Order N^o : ../../..

PEOPLE'S DEMOCRATIC REPUBLIC OF ALGERIA
MINISTRY OF HIGHER EDUCATION AND SCIENTIFIC RESEARCH
UNIVERSITY KASDI MERBAH OF OUARGLA

Faculty of New Information Technologies and Communication
Department of Electronics and Telecommunications

THESIS

Thesis submitted in partial fulfillment of the requirements for the degree of

3^{rd} **Cycle LMD Doctorate**

Option : **Systems of Telecommunications**

By : **TRABELSI Selma**

Theme

Development of Efficient Biometric Systems for Persons Recognition

Publicly defended on :27/10/2022 before the jury composed of :

Fouad CHEBBARA	*Pr.*	*at Ouargla University*	*President*
Djamel SAMAI	*MCA*	*at Ouargla University*	*Thesis Director*
Abdallah MERAOUMIA	*Pr.*	*at Tebessa University*	*Thesis Co-director*
Mohamed Ridha LAOUAR	*Pr.*	*at Tebessa University*	*Examiner*
Abderrazak BENCHABANE	*MCA*	*at Ouargla University*	*Examiner*
Fella CHARIF	*MCA*	*at Ouargla University*	*Examiner*


بسم الله الرحمن الرحيم


وقل رب زدني علما

صدق الله العظيم

To my beloved parents, **Leila BENAOUDA** *and* **Mohammed**, *for always believing in me and encouraging me to excel in my studies. May Allah keep them safe.*

I am very grateful to Allah for being with me and for the unconditional support that I received from my family: my sister: **Imene** *and her daughter* **Lina** *and my brothers:* **Moussa**, **Mohamed**, *and* **Younes**. *I ask Allah to protect them.*

Many thanks to my supervisors: **Dr. Djamel SAMAI**, **Pr. Abdelmalik TALEB-AHMED** *and* **Pr. Fadi DORNAIKA** *for their support, help, and encouraging words.*

All my friends and colleagues.

Selma TRABELSI

acknowledgments

First and foremost, I thank **ALLAH** the Almighty for allowing me to reach this modest scientific level and for providing me with the courage and patience to complete the work in this thesis.

I would like to thank my mother ***Leila BENAOUDA*** *for her friendship, encouragement, and caring over all these years, for always being there for me through thick and thin, and without her, this project would not be possible. I would also like to thank my sister and my brothers for their understanding and support throughout all these years.*

I would also like to my sincere thanks go to my dissertation supervisors ***Dr. Samai Djamel, Pr. Abdallah Meraoumia, Pr. Abdelmalik TALEB-AHMED, Pr. Fadi Dornika, Dr. Azeddine BENLAMOUDI, and Dr. Khaled BENSID*** *this research could not have been accomplished without their sustaining support, guidance, patience, and encouragement all the way.*

I would like to acknowledge my thesis committee ***Pr. Fouad CHEBBARA, Pr. Med Ridha LAOUR, Dr. Abderrazak BENCHABANE, and Dr. Fella CHARIF****, for accepting and evaluating my thesis work.*

My special thanks are extended to my friends ***Leila, Yamina, Fatima, Chahera, Maberouka, Alla, Ouassama, Fouad*** *and all colleagues that helped me grow as a person and were always there for me during the good and bad times in my life. Thank you.*

To each and every one of you – Thank you so much.

Résumé

Face aux inquiétudes croissantes concernant les failles de sécurité et les transactions frauduleuses, les technologies fiables et pratiques d'identification et de vérification des personnes sont de plus en plus demandées dans nos activités sociales et nos services nationaux. La biométrie, qui utilise des caractéristiques physiologiques et comportementales distinctives pour connaître l'identité d'un individu, gagne en popularité dans un large éventail d'applications de sécurité gouvernementales, médico-légales, militaires et commerciales.

L'empreinte palmaire et l'empreinte articulaire du doigt sont deux modalités physiologiques obtenues à partir de la main humaine et ont prouvé leur fiabilité et leur acceptabilité par l'utilisateur dans une large gamme d'applications de sécurité. Dans notre travail, nous avons d'abord développé une approche efficace appelée Simplified PalmNet—Gabor qui se concentre sur l'amélioration du PalmNet pour la reconnaissance rapide d'images d'empreintes palmaires multispectrales et sans contact. De plus, nous utilisons des procédures de sélection de caractéristiques et de réduction de la dimensionnalité pour surmonter les problèmes de complexité de calcul. Les résultats expérimentaux montrent que notre approche permet d'atteindre un taux de reconnaissance élevé en utilisant un nombre de caractéristiques nettement inférieur.

Nous avons également conçu des systèmes d'identification unimodaux et multimodaux basés sur des images multispectrales d'empreintes palmaires et empreintes des articulations des doigts. L'extraction de caractéristiques est une étape cruciale dans le système biométrique. Pour cette raison, nous proposons une méthode d'apprentissage profond par réseau de neurones convolutionnels (CNN) pour extraire les caractéristiques profondes. Les résultats obtenus indiquent clairement que les techniques d'extraction de caractéristiques basées sur l'apprentissage profond proposé peuvent atteindre des performances élevées par rapport aux meilleures techniques de pointe.

Mots-clés : Biométrie, Apprentissage profond, PalmNet–Gabor, Sélection de caractéristiques, Réduction de la dimensionnalité, Empreinte palmaire multispectrale, Empreinte palmaire sans contact, Empreintes des articulations des doigts, Réseau de neurones convolutionnels.

Abstract

With growing concerns about security breaches and transaction fraud, reliable and convenient personal identification and verification technologies are increasingly demanded in our social activities and national services. Biometrics, which uses distinctive physiological and behavioral characteristics to learn an individual's identity, is gaining popularity in a wide range of government, forensic, military, and commercial security applications.

Palmprint and finger knuckle print are two physiological modalities obtained from the human hand and have proved their reliability and user acceptability in a wide range of security applications. In our work, we first developed an effective approach called Simplified PalmNet—Gabor that concentrates on improving the PalmNet for fast recognition of multispectral and contactless palmprint images. Moreover, we use feature selection and dimensionality reduction procedures to overcome computational complexity issues. Experimental results show that our approach achieves a high recognition rate by using a substantially lower number of features.

We also designed unimodal and multimodal identification systems based on multispectral palmprint and finger knuckle print images. Feature extraction is a crucial step in the biometric system. For this reason, we propose the Convolutional Neural Network (CNN) deep learning method to extract deep features. The results indicate that the proposed deep learning-based feature extraction techniques can achieve high performance compared to the best state-of-the-art techniques.

Keywords : Biometrics, Deep learning, PalmNet–Gabor, Feature selection, Dimensionality reduction, Multispectral palmprint, Contactless palmprint, Finger knuckle print, Convolutional Neural Network.

الملخص

مع تزايد المخاوف بشأن الاتهاكات الأمنية والاحتيال في المعاملات ، أصبحت تقنيات التعرف والتحقق من الشخصية الموثوقة والمريحة مطلوبة بشكل متزايد في أنشطتنا الاجتماعية والخدمات الوطنية. القياسات الحيوية ، التي تستخدم الخصائص الفسيولوجية والسلوكية المميزة لمعرفة هوية الفرد ، تكتسب شعبية متزايدة في مجموعة واسعة من تطبيقات الأمن الحكومية والطب الشرعي والعسكري والتجاري.

بصمة الكف وبصمة الإصبع هما طريقتان فسيولوجيتان تم الحصول عليهما من اليد البشرية وأثبتا موثوقيتهما ومقبولية المستخدم في مجموعة واسعة من تطبيقات الأمان. في عملنا ، قمنا أولاً بتطوير نهج فعال يسمى Simplified PalmNet—Gabor يركز على تحسين PalmNet للتعرف السريع على صور بصمات اليد متعددة الأطياف والتي لا تلامس. علاوة على ذلك ، نستخدم إجراءات تحديد الميزات وتقليل الأبعاد للتغلب على مشكلات التعقيد الحسابي. تظهر النتائج التجريبية أن نهجنا يحقق معدلتمييز مرتفع باستخدام عدد أقل بكثير من الميزات.

لقد صممنا أيضًا أنظمة تعريف أحادية الوسائط ومتعددة الوسائط تعتمد على بصمة الكف متعددة الأطياف وصور بصمات الأصابع. استخراج الميزات هو خطوة حاسمة في نظام القياسات الحيوية. لهذا السبب ، نقترح طريقة التعلم العميق للشبكة العصبية التلافيفية لاستخراج الميزات العميقة. تشير النتائج التي تم الحصول عليها بوضوح إلى أن تقنيات استخراج الميزات القائمة على التعلم العميق يمكن أن تحقق أداءً عاليًا مقارنة بأفضل التقنيات الحديثة.

الكلمات المفتاحية القياسات الحيوية ، التعلم العميق ، شبكة اليد غابور، اختيار الميزات ، تقليل الأبعاد ، بصمة الكف متعددة الأطياف ، بصمة الكف غير التلامسية ، بصمة الإصبع ، الشبكة العصبية التلافيفية.

Contents

List of Figures

List of Tables

Abbreviations

CCD :	Charged Coupled Device	**LMF :**	Left Middle Fingers
CMC :	Cumulative Matching Characteristic	**MCI :**	Mean Curvature Image
CNN :	Convolutional Neural Network	**MUL :**	Product score
CPU :	Central Processing Unit	**NIR :**	Near Infra-Red
DBN :	Deep Belief Network	**PCA :**	Principal Component Analysis
DCT :	Discrete Cosine Transform	**RIF :**	Right Index Finger
DFT :	Discrete Fourier Transform	**RLOC :**	Robust Line Orientation Code
DWT :	Discrete Wavelet Transform	**RMF :**	Right Middle Fingers
EER :	Equal Error Rate	**ROC :**	Receiver Operating Curve
FAR :	False Acceptance Rate	**ROI :**	Region Of Interest
FKP :	Finger Knuckle Print	**ROR :**	Rank One Recognition
FRR :	False Rejection Rate	**RPR :**	Rank of Perfect Recognition
FS :	Feature Selection	**SIFT :**	Scale Invariant Feature Transform
GAR :	Genuine Acceptance Rate	**SUM**	Sum Score
GCI :	Gaussian Curvature Image	**SVM :**	Support Vector Machine
kNN	k-Nearest Neighbor	**WHT MUL**	Weighted Product Score
LBP :	Local Binary Pattern	**WHT SUM**	Weighted SUM Score
LIF :	Left Index Fingers	**WPCA**	Whitening Principal Component Analysis

Part I

Context And Motivations

Chapter 1

General Introduction

Individual authentication and identification are becoming increasingly important in the modern automated world. The current technology uses personal identification codes (PINs) or passwords. These reasons fall far short of the standard of an identification scheme since it requires an excessive amount of passwords to be remembered, and the password or PIN is highly insecure. As an outcome, in today's complex, geographically mobile, and increasingly electronically wired information society, the issue of identifying an individual remains a significant challenge. Biometrics-based authentication and identification are emerging as the most reliable method. Biometrics necessitates the individual to be physically identified and present at the moment of identification. It depends on "something which you are or you do" to provide high security, improved accuracy, and increased efficiency [1],[2].

It overpowers some of the shortcomings of traditional identification technology, including ID cards and PINs: ID cards can be misplaced, thieved, or unremembered, whereas PINs can be forgotten or guessed by impostors. Furthermore, traditional identification methods cannot distinguish between an authorized user and an imposter who illegally obtained the authorized user's "information" or "token." Automated biometrics are concerned with physiological or behavioral-related characteristics like fingerprint [3], signature [4], palmprint [5], iris [6], voice [7], and face [8]; these traits are used to verify the individual's identity or create an identity from a database. Creating an automated biometric system

that can authenticate many people with accuracy and reliability is a difficult task.

To develop a biometric system, it is necessary to choose which biometric method will be used. Overall, this biometric modality enables us to select the most appropriate feature extraction technique that may provide the best recognition rate. Indeed, acceptability and precision rates are two essential parameters implemented to choose the suitable biometric method within a particular security application. Human behavior modalities have a greater acceptability rate with inferior precision because of their higher inter-class variability [9]. In contrast, the physiological modalities offer a good compromise between acceptability and precision rates. Even within the usual range of physiological traits, biometric modalities with low acceptability and others characterized by poor accuracy. For example, face traits are very acceptable but result in low precision. Besides, fingerprints provide high precision but are not accepted by users in several applications. Various physiological modalities are currently required, and those obtained from the human hand have confirmed their reliability and acceptability by the user in a wide range of security applications [10]. In particular, from the palm of the human hand, two main biometric modalities can be obtained: palmprint and finger knuckle print.

Specifically, palmprint is concerned with the inner surface of a hand and looks at line patterns and surface shapes. A palm is covered with the same kind of skin as the fingertips and is larger than a fingertip in size. As a result, it is quite natural to consider using palmprints to identify an individual. Because of the rich texture features, principal lines and wrinkles on palm prints are considered sufficiently stable and distinctive information for identifying an individual from a wide population. On the other hand, Finger Knuckle Print (FKP) has several features that can be used, such as structure and shape, length, width, thickness, and joint characteristics of the skin surface, such as creases and ridges in fingers. Several major factors make a person's FKP unique. Among these factors, the ease of use, including the rich texture information, appears to be the most significant, allowing the biometric system to work with higher accuracy.

In general, a biometric system is a type of pattern recognition system where a feature set is first extracted from the obtained data and then compared with the stored template set to decide on the identity of an individual. A biometric system is implemented for both verification and identification. In verification mode, the decision looks into "whom the person claims to be," whereas, in identification mode, the decision looks into "to whom this biometric data belong?" As a result, a biometric system is formalized as a two-class or multi-class pattern recognition system. A biometric system typically consists of four main modules: data acquisition, feature extraction, matching, and system database, where feature extraction and matching are two of the most challenging issues in biometric recognition research, attracting researchers from diverse fields including biometrics, computer vision, pattern recognition, signal processing, and neural networks.

1.1 Problem statement and objectives

Developing an effective biometric system must consider five essential and relevant factors: accuracy, user acceptance, environmental constraints, security, cost, and computation speed (see figure 1.1). Indeed, decreasing accuracy can increase speed, reduce user acceptance, enhance precision, and increase cost, which may enhance security [11] [12].

Therefore, a system based on palm prints or finger knuckle prints is very appropriate because they do not cause anxiety to the users. In particular, finger knuckle print recognition offers many features that can be used, including structure and shape (length, width, and thickness), attributes of the skin surface, including creases and ridges in fingers, and traits of the skin. In addition, a person's FKP is distinctive due to several major factors, the most important of which appear to be the rich texture data, low cost, and simplicity of use. This permits the biometric system to function more accurately.

On the other hand, biometric systems based on palm prints are generally well accepted by users because they are not viewed as very intrusive or privacy-sensitive. Additionally, palm prints can be acquired using low-cost devices, making them suitable for various

low-cost applications in daily life. Palm prints are also suitably redundant to facilitate the accurate recognition of even a partially damaged palm surface. Unfortunately, traditional systems for palm print recognition depend on touch-based acquisitions with pegs that restrict the posture of the hand, making them harder to use. For this reason, recent research has focused on contactless and contact-free acquisition systems, making them more convenient and comfortable by eliminating the contact obligation. However, the liberty of presenting one's hand offers a variety of variabilities such as scaling changes, position variability, hand orientation changes, illumination changes, etc. Moreover, high-dimensional data with many uncorrelated and redundant features remains challenging due to computational complexity issues.

Research in this field is certainly interesting via the multiplicity and diversity of these problems. Hand biometric modality has received much attention from research laboratories and industrial ones. To provide the design of our hand biometric system with success, our purposes are concentrated on the proposition of a solution that enhances the accuracy and the speed of the individual recognition process, which reduces the cost of the biometric system and increases user acceptance. Hence, our solution is based on multimodal biometric systems based on deep learning and feature selection methods for contactless and contact-based recognition systems. Then, we proposed unimodal and multimodal identification systems for multispectral and touchless palmprint images. Also, feature selection and dimensionality reduction procedures are applied to reduce computational complexity. For the multimodal system, we used the matching score fusion method to improve the performance of the unimodal system. On the other hand, two multimodal identification systems have been developed based on palmprint and finger-knuckle print recognition.

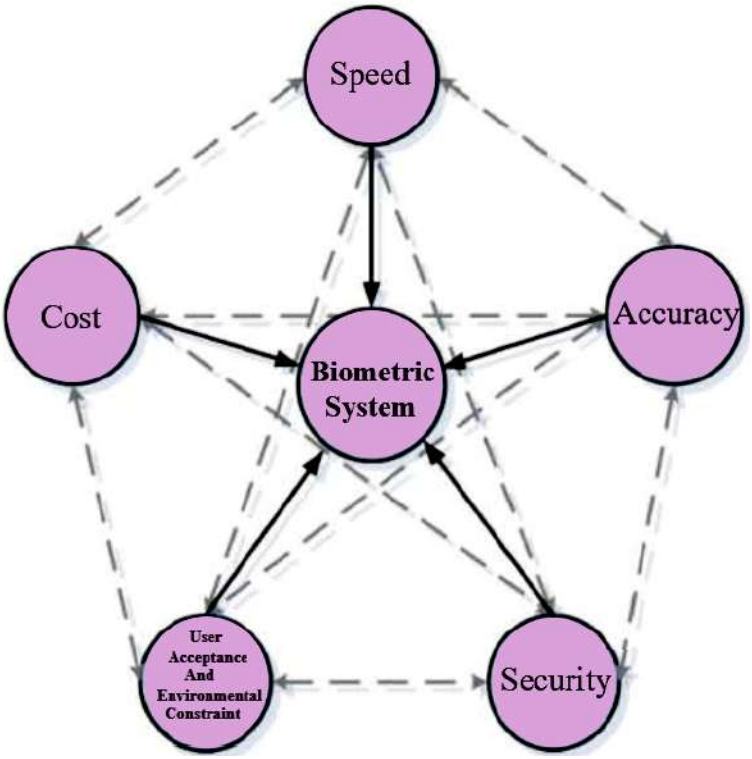

Figure 1.1 – Interrelationships between different factors for biometric system design.

1.2 Contributions

In order to achieve the objectives detailed in the previous section, some contributions are suggested for identification systems based on hand biometric modalities. The main contributions of this thesis are detailed as follows:

1. Our first contribution is to design an efficient approach called simplified Palm-Net–Gabor based on deep learning and feature selection. Our approach focuses on enhancing PalmNet for multispectral and contactless palmprint recognition. Therefore, in the preprocessing stage, we applied Log-Gabor filters to adjust the pixel luminance of palmprint images. Then, we reduced the number of features using feature selection and dimensionality reduction procedures. Our objective is to select a subset of relevant features, decrease the dimensionality, reduce the running time, and improve the accuracy. After that, SVM and K-NN classifiers are used for classification. Finally, we fused modalities at the matching score level for the multimodal system to improve system performance. The proposed method

effectively improves the accuracy of the PalmNet and reduces the number of features and computational time. Experiments show that our approach achieves a high recognition rate while using a substantially lower number of features.

2. Our second contribution is constructing a reliable recognition system based on Convolutional Neural Networks (CNN). CNN is a deep neural network used in pattern recognition and image processing. We aim to develop palmprint and palm-vein-based biometric systems in which biometric images are analyzed using the CNN feature extraction technique. In our experiments, we first evaluate each biometric identification system based on a single spectral band (a unimodal system). Also, the results of two or more unimodal systems are fused at the matching score level to create an efficient and robust multimodal identification system.

3. Finally, we presented an approach to extracting deep features from finger knuckle print images. The proposed method uses a CNN deep learning technique. The proposed CNNs are designed to extract highly discriminative features specific to finger knuckle print samples. This work aims to improve the recognition rate using multimodal biometric systems based on the fusion at the matching score level for multi-sample FKP images, which are Left Index Finger (LIF), Left Middle Finger (LMF), and Right Index Finger (RIF), and Right Middle Finger (RMF) modalities. Experimental results on FKP images show that the proposed scheme yields the best performance and can provide an excellent recognition rate, mainly when fusing spectral bands of biometric modality.

1.3 Organization of the Manuscript

The rest of the thesis is organized as follows.

Chapter 2: Chapter 2 illustrates the state of the art of hand modalities represented by palmprint recognition, including different representations of palmprint images

and classical and deep learning methods for palmprint feature extraction. Then, the state of the art of finger knuckle print recognition is detailed. Also, the performance evaluation metrics of the detectors are presented.

Chapter 3: This chapter describes the proposed unimodal and multimodal identification systems based on deep learning and feature selection methods. Various experiments were carried out using contact-based and contactless palmprint images. Besides, this chapter includes multimodal system experiments at matching score fusion levels to overcome the drawbacks of the unimodal system.

Chapter 4: This chapter presents the proposed approach based on Convolutional Neural Network (CNN) for palmprint recognition. The architecture of the CNN is detailed. Then, the experimental results of the unimodal and multimodal systems are demonstrated to evaluate the robustness and efficiency of the proposed method.

Chapter 5: Chapter 5 demonstrates ourunimodal and multimodal systems based on finger knuckle print (FKP) images. Then, a description of the deep CNN-based feature extraction method and a classification. Finally, the experimental results obtained using different samples of FKP images are presented and discussed.

Chapter 6: This chapter gives a general conclusion with the perspectives that we will consider.

Chapter 2

Hand Biometric Traits: State of the Art

2.1 Introduction

The ease of use of a biometric system depends on the constraints related to the acquisition, and use of the chosen biometric modality [13]. In order to satisfy this requirement, hand-related biometric modalities are potentially powerful technologies. People readily accept biometric technologies based on different hand-related modalities because of their ergonomics. Moreover, these technologies are easy to install at a reasonable cost. This chapter is organized as follows: Section 2 introduces state-of-the-art palmprint recognition, including different representations of palmprint images and classical and deep learning methods for palmprint feature extraction. Section 3 exhibits the state of the art of finger knuckle print recognition. The performance evaluation metrics of the detectors are detailed in Section 4. Finally, section 5 refers to the conclusion of this chapter.

2.2 Palmprint Recognition

The palm is defined as the inner part of the hand, from the wrist to the roots of the fingers. A print is an impression made on or over a surface through pressure. A palm print is defined as a palm skin pattern composed of the physical characteristics of skin patterns, such as lines, points, and texture (see fig 2.1) [2].

Figure 2.1 – The palm of the hand.

Many unique features in a palmprint image can be used to identify a person. Figure 2.2 shows an inked palmprint, and a palmprint without ink from the same palm [2]. Both were obtained using a resolution of 500 dpi. On the palm, six main types of features can be observed. The first four can be taken from inkless or inked palm prints, while the last two can only be obtained from inked palm prints with relatively high accuracy [2].

— Geometry Properties: Based on the shape of the palm, we can easily get the corresponding geometric features like length, width, and area.

— Principal Line Features: In a palmprint, the location and shape of the main lines are significant physiological characteristics for identifying individuals because they vary slightly over time.

— Wrinkle Features: Many wrinkles in a palmprint differ from the main lines in that they are thinner and more irregular. They are categorized as fine and coarse wrinkles so that more features can be captured in detail.

— Datum points: Two endpoints called "data points" are acquired using the main lines (see Figure 2.2). These crisscross both sides of the palm and provide a stable method for registering palm prints. Palm size can be determined using the Euclidean distance between these endpoints.

— Delta Point Features: The delta point is represented as the center of a delta-like area of the palmprint. The delta points are usually located in the finger-root region. These offer reliable and unique measurements for palmprint verification.

— Minutiae Features: A palmprint is essentially comprised of the ridges, giving the minutiae features the ability to be employed as another vital measurement.

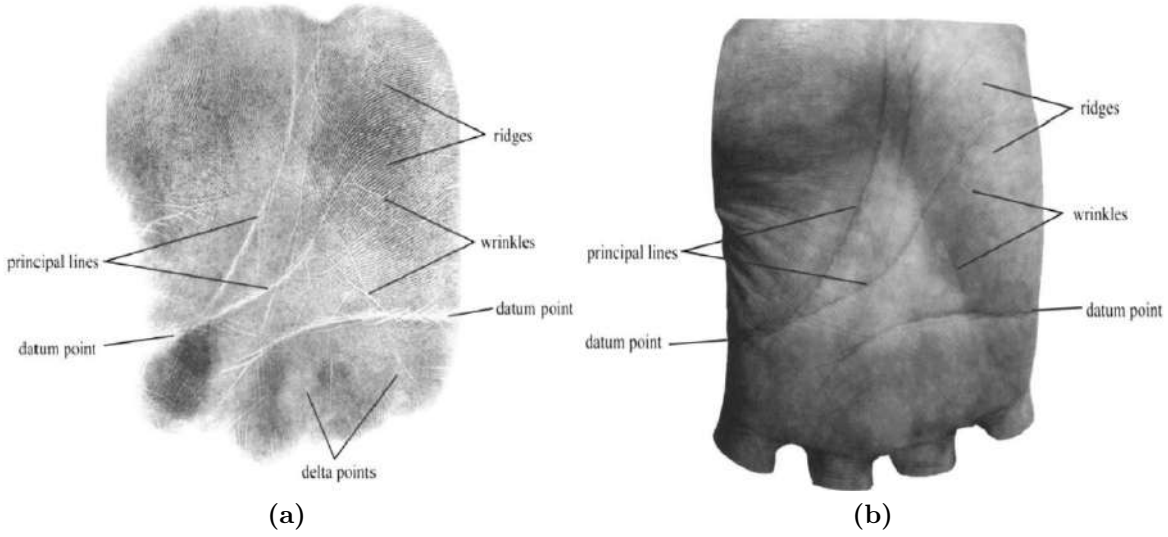

Figure 2.2 – Palmprint features. (a) inked palmprint, (b) inkless palmprint.

The palmprint approach can be classified into different categories based on the palmprint image data type, such as grayscale [14] [15], 3D [16] and multispectral/hyperspectral. In addition, the palmprint images can also be classified based on the method of palmprint image acquisition, and thus, they can be grouped into contact-based [17] and contactless palmprint images. The main difference is whether the hand is in contact with the acquisition device. Specifically, the former is captured by placing the palms on the device and user-pegs' aids. By contrast, the latter is collected with hands not touching the device. Fig. 2.3 illustrates two typical contact-based and contactless palmprint image acquisition modes [18].

(a) (b)

Figure 2.3 – The devices used to collect palmprint images. (a) contact-based palmprint image acquisition device. (b) contactless palmprint image acquisition device.

2.2.1 GrayScale representation

Zhang et al. [19] created a camera to capture palmprints in 2003 based on the Gabor wavelet decomposition. They have recommended a system of detection and extraction of local peculiarities of the palmprint. The efficiency of this system was confirmed under two operational procedures; verification and identification, adding to the help of a database of 775 of 7752 images of 386 persons, with variations in light and pose. A recognition rate of 98% on average and an error of 0.04% have been reported, demonstrating that the recognition rate is exceptionally high. This indicates the strength of this approach.

Kumar et al. [20] have introduced a DCT-based system. The goal is to show the objective and utility of DCT coefficients in palmprint verification. This system collects data and information from the hand shape and the palmprint to strengthen identification. These two components are fused and used at the score level. The results of this experiment on a database of 100 people revealed that both the handprint and palmprint are the same. Besides that, the product rule of the scores produces positive results with a 0.6% error.

Moreover, a DWT-based palmprint description was suggested by Zhang et al. [21], along with directional context for each subband. The goal is to gather dominant coefficients for all main lines and wrinkles. A series of traits, including the center of gravity, density, and energy, would then be defined to distinguish the palmprint from the selected values of the directional context. Tests performed on a database of 200 images of 50 people show that the system can produce impressive results.

Furthermore, Zhang et al. [22] proposed an approach based on lines. It uses two main and new features for palmprint identification: datum point invariance and line feature matching. The palmprint's reference points are defined. The retrieval of line features and their matching are then recommended to evaluate whether the two palm prints are from the same palm. The experimental results reveal that the recognition algorithms' performance remains poor. Following what has been preceded, Jay Kumar et al. [23] developed another effective method based on palmprint lines. They combined the traits of the palmprint with the hand geometry to enhance the system's performance. The palmprint's traits and the hand's geometry can be obtained simultaneously, from the same image, using a digital camera. Their test results on a database of 100 people demonstrate the fusion of hand geometry traits with palmprint traits with the help of a simple image sensor.

The Fisherpalms method was also presented by Wu et al. [24]. A Fisher Linear Discriminant Analysis (LDA) linear selection is utilized to forecast all of the initial high dimensional palmprints to an even smaller area (Fisher space). The connection between the accuracy of recognition and the palmprint image is investigated. The proposed method gave high precision ($>$ 99 percent). Besides, the results show that this approach is easy, quick, and allows for real-time recognition (identification or verification). Also, Lu et al. [25] recommend a palmprint system grounded on eigenpalms(eigenspace). As used in PCA, the initial images are converted into a small set of primary components known as Eigen palms, which are the eigenvectors of the learning set. The recognition process involves projecting the image into a subspace composed of the selected principal compo-

nents, computing the Euclidean distance between them, and determining the Euclidean spacing between the image and its projection. The outcomes of the studies proved the method's efficacy in terms of recognition rate. In addition, Zuo et al. [26] have improved on the PCA-based approach by using a two-dimensional primary component subspace to distinguish palmprints (2D-PCA). The two-dimensional PCA is a new image portrayal approach for recognition. The authors propose an Arranged Matrix Distance (AMD) to calculate the distance between two matrices. The test findings exhibit that this approach is efficacious for recognition.

2.2.2 Multispectral and hyperspectral representation

Recently, biometric recognition has made use of multispectral and hyperspectral images. If we can successfully evaluate and process images captured in the multispectral or hyperspectral domain, we can acquire valuable information about the human body. For example, in the presence of certain waves, the temperature of the skin and its physiological traits can deliver information on the thermal regulation of human tissues and the vascular mapping unique to each individual. Rather than only a few researchers having studied biometric identification employing hyperspectral images, most of them focus on biometric identification using multispectral images.

1. **Multispectral representation**

   Han et al. [27] provided a multispectral palmprint recognition method that uses various spectral bands to identify palmprint image data, which includes red, green, blue, and infrared. Although, as a comparison algorithm, the Competitive Coding Strategy is used (similarity measure) by combining the entire spectral bands (by employing the image level merging method formed on wavelet transform), the outcomes of the verification tests revealed that the fusion produced better results than a single spectral band. Guo et al. [28] differentiated the performance of a palm print recognition biometric scheme employing white and non-white lights (six other lights of different colors). However, the tests on an extensive database showed that white light does not offer the optimal illumination for palm print recognition.

Hao et al. [29] proposed pixel-level fusion of multispectral palm print images for increasing the performance of a palm print authentication system. The findings of the studies obtained using several image fusion methods exhibited an enhancement in recognition accuracy compared to a scheme that only utilizes monochrome images.

David Zhang et al. [30] suggested a multispectral palmprint verification method. Their work contained a data acquisition device to obtain palmprint images in different illuminations and then use an orientation-based representation for the multispectral palm print images. At the score level, the fusion scheme was used. The experimental results showed the efficiency of merging all of the multispectral bands compared to a particular spectral band. On the other hand, Khan et al. [31] created a sample of a multispectral palmprint system based on contour representation. This representation is obtained from the contourlet transform. The verification results demonstrated that the contour representation outperforms methods found in various literature. Cui et al. [32] used Image-Based Linear Discriminant Analysis (IBLDA) and the synthesis of the four bands of the palmprint image. The images of the four bands are classified into two groups, and a complex matrix is constructed using the two bands from each group. The results have revealed that using the IBLDA technique results in the highest recognition rate. Xu et al. [33] proposed a new technique for multispectral images using a quaternion model. A quaternion matrix represents the multispectral palmprint image. A PCA and DWT alteration were implemented on the matrix to retrieve the palm print characteristics. According to the test results, the quaternion matrix can achieve a high recognition rate.

2. **hyperspectral representation**

   Multispectral imaging delivers additional information compared to the traditional observed palmprint image. This image presents many measured spectral bands

of less than ten. Therefore, additional information is added to the multispectral image by using a hyperspectral representation. The hyperspectral image consists of several bands varying from ten to two hundred. While a database of hyperspectral palm prints is now available, few studies on biometric identification centered on hyperspectral imaging have been conducted. Zhenhua Guo et al. in [34] have created a system for acquiring hyperspectral images in several consecutive bands (420 nm–1100 nm). These images were analyzed in order to select the best spectral bands. First, a feature vector is obtained (using 2D-PCA) and compared with each spectral band. Then, several combinations are evaluated using score level merging to select the best combination. The experimental results show that two spectral bands can provide the desired discriminating information for the palm print. This work could also guide future systems identification based on hyperspectral palm prints. In another work, Zhenhua Guo et al. [34] did the same with the use of a classification algorithm. The authors propose a new algorithm for classifying spectral bands using a k-means clustering algorithm. The test results disclosed that three spectral bands delivered can provide the most significant discriminating power of the palmprint.

3. **Three-dimensional representation**

   Several methods have been developed for palmprint recognition (2D representation). However, they have several limitations related to palm print orientation, pose, lighting, etc. In recent years, 3D palmprint recognition methods have been debated as a substitute solution to the mentioned problems. The wealth of information delivered by 3D measurements permitted the renovation of the palmprint's three-dimensional form. This kind of exemplification is unaffected by variations in lighting and pose. Overall, the methods developed employed 2D-3D multimodal methods that integrated 2D and 3D measurements to maximize the benefits of both methods (2D and 3D). In their work, Zhang et al. [35] contained the biometric identification framework devoted to the 3D demonstration of palmprints.

The study proposed three methods for feature extraction: Mean Curvature Image (MCI), Gaussian Curvature Image (GCI), and Surface Types (ST). The 3D palmprints are then classified using a rapid technique for measuring similarity and a score-level fusion strategy. These tests demonstrate that 3D palmprint identification has an excellent recognition rate and that 3D demonstration also has a powerful anti-counterfeiting ability.

Li et al. [16] employed image curvatures (MCI) to demonstrate palmprint characteristics after proposing a palmprint database based on the assistance of 200 volunteers. The 3D palmprint design is then coded using the "Competitive Coding" method based on their MCI. The scheme can attain excellent performance with an error of 0.284 % by using fusion at the level of MCI scores and their CompCode. Zhang et al. [36] developed the precision and robustness of the palmprint recognition scheme by utilizing both the 2D and 3D characteristics of the palm prints simultaneously. The feature extraction procedure employs a "surface curvature maps" method for 3D images and the Gabor filter for 2D images. The fusion of these two characteristics is used at the score level. Experiments on a database of 73 people show that the identification scheme can achieve satisfactory results. In the work of Cui [37], the feature vector is exemplified by the "Two-Phase Test Sample Representation-TPTSR" algorithm. PCA is used to acquire the overall palmprint characteristics before adding TPTSR. The two modalities, 2D and 3D, are combined at the score level. The experimental results on a database of 8000 images show that the combination of the two methods makes it possible to achieve identification rates above 95%.

2.2.3 Classical Methods for Palmprint feature extraction

Recognizing an individual employs a specific criterion to determine a person's identity. To do this, a certain number of clues (or characteristics) collected from an anonymous form, the individual to be recognized, must be exploited and interpreted to generate a theory concerning his identity. Performing this recognition task with exact accuracy is

difficult [38]. This is primarily due to the choice of the extracted features that must be reflective of the person's identity to be identified. This decision is significant because it influences the entire recognition methodology. Finally, even if these characteristics are known, it is frequently hard to exploit them to describe a set of rules. Many features, such as lines and texture, can be implemented to represent and characterize the palmprint image. Numerous methods for extracting many biometric characteristics have already been suggested. The classical methods for palmprint recognition can be divided into line-based, coding-based, texture-based, subspace-based, and local-texture-descriptor-based approaches [39]. In this chapter, we focus on online-based, and coding-based approaches that are most commonly studied in the literature and demonstrate the best recognition accuracies for palmprint recognition [18].

1. **Line based algorithms**

   To extract palm lines, Wu et al. [15] used the second-order derivatives of a Gaussian to show the magnitude of the line and the first-order derivatives of a Gaussian to detect the line location. The last result is acquired by combining all the directional line detection results and then encoded using the chain code. Liu et al. [40] proposed a wide line detector using an isotropic nonlinear filter to obtain the location and width information of palm lines. Additional techniques, such as two-stage filtering, have similarly been used to detect palm lines [41]. Wu et al. [42] propose another algorithm that computes the magnitude of palm lines by applying Sobel masks. Histograms are formed by projecting these magnitudes in the same directions. These histograms are considered inputs to Hidden Markov Models (HMMs). Boles et al. [43] built binary edge images with Sobel masks and thresholds. After that, they applied the Hough transform to collect the parameters of the six lines with the highest densities in the accumulator array for matching. Kung et al. [44] developed a low-resolution edge map to generate a feature vector. Finally, the feature vector is passed into decision-based neural networks. To retrieve main wrinkles and lines, Huang et al. [45] recommended a two-level improved finite radon

transform and a dynamic threshold to extract major principal lines and wrinkles. A matching scheme known as the pixel-to-area comparison is used to evaluate the difference between two binary edge maps. Leung et al. [46] used Sobel masks to obtain palm lines and line segment Hausdorff distance to compare two palmprints. Rafael Diaz et al. [47] made use of Sobel masks and morphologic operators as two separate feature extractors to obtain the gradient of the images. Neural networks categorize these feature values.

2. **Coding based algorithms**

The coding-based technique encodes the output of a bank of filters into bitwise code. Zhang et al. [19] developed a PalmCode method that first convolved the palmprint image with a 2D Gabor filter and then encoded the phase of the filter responses as bitwise features. PalmCode achieved significant rates of accuracy and speed in verifying the palmprint information extracted from low-resolution sets. Inspired by the PalmCode method, Kong et al. [48] introduced a new palm recognition method called Competitive Coding Scheme (CompCode). The scheme uses the real part of a neurophysiology-based 2D Gabor filter to extract the orientation information of the palmprint, accompanied by an encoding process to create a feature vector to uniquely describe the original palmprint. The filter is none other than the original Gabor filter, whose degrees of freedom were repartitioned corresponding to the results of the neurophysiological system such that the palm line pattern was modeled as an inverted Gaussian function.

Kong et al. [49] presented the FusionCode method to improve performance through convolving a palmprint image along with a bank of Gabor filters with distinct orientations and then encoding the phase of the filter response with the maximum magnitude. Recent advances in coding-based techniques indicate that the orientation information of palm lines is one of the most promising features for personal identification. Jia et al. [50] employed a modified version of the Radon transform (FRAT), called the Modified Radon Transform (MFRAT), which attempted to

increase the robustness of coding-based palmprint recognition techniques against small image transformations. Moreover, they demonstrated a new matching technique that considers small geometric differences by considering the neighborhood of each pixel in the Radon-filtered image. This is referred to in the literature as the robust line orientation code (RLOC). Although RLOC produces a slight advantage over its associated competitors in the presence of geometric distortions, it suffers from significant computational complexity.

Zuo et al. [51] suggested the competitive code method that processes the image using several Gabor filters with distinct orientations, and after that, it encodes merely the index of the filter matching to the minimum magnitude reaction for each pixel separately. This encoding creates a map of the image's most crucial palmprint line orientations. Fei et al. [52] employ multiple Gabor filters with various orientations to filter the image, encoding statistics signifying the two most demonstrative filters for every pixel and matching them by using the nonlinear angular distance. Likewise, the neighboring direction indicator (NDI) technique [53] encodes the main orientation and the relations with the orientations of the neighboring areas for every pixel. More recently, the robust competitive code approach has been proposed by Xu et al. [54], which combines the competitive code algorithm with the NDI technique. Specifically, the robust competitive code method encodes the most relevant orientation and a weighted combination of the orientations in nearby regions for each pixel.

3. **Other algorithms**

Jing et al. [55] used a two-dimensional (2D) separability judgment to select DCT frequency bands with appropriate linear separability. Then, from the given bands, it extracts the linear discriminant features using the optimized Fisherface method and classifies them with the nearest neighbor classifier. Luo et al. [56] proposed a new image descriptor, local line directional patterns (LLDP). This work shows

that different implementations of LLDP descriptors perform competitively in palm print recognition. Kang et al. [57] presented a novel recognition approach for contact-free palm-vein recognition that performs feature extraction and matching on all vein textures distributed over the palm surface, including finger veins and palm veins, to minimize the loss of feature information. First, a hierarchical enhancement algorithm is adopted, which combines a DOG filter and histogram equalization to alleviate uneven illumination and highlight vein textures. Second, a Root Scale Invariant Feature Transform (RootSIFT), a more stable local invariant feature extraction method compared to the Scale Invariant Feature Transform (SIFT), is used to overcome the projection transformation in contact-free mode.

2.2.4 Deep Learning Methods for Palmprint feature extraction

Palmprint recognition technologies in deep learning [58] [59] have flourished on a large scale. Deep learning is classified into two types: supervised learning, such as convolutional neural networks (CNN), and unsupervised learning, such as deep belief networks (DBN). The three crucial points in a particular learning system are the activation function, the loss function, and the optimization strategy. Generally, a typical deep learning system comprises various layers, such as the input layer, convolutional layer, fully connected layer, pooling layer, softmax layer, and output layer [60]. In this context, Wang *et al.* [61] proposed 2D Gabor wavelets for palmprint images. They used a Pulse-Coupled Neural Network (PCNN) to imitate the creatural vision perceptive process and decompose each Gabor subband into a series of binary images. Entropies for these binary images are calculated and regarded as features. An SVM classifier is employed for classification. Minaee and Wang [62] proposed a Deep Scattering Convolutional Network with a two-layer for palmprint recognition. Then Principal Component Analysis (PCA) is applied to reduce the dimensionality of the data. For classification, a multi-class SVM and the nearest neighbor classifier are used. Svoboda [63] proposed a Convolutional Neural Network (CNN) based on the AlexNet model and trained by optimizing a loss function related to the d-prime index to achieve a better genuine/impostor score distribution separation of

touchless palmprint databases.

Meraoumia *et al.* [64] proposed Principal Component Analysis Network (PCANet) deep learning-based feature extraction using two stages. Then, the supervised procedure uses four classifiers (SVM, Radial Basis Function (RBF), Random Forest Transform (RFT), and KNN). The testing was performed on multispectral palmprint databases. Cheng *et al.* [65] proposed Deep Convolutional Features-Based Supervised Hashing (DCFSH). They used the CNN-F architecture to extract the palmprint convolutional features, followed by learning binary coding from distilled deep features. The DCFSH is evaluated on a multispectral palmprint database. The Hamming distance is employed in the matching steps. Zhong et al. [66] proposed a new method to achieve end-to-end palmprint recognition using a Siamese network. In their network, two parameter-sharing Visual Geometry Group-16 (VGG-16) networks were used to extract the convolutional features of two input palmprint images, and the top network directly obtained the similarity of two input palmprints based on their convolutional features. Bensid et al. [67] proposed a simple new deep learning feature extraction algorithm for an efficient multispectral palmprint identification system called the Discrete Cosine Transform Network (DCTNet).

Genovese *et al.* [68] proposed PalmNet, a Convolutional Network that uses Gabor responses and PCA filters through an unsupervised procedure applied to different touchless palmprint databases and uses the 1-NN classifier based on the Euclidean distance for classification step. Besides, Zhao *et al.* [69] proposed a joint constrained least-square regression (JCLSR) model with deep convolutional neural networks to solve the undersampling classification problem by extracting different deep local convolution features using different patches of the same palmprint image. The experiments of the proposed method (JCLSR) were performed on touchless and multispectral palmprint databases. Table 2.1 includes a summary of deep learning methods for palmprint recognition.
Fei et al. [70] proposed LRRIPLD, a new Low-Rank Representation (LRR) model Integrated with Principal Line Distance for contactless palmprint recognition. LRRIPLD generates a graph that is more distinct than LRR because the main line distances effec-

tively improve clustering results by increasing the weights of the links between similar samples. The approach has been tested on three palmprint databases: IITD-Touchless, GPDS-Touchless, and CASIA.

Table 2.1 – A summary of published Deep Learning approaches for Palmprint Recognition.

Notes:
-N. ind = Number of individuals;
-N. samp = Number of samples;
-M= Multispectral database;
-T= Touchless database.

Authors	Year	Methods	DATABASES			Performance		Train
			Name	N. ind	N. samp	EER (%)	ROR (%)	/ Test (%)
Wang et al. [61]	2012	2-D-Gabor wavelet and pulse-coupled neural network	PolyU	193	7752	-	97.37	50/50
Minaee and Wang [62]	2016	Deep scattering convolutional network	PolyU	500	6000	-	100	50/50
Svoboda et al. [63]	2016	AlexNet, Discriminative Index Learning	IITD	460	2300	1.640	-	50/50
			CASIA	312	2751	1.860	-	
Fei et al. [70]	2016	LRRIPLD	$IITD_T$	230	2600	-	91.78	-
			$GPDS_T$	100	1000	-	91.30	
			$CASIA_T$	312	5500	-	95.05	
Meraoumia et al. [64]	2017	PCANet with two stages	PolyU	500	6000	0.000	100	33.33/
			$CASIA_M$	100	1200	0.125	99.50	66.67
			CASIA	100	1200	0.006	99.83	50/50
Cheng et al. [65]	2017	DCFSH	PolyU	193	7752	0.000	-	-
Zhong et al. [66]	2018	Siamese Network	PolyU	500	6000	0.281	-	-
			XJTV	114	2078	4.559	-	
Bensid et al. [67]	2018	DCTNet with Two-stages	PolyU	500	6000	0.000	100	25/75
			$CASIA_M$	100	1200	0.111	99.33	
			PolyU	500	6000	0.000	100	50/50
			CASIA	100	1200	0.003	99.83	
Genovese et al. [68]	2019	PalmNet-GaborPCA	$CASIA_T$	624	5455	0.720	99.77	50/50
			$IITD_T$	467	2669	0.520	99.37	
			$REST_T$	358	1937	4.500	97.16	
			$Tongji_T$	600	5182	0.160	99.83	
Zhao et al. [69]	2020	JCLSR	CASIA	312	2750	-	99.84	70/30
			PolyU	500	6000	-	100	
			$IITD_T$	230	2601	-	98.17	
Arora et al. [71]	2021	PalmHashNet	CASIA	312	2496	0.031	99.98	-
			$ITTD_T$	460	1841	0.390	99.62	
			$Tongji_T$	193	6000	0.530	97.85	
			PolyU II	300	3860	0.011	99.83	

2.3 Finger Knuckle Print Recognition

The external surface of the finger has distinguishing characteristics, especially in the vicinity of the joints, such as major lines, minor lines, and ridges, which can be extracted from low-resolution images. Recently, a new biometric technology centered on the outer of the finger, known as finger knuckle print [72], has been harnessed (see Figure 2.4). Because the hand has multiple fingers, numerous studies have shown that the finger knuckle print can be employed in the area of individual identification for robust and accurate recognition [73] [74].

Figure 2.4 – Finger Knuckle Print.

The schematic diagram of the personal identification system based on the FKP image is shown in Figure 2.5. The system consists of two major modules. One is an information acquisition module, while the other is a data processing module. The data acquisition module comprises a finger holder, an LED light source ring, a lens, a CCD camera, and an acquisition board. The LED light source and CCD camera are enclosed in a box to provide almost constant illumination. In addition, a basal block and a triangular block are utilized to fix the position of the finger knuckle. The data processing module has three main stages: region of interest (ROI), feature extraction, and matching. During the data acquisition step, the user puts the finger on the basal mass in a particular pattern by trying to touch the two slopes of the triangular block (see Figure 2.6). This design aims to decrease finger position alteration across various capture sessions.

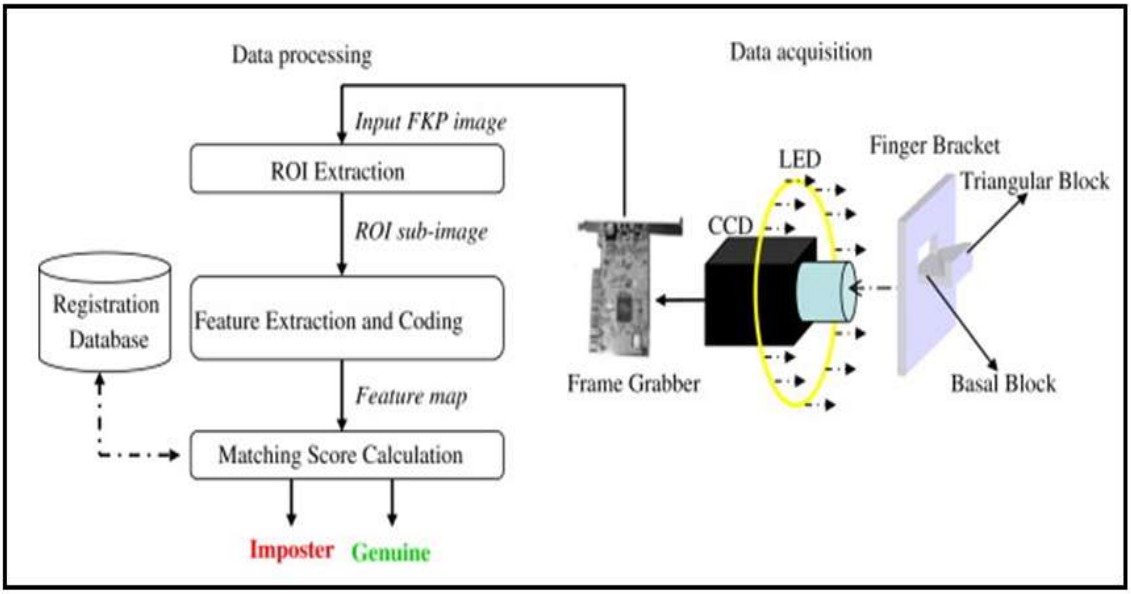

Figure 2.5 – Structure of the proposed FKP based personal identification system

Figure 2.6 – The device used to collect finger knuckle print images.

An FKP-based biometric system aims to determine the characteristics of an individual's finger knuckle print to distinguish among individuals in the recognition tasks. Generally, the methods used for an FKP-based biometric identification system are similar to those used for palmprint-based biometric identification systems. However, the major benefit of the FKP method is that the hand has many fingers (Figure 2.7), allowing for a high recognition rate if some of these fingers are fused. On the other hand, because it has a greater surface area, it is rich in biometric data, allowing the biometric method's

identification rate to be increased.

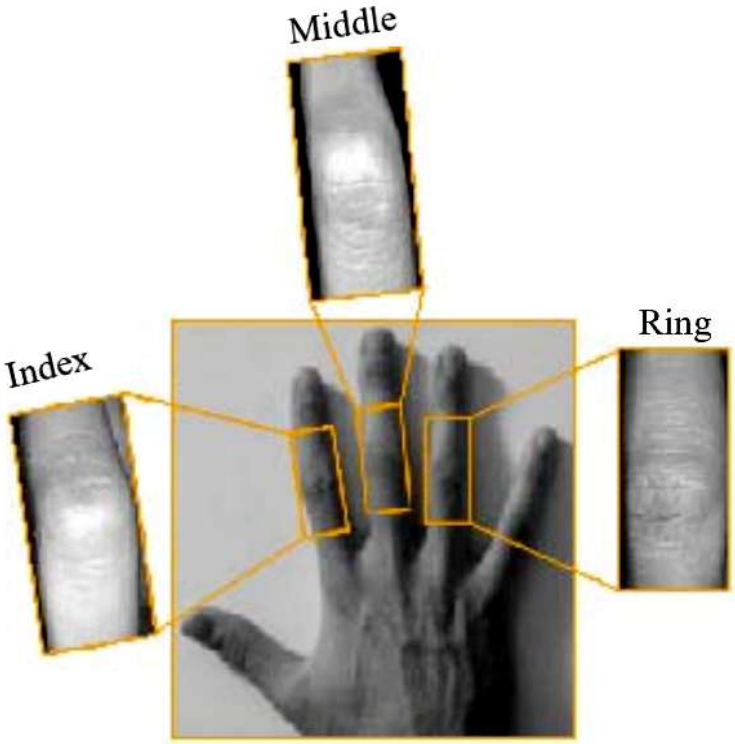

Figure 2.7 – Finger knuckle print: middle, index, and ring finger.

Zhang et al. [75] used the Gabor wavelet for feature extraction. They contribute to developing a biometric system based on the fusion of local and global data relevant to the FKP method. Gabor filters are used to acquire the biometric traits that characterize the local orientation scale. However, as the scale of the Gabor filters rises, the transformation with these filters converges to the overall image's Discrete Fourier Transform (DFT). As a result, the DFT of the entire image offers a set of coefficients to demonstrate the FKP modality's relevant data. The experimental results on a database of 165 people show that this scheme can operate with an error of 0.402%. The same authors [76] integrated the orientation and amplitude of the information extracted by the Gabor filtering. They validated that combining all fingers allows for zero error rates.

Hedge et al. [77] identify the peak points in the Gabor Wavelet graph. Then, the distances between these points are measured and saved in a feature vector. The experimental results acquired using the same database proved its minority compared to Zhang et al.'s algorithms [75]. Badrinath et al. [78] introduced a novel integration of local data for

an FKP identification system that is robust to scale and rotation. The FKP's varying brightness is adjusted, and the texture is upgraded, owing to the comparatively curved surface. The local features are extracted by employing the scale-invariant feature transform (SIFT) and accelerated robust features (SURF) of the enhanced FKP. Aoyama et al. [79] developed an algorithm for individual identification-related FKP recognition system depending on Band Limited Phase Only Correlation (BLPOC). The scheme is designed to generate phase information using the 2D Discrete Fourier Transform (DFT), which is then accompanied by phase-based correspondence matching. Lastly, the BLPOC-based local block matching is employed to estimate the matching score by applying the global and local demonstrations of FKP images.

Jaswal et al. [80] introduced a recognition system relying on the dorsal surface of the finger. First, the images acquired are processed using a median filter. Then, the Scale Invariant Feature Transform (SIFT) and PCA-related LDA approaches are merged to extract features. Later, the feature vectors are classified and identified by the nearest neighbor classifier (KNN) depending on three estimation methods: Euclidean Distance, Spearman Correlation Coefficient, and City Block Distance. Nigam et al. [81] proposed an FKP recognition scheme using the concatenation of multiple texture features. However, the FKP image is processed before employing the curvature Gabor filter to extract the Region of Interest (ROI). Next, the Gradient-related Ordinal Connections are applied to acquire robust image representation to improve ROI. Finally, the Distinction Incorrectly Tracked Corners (ITC) amount is applied in the matching stage. Waghode et al. [82] introduced a subspace-based method for an FKP recognition system. The Gabor filter was originally employed to eliminate the noise. Also, PCA is applied to extract features. Lastly, LDA and Probabilistic Neural Network (P-NN) classifiers were utilized for the matching stage. Zhai et al. [83] presented an FKP recognition scheme that employs a Batch Normalized Convolutional Neural Network (CNN) architecture accompanied by histogram equalization for data augmentation. Chaa et al. [84] proposed a novel technique for combining two histograms of oriented gradients (HOG) derived from reflection and illumination. The Adaptive Single Scale Retinex (ASSR) procedure obtains a large

feature vector from FKP images. Dimensionality was reduced using the PCA + LDA method. Lastly, cosine distance is employed for classification. Attia et al. [85] provided an FKP identification system based on the feature-level fusion of imaginary and real images extracted using the 1D Log Gabor filter. The feature vectors of the images are extracted together using Three Patch Local Binary Patterns (TPLBP). All the feature vectors extracted are concatenated to form a single feature vector. Afterward, LDA is utilized to reduce dimensionality. Eventually, the nearest neighbor classifier is matched by using cosine Mahalanobis.

Kim et al. [86] introduced a novel method for extracting line features from FKP images. First, the horizontal and vertical knuckle lines are extracted using a shift-and-difference matrix, activated with the sigmoid function for contract improvements. Following that, line features are extracted using a Fourier spectrum analysis. Finally, the two-directional line features are combined at the score level using Total Error Rate Minimization that Adopts the Extreme Learning Machine Kernel (TERELM). Muthukumar et al. [87] developed an FKP biometric scheme that uses the Short and Long Gabor features. The Hamming Distance (HD) and Support Vector Machines (SVM) are implemented in the matching phase. Finally, the scores of both techniques are combined and then utilized to identify the individual.

Chlaoua et al. [88] introduced a multimodal biometric system based on FKP images. The Principal Component Analysis Network (PCANet) method was employed. The PCANet processes an FKP image in two stages involving filter banks and a simple binary hashing and block histogram for clustering feature vectors. Finally, a linear multiclass Support Vector Machine (SVM) is used for the classification step. Attia et al. [89] introduced an FKP recognition system that uses a Multi-Scale Bank of Binarized Statistical Image Features (BBSIF). This scheme extracts features to encode FKP images using top-performing complex filters. Following that, the encoded FKP images were used to extract histograms, which were then connected in series to produce a large feature vector later utilized for dimensionality decrease. Concerning recognition, the PCA+LDA

method was utilized, along with the nearest neighbor classifier.

2.4 Biometric System Evaluation

Evaluating the performance of a biometric system is an essential task in conceiving the biometric verification and identification system. This section discusses techniques for testing a biometric system and reviews different performance statistics and charts related to visualizing. There are two types of biometric applications, namely verification and identification. It is helpful to distinguish between them here as they will impact the choice of performance evaluation.

2.4.1 Error Rate Metrics

In general, there are several metrics used in the context of biometric system conception and evaluation. Some are used in the verification system and others in identification. The identification system can operate in two modes: open-set and closed-set identification. In the first mode, the person to be identified is not guaranteed to exist in the database but is assumed to exist in the second mode. First, however, The principal criteria used to evaluate the performance of a biometric system are:

— False Rejection Rate, or FRR: It reflects the percentage of persons required to be accepted, but the system rejects them. The following equation describes it:

$$FRR(\%) = \frac{Number\ of\ rejected\ genuine\ (FR)}{Total\ number\ of\ genuine\ access} \tag{2.1}$$

— False Acceptance Rate, or FAR: This rate reflects the percentage of persons expected to be not recognized, but the system accepts them. The following equation describes it:

$$FAR(\%) = \frac{Number\ of\ accepted\ imposter\ (FA)}{Total\ number\ of\ imposter\ access} \tag{2.2}$$

— Equal Error Rate, or EER: This rate is defined as the percentage where the false acceptance and rejection rates are equal (FAR = FRR). That is the best trade-off between false rejections and false acceptances.

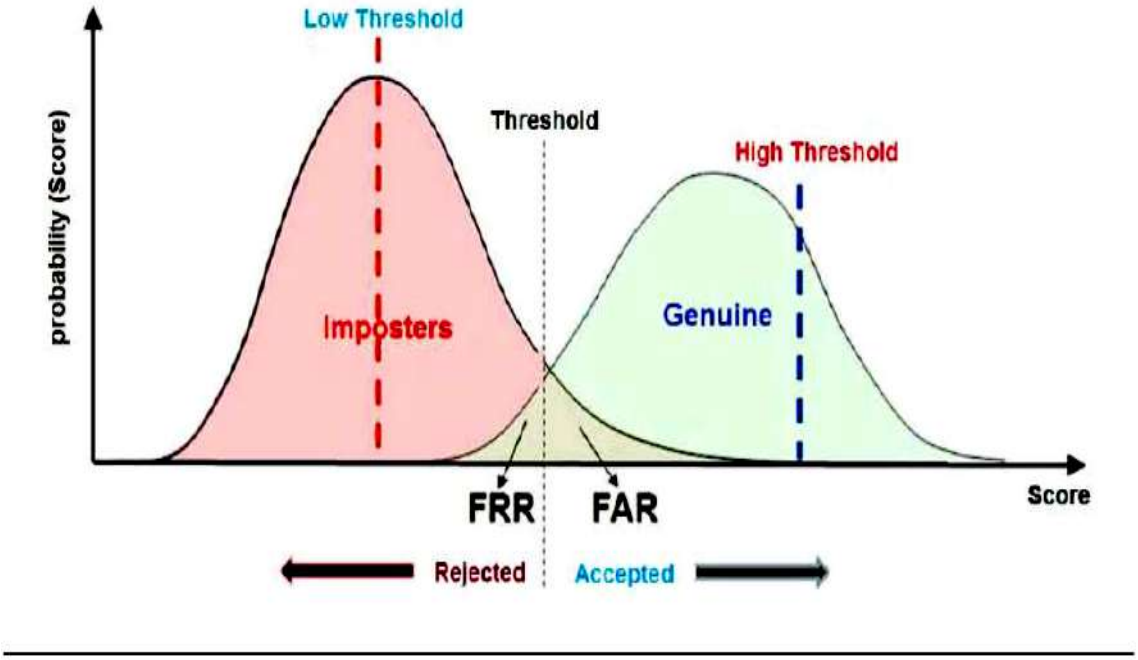

Figure 2.8 – Distributions of genuine users scores and impostor scores.

We can use another performance measurement, the Genuine Acceptance Rate (GAR). It represents the system identification rate. This rate is defined as the percentage of genuine users accepted by the system, which is expressed as follows:

$$GAR(\%) = 100 - FRR(\%) \tag{2.3}$$

So, we can display the Receiver Operating Characteristics (ROC) curves, which are the GAR against the FAR or the FRR against the FAR [90].

In closed-set identification, we use the Cumulative Matching Characteristic (CMC) curve to measure the accuracy performance of a biometric system. It shows the ranking of individual templates based on the match rate. This curve is associated with two criteria. The rank of Perfect Rate (RPR), defined as the rank at which the identification rate attempts 100%, and Rank-One Recognition (ROR), defined as the percentage of persons recognized by the system as a function of a variable "rank."

2.4.2 Curves of Performance

The performance of a biometric system for various criteria (decision threshold) is graphically represented using specific curves. The logarithmic scale is frequently applied to represent them as more precise and readable, principally in comparing biometric systems with similar performance. The most used performance curves are:

2.4.3 Receiver Operating Characteristic curve (ROC)

The Receiver Operating Characteristic (ROC) curve is a typical technique for describing the technical presentation of a biometric scheme in a precise application (generally in verification and open-set tasks). The ROC curve is a diagram that depicts the connection between FAR and FRR (GAR against FAR). Figure 2.9 shows a demonstration of the ROC curve.

2.4.4 Cumulative match characteristic curve (CMC)

A CMC curve is a graphical representation employed to evaluate the performance of a biometric identification system in closed-set mode. A CMC curve plots the identification rate against the rank. An example of this curve is shown in Figure 2.10.

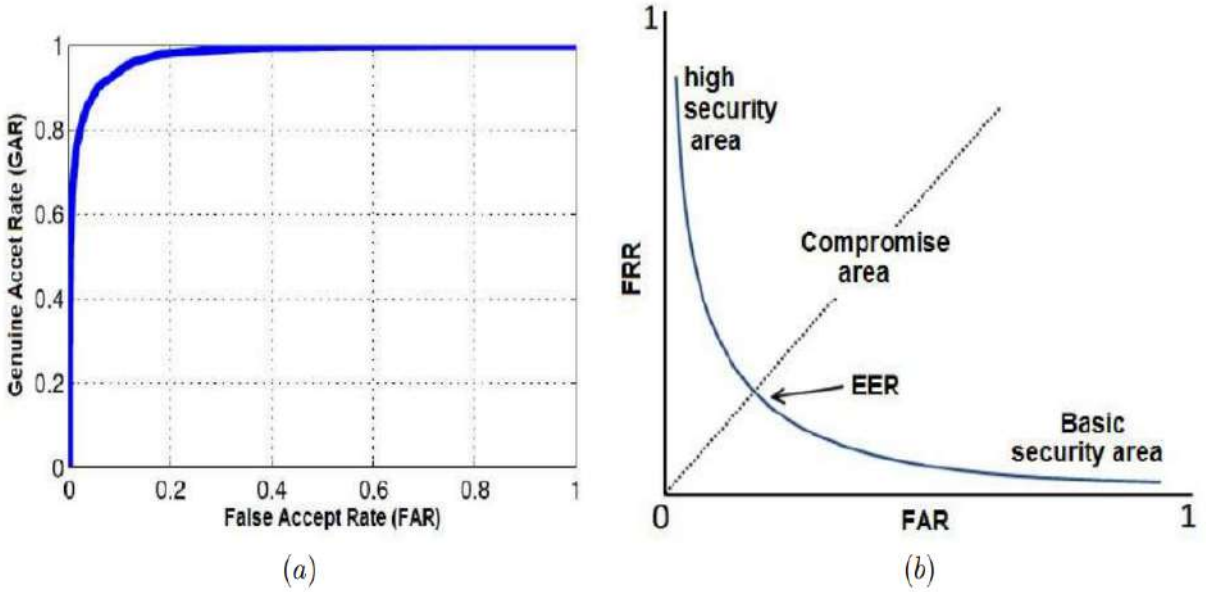

Figure 2.9 – Receiver Operating Characteristic (ROC): (a) GAR against FAR when the decision threshold varies, (b) FRR Variation according to the FAR when the decision threshold varies

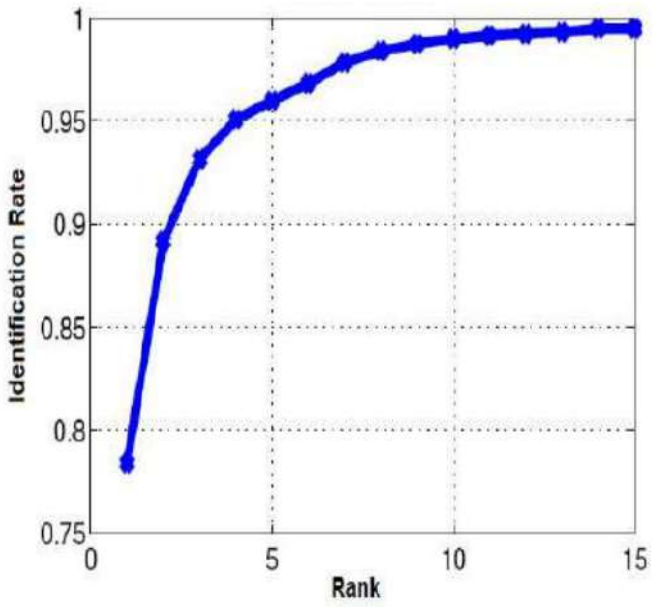

Figure 2.10 – Cumulative match characteristic curve (CMC).

2.5 Conclusion

Biometric systems that use different biometric modalities of the hand are superior to systems using a single biometric modality. This superiority is due to their efficiency, and users accept them easily because of their ergonomics. Furthermore, the installation of these systems is easy and less expensive. Several biometric modalities can be extracted

from the hand.

In this chapter, we have reviewed the main biometric modalities related to the hand. Then, we have detailed the two most commonly used biometric modalities currently, namely the palmprint and the finger knuckle print. Therefore, the state-of-the-art on the various works realized in the literature was given in this chapter.

Part II

Contributions

Chapter 3

Efficient palmprint biometric identification systems using deep learning and feature selection methods

3.1 Introduction

The fast growth of modern human civilization has led to an increasing demand for new and efficient technologies to sustain it. Alongside, security and privacy concerns have emerged, and the usage of highly reliable and accessible individual authentication and identification techniques became crucial. Biometrics has emerged to address this need and has become a science that studies physiological and behavioral characteristics of the human body to recognize an individual's identity. Biometric technologies focus on techniques that automatically authenticate both stable human traits, such as DNA, fingerprint [91], faces [92], iris [93], palmprint, and human behavioral traits such as gait [94], voice [95], keystroke [96], and signature [97]. Among these, palmprint recognition has shown itself to be one of the essential biometric technologies, attracting significant

attention.

The palmprint images contain rich features such as principal lines, wrinkles, and minutiae. They are relatively stable, and their captured images are easy to obtain [98] [99]. They can be categorized according to the way of their acquisition. Therefore, they can be divided into two categories of palmprint images, contact-based and contactless. The main difference between them is whether the hand is in touch with the acquisition device or not [100]. The first type of image is gathered by placing the palms on the device and using user-pegs, while the second type is obtained without contacting the device's surface [18]. A biometric system can be divided into two categories, unimodal and multimodal biometric systems. The unimodal biometric system is designed to recognize individuals based on a single biometric trait's information. That system suffers from some limitations and cannot provide satisfactory recognition accuracy. The multimodal biometric system integrates information from multiple biometric traits. It is more secure than a unimodal system and can solve a variety of problems, including noisy sensor data, non-universality, distinctiveness, and the lack of biometric traits. The combination of modalities provides efficient means for improving the performance and reliability of the biometric system [101].

The main component of a biometric system is feature extraction. It extracts only the discriminant information from the acquired image to create a new representation that should be essentially unique to each person [102]. Deep learning techniques, which provide a better representation of the image, have become popular methods for this purpose. The main benefit of deep learning methods is their ability to generate efficient and discriminative features from the biometric image. Recently, many feature extraction methods based on deep learning techniques have been proposed in the literature [64] [62].
Since feature extraction is an essential part of the recognition task, predicting performance and reducing the computation required can be achieved by using Feature Selection (FS). This latter is an essential component of machine learning and data mining, which has been studied for many years under different conditions and in diverse scenarios [103]. These algorithms aim to rank and select a subset of related features based on their de-

grees of preference, relevance, or importance, as defined in a particular application. Since feature selection may reduce the number of features needed to train classification models, it mitigates the effect of dimensionality's curse, speeds up the learning process, improves model performance, and promotes data understanding. In this chapter, inspired by the work of PalmNet [68], we will propose efficient biometric identification systems based on palmprint traits. To accomplish this, we suggest applying Log-Gabor filters in the preprocessing step to adjust the pixel luminance of palmprint images. After, we process to extract the discriminant information by using an adaptive Gabor-based filter tuning procedure [68]. To improve the recognition rate as well as reduce the size of large feature vectors and the computational time, we use feature selection and dimensionality reduction procedures. Additionally, we employ a Support Vector Machines (SVM) classifier instead of the K-Nearest Neighbor (KNN) classifier based on the Euclidean distance, with K=1 (denoted by 1-NN in the following). For the multimodal system, we fuse modalities at the matching score level to improve system performance. To validate our method, we applied it to several public palmprint databases containing images of distinct qualities, resolutions, and dynamic ranges. We also carried out comparisons with several recent state-of-the-art methods.

The main contributions of this work are as follows:

- The development of effective unimodal and multimodal biometric systems for palmprint recognition.
- Improvement of palmprint images using log-Gabor filters by adjusting pixel luminance.
- Using feature selection with dimensionality reduction significantly reduced the features vector size with a reduction rate of 0.003 %, which allowed reducing computational time without degrading the performance of our recognition systems.
- Employing the SVM classifier instead of the 1-NN classifier as in the chapter [68]. Experimental results demonstrate that our methodology scored a higher recognition accuracy than existing approaches in the literature.

The rest of the chapter is organized as follows: Section 3.2 introduces the proposed approach of unimodal and multimodal identification systems for palmprint recognition.

The experimental results are given in Section 3.3, which reports the obtained experimental results. Finally, Section 3.4 concludes the chapter.

3.2 Proposed approach

Figure 3.1 shows the block diagram of the proposed unimodal palmprint identification system, composed of five steps: Preprocessing; feature extraction; feature selection and dimensionality reduction; classification and matching; decision. Every unimodal system calculates its own matching score. For the multimodal system, these individual scores are eventually combined or fused at the matching score level into a total score used by the decision module. A final decision is made based on this matching score (the user is identified or not). This structure can improve the proficiency of a unimodal system and be used to solve some of its limitations.

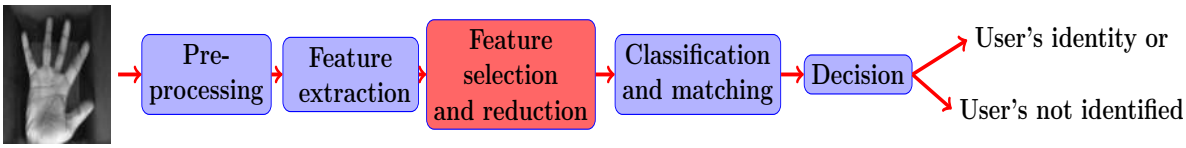

Figure 3.1 – Flowchart of the proposed approach.

3.2.1 Preprocessing

The preprocessing step can be divided into three separate tasks: a) extracting the Region of Interest (ROI) from the palmprint image, b) resize the ROI palmprint images, and c) applying the Log-Gabor filter (see Figure 3.2). First, the surface of the palm image is segmented for extracting the Region Of Interest (ROI). The ROI attempts to get only the area where the hand has useful information. For that, we have to align the palmprints by using the algorithm mentioned in [19]. The central part of the image, which is 128×128, is then cropped to represent the whole palmprint. Second, we resize the ROI to dimensions of 32×32 pixels in order to reduce the computational time. In the last step of the preprocessing module, and to enhance the ROI image of palmprint, a Log-Gabor filter is applied to provide a better enhancement with its good smoothening characteristics based on performance and quality measurements that have been empirically observed (Fig. 3.2. d). The log-Gabor filter is a derivative of the standard Gabor

filter. The log-Gabor frequency response is Gaussian in the logarithmic frequency scale, as opposed to the standard Gabor that has Gaussian frequency response in a linear scale. The log-Gabor frequency response is described by (Eq. 3.1):

$$G(w) = \exp\left(\frac{-\left(\log(w/w_0)\right)^2}{2\left(\log(k/w_0)\right)^2}\right) \tag{3.1}$$

Where w_0 is the centre frequency of the filter and the bandwidth is determined by the $\frac{k}{w_0}$ term. The parameters of Log-Gabor filter were experimentally selected as $w_0 = 1/3$ and $k = 0.65$.

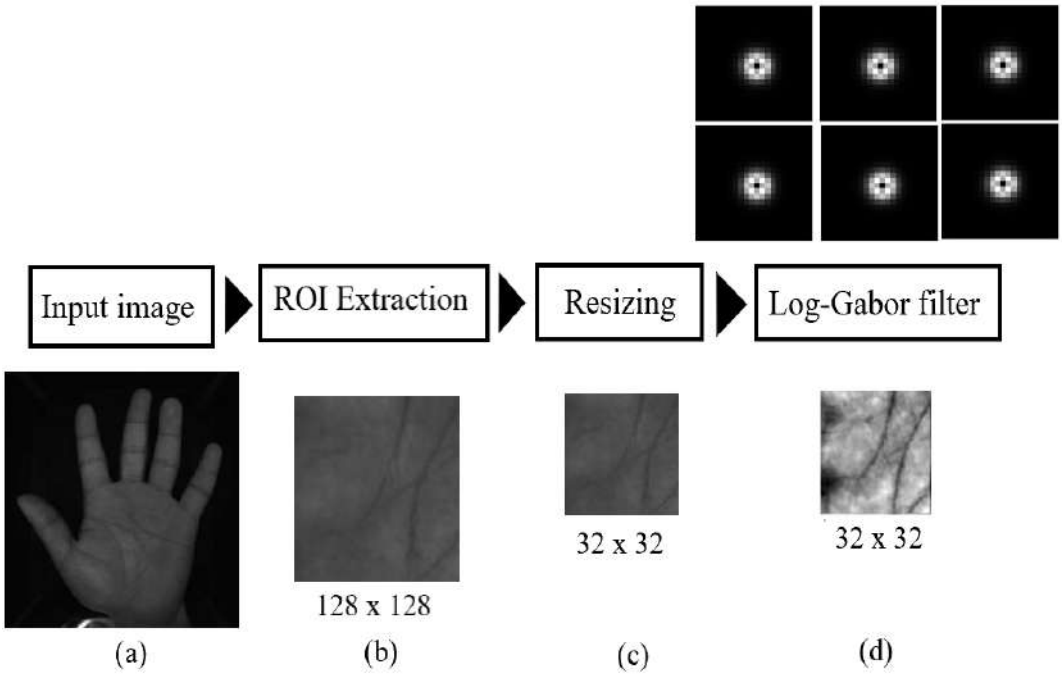

Figure 3.2 – The main tasks of preprocessing step. (a) input image, (b) ROI palmprint extraction, (c) image resizing, and (d) results of Log-Gabor filter.

3.2.2 Features extraction

Feature extraction is a key module for recognition systems. The acquired biometric data are processed, and only the salient information is extracted to form a new representation of the data. Ideally, for each person, this new representation should be unique. In our scheme, to extract highly discriminative palmprint features, PalmNet deep learning is used to extract the features vector of each data type. It is a particular case of an image

classification deep learning baseline, which consists of three stages: 1) convolutional stage, 2) binarization stage, 3) histograms stage. Thus, the block diagram of PalmNet algorithm is presented in Fig. 3.3 and can be summarized as follows [68]:

1. **Convolutional stage**

   As shown in Fig. 3.3, the convolution process is ensured by two layers of the Gabor filter bank:

   — First convolutional layer (L_1), consisting of k_1 filters. Each filter is convolved with the input image (layer L_0 with dimensions of $u \times v$). Thus, the output of this layer consists of k_1 images with dimensions of $u \times v$. So,

   $$I_{l_1}(i,j) = \sum_m \sum_n h_{l_1}(m,n) I_{l_0}(i-m, j-n), \qquad 1 \leq l_1 \leq k_1 \tag{3.2}$$

   Where, I_{l_0} represents the input image of layer L_0 to be convolved with the filter h_{l_1} to produce the output image I_{l_1} of layer L_1. The indices i and j deal with the images while m and n work with the filters.

   — Second convolutional layer (L_2), consisting of k_2 filters. Each filter is convolved with the output of layer L_1. Thus, the output of this layer consists of $k_1 k_2$ images with dimensions of $u \times v$.

   $$I_{l_1 l_2}(i,j) = \sum_m \sum_n h_{l_2}(m,n) I_{l_1}(i-m, j-n), \qquad 1 \leq l_1 \leq k_1 \, and \, 1 \leq l_2 \leq k_1 k_2 \tag{3.3}$$

   Where, I_{l_2} represents an image of the $k_1 k_2$ output filtered images. h_{l_2} is a filter of layer L_2.

   The significance of this part is that we used two types of filters, fixed-scale Gabor filters and adaptive multiscale Gabor filters. In the first type, we created a set of fixed scale $2-D$ Gabor filters with dimensions of $h_1 \times h_2$, as products of a sinusoidal wave with a Gaussian function [68]. In the second type, we first computed a set of adaptive orientations from the training subset of palmprint ROI. Then, we computed a bank of multiscale Gabor filters with the computed orientations. Finally, we selected the filters that get the greatest magnitude responses with dimensions of $g_1 \times g_2$ where $g_1 \times g_2 = 4 \cdot 2^{m_f}$. The value of m_f is computed as $m_f = [0, 1, \cdots, \cdots M]$, where M equal to $M = [log_2(u/2)]$ and u is the horizontal size of the ROI images [68]. So, the number of filters chosen for each layer of the

network, i.e., k_1 and k_2, consists of $F + A'$ filters, corresponding to F fixed-scale $2-D$ Gabor filters and A' adaptive multiscale $2-D$ Gabor filters.

2. **Binarization stage**

   In this stage, the $k_1 k_2$ output images obtained from the output of the second layer are converted to binary format using a Heaviside step function illustrated by the following equation:

$$B_{l_2}(i,j) = \begin{cases} 1 & if\ I_{l_2}(i,j) > 0 \\ 0 & otherwise \end{cases} \tag{3.4}$$

   Where B_{l_2} is a binary image. In total, we obtain k_1 groups of binary images, each containing k_2 binary images B_i, with $i = 1, 2, \cdots, k_2$. These images have the same dimensions of $u \times v$. For each position (i,j), by concatenating the binary values of all $k_2 \times k_1$ binary images, we obtain:

$$b = [B_1(i,j), B_2(i,j), \cdots, B_{k_2}(i,j)] \tag{3.5}$$

   We convert the binary vector b into a decimal number as follows:

$$d = \sum_{k=1}^{k_2} 2^{k-1} b(k) \tag{3.6}$$

   This process is repeated for each position (i,j). Finally, we obtain a decimal matrix $D(i,j)$ that describes the whole k_2 binary output image group.

   Likewise, the decimal matrices D_l are determined for all k_1 binary images groups, with $l = 1, 2, \cdots, k_1$.

3. **Histograms stage**

   In this stage, each D_l matrix is partitioned into n_B non-overlapping (disjoint) blocks with dimensions of $b_l \times b_2$, and their histograms are computed. Each histogram consists of 2^{k_2} bins. Thus, a features vector H is obtained by concatenating the histograms for all blocks of all images D_l, where:

$$|H| = k_1 n_B 2^{k_2} \tag{3.7}$$

In conclusion, to achieve the best recognition accuracy, the hyperparameters of the PalmNet include the number of filters in each layer k_1 and k_2, and the values of b_1 and b_2 are experimentally tuned.

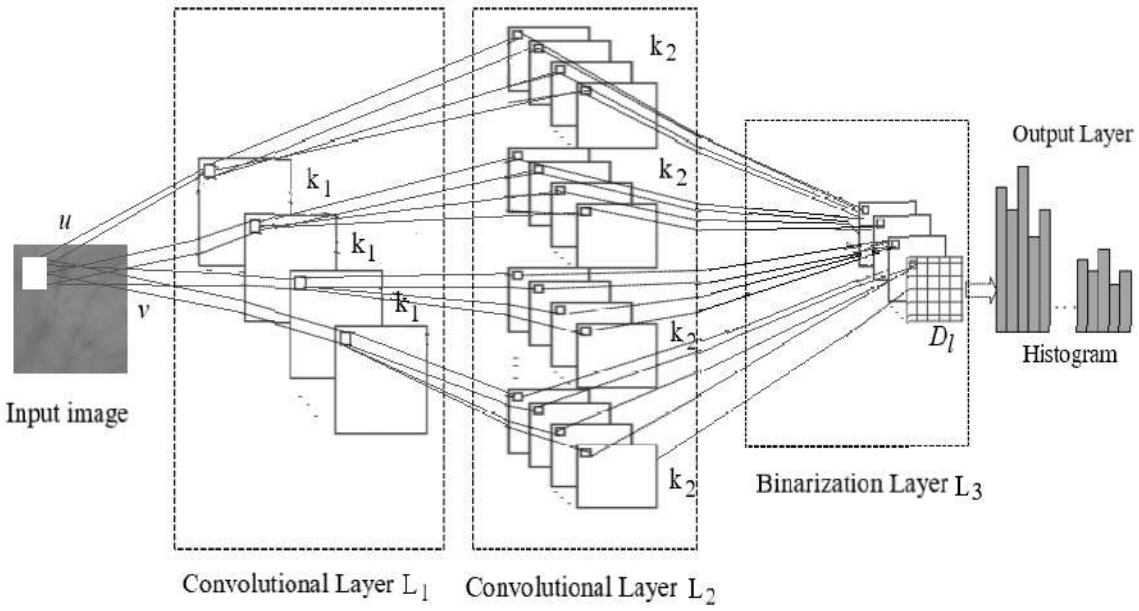

Figure 3.3 – Topology of the proposed network.

3.2.3 Feature selection and dimensionality reduction

Feature selection (Fs) is a significant component of machine learning, computer vision, artificial intelligence, and data analysis. The aim of feature selection is to select useful features and remove redundant information. In this section, we use the feature selection and dimensionality reduction methods as follows: *i*) Fisher score algorithm (as feature selection method), *ii*) ReliefF algorithm (as feature selection method) and *iii*) Whitening Principal Component Analysis (WPCA) algorithm (as dimensionality reduction method). Feature selection algorithms can be divided into three groups [104]:

— Wrappers method that uses classifiers to score a particular subset of features;

— embedded methods that insert the selection process into the classifier's learning process;

— filter methods that analyse intrinsic properties of data, ignoring the classifier [105].

We aim to use feature selection algorithms to rank and select a subset of pertinent features based on their degree of importance, preference, or significance as specified in an application, since the number of features used for training classification models can be decreased by the selection of features. Furthermore, dimensionality reduction reduces the impact of the dimensional curse, reduces time and over-fitting, improves training model, and data comprehension.

While feature selection can be used in both supervised and unsupervised learning, we will focus our study on supervised learning (classification) methods in which the class labels are known ahead of time. The interesting topic of feature selection for unsupervised learning (clustering) is a more complicated issue, and research in this field is recently getting more attention in several communities. In recent years, a variety of feature selection methods have been exploited for clustering paradigms, for example [106] [107] [108] [109] [110].

1. **Fisher score algorithm**

   Fisher score is one of the most common supervised feature selection methods. We used a linear discriminant approach based on Fisher's score, which evaluates the discriminating power of features. The score is given by:

$$W_i = \frac{\sum_{j=1}^{c} N_j.(m_j - \bar{m})^2}{\sum_{j=1}^{c} N_j \sigma_j^2} \tag{3.8}$$

   Where W_i is the score of features i, c is the number of classes, N_j is the number of samples in class j, $\bar{m}$ is the feature mean. m_j and σ_j^2 are the mean and the variance of the class j in the intended feature.

2. **ReliefF algorithm**

   Kira and Rendell [111] formulated the original Relief algorithm inspired by instance-based learning, which is optimized for two-class problems without losing values. The basic idea of the algorithm, when analysing learning instances, is to take into account not just the difference in features values and the variation in classes but also the distance between the instances. In the features space, distance is calculated so that similar instances are close to each other and far apart, and dissimilar

ones are far away. By taking into account the similarity of instances, the context of all the features is implicitly considered [104]. For each instance, from a random subset of m ($m \leqslant M$), learning instances compute the closest instance of the same class (near hit x_H) and the closest instance of the opposite class (near miss x_M). Then it updates the quality of each feature (see Eq. 3.8).

$$W[i] = W[i] - diff(i, x_k, x_H)/m + diff(i, x_k, x_M)/m \tag{3.9}$$

Kononenko *et al.* [112] propose a number of updates to Relief. First, they found the near hit (x_H) and near miss (x_M) instances using the Manhattan ($L1$) norm rather than the Euclidean ($L2$) norm, although the rationale is not specified. Second, they found taking the absolute differences between x_k and near hit (x_H), and x_k and near miss (x_M) to be sufficient when updating the weight vector (rather than the square of those differences), which can deal with multiclass problems.

3. **Whitening Principal Component Analysis (WPCA) algorithm**

   Principal Component Analysis (PCA) is the most popular dimensionality reduction technique widely used in machine learning to reduce the features' redundancy for efficient palmprint recognition. However, PCA has two weaknesses: The performance of PCA is degraded when using its leading eigenvalues and the weak discriminating in its eigenvectors. WPCA is PCA with an extra step: whitening the eigenvectors by eigenvalues. The whitening step is simple but very effective; it helps to rectify the deficiencies of PCA, where (i) the features are less correlated with each other, and (ii) the features all have the same variance. Therefore, making the palmprint recognition system achieve better performance.

3.2.4 Classification and Feature Matching procedures

A person's identity can be ascertained through the classification and feature matching process. The feature vectors of the training set issued by the feature extraction module are used for classification. In our work, we used two classifiers, a 1-NN classifier based on

the Euclidean distance and a multi-class SVM classifier with Gaussian kernel. The first classifier arranges a sample based on the category of its nearest neighbour. It basically consists of finding the similarity between the test model and each model of the training set. The second classifier uses a set of training data that enables a hyperplane to separate the best points [113].

A matching process is intended to compare the test features vectors against the stored templates (training set) to generate match scores. The match score is a measure of the similarity or dissimilarity between the template and the test. Therefore, a higher match score indicates a greater similarity between the template and the query. If a matcher measures the dissimilarity between the two feature sets, the score is denoted as a distance score. A lower distance score points to higher similarity.

3.2.5 Normalization and Fusion Procedures

In multimodal systems, the normalization method widely used allows each measured score to be converted into a common interval. $Min-Max$ is the type of normalization mostly used in biometric recognition systems. This technique is most appropriate where the limits (minimum and maximum values) of the scores produced by the systems are known [114]. So, we can conveniently convert the minimum and maximum values of the scores vector into 0 and 1, respectively. The following formula gives the score normalized by the $Min-Max$ method.

$$\widehat{V_d} = \frac{V_d - min(V_d)}{max(V_d) - min(V_d)} \tag{3.10}$$

Where the vector V_d includes all the scores calculated between the test and all the stored feature vectors, while the vector $\widehat{V_d}$ comprises the normalized scores.

Score level fusion is the most commonly used biometric information fusion strategy since matching scores are readily available, and they retain enough information to distinguish genuine matching from impostor matching. There are several matching score fusion rules that integrate normalized matching scores of a user to produce the final matching score. In our work, we conducted the experiment with four fusion rules: sum-score

rule (SUM), product score rule (MUL), SUM-weighted-score (SUM MUL) and product-weighted-score (WHT MUL) [114].

— Simple Sum rule: This rule takes the sum of the N unimodal systems matching scores of the k^{th} user as the final matching score S_k of this user. S_k is calculated as follows:

$$S_k = \sum_{i=1}^{N} S_{k_i} \tag{3.11}$$

— The product rule: This rule presents the multiplication result of the N unimodal systems matching scores of the k^{th} user as the final matching score of this user, which is expressed as follows:

$$S_k = \prod_{i=1,2,...,N} S_{k_i} \tag{3.12}$$

— The weighted Sum rule: This rule can define the final matching score of the k^{th} user, which is calculated as follows:

$$S_k = \sum_{i=1}^{N} w_i S_{k_i} \tag{3.13}$$

— The weighted Product rule: This rule can determine the final matching score of the k^{th} user, which is shown as follows:

$$S_k = \prod_{i=1,2,...,N} S_{k_i}^{w_i} \tag{3.14}$$

Where w_i represents the weight of the matching score of the i^{th} biometric trait of the k^{th} user, which is calculated as follows:

$$w_i = \frac{\frac{1}{EER_i}}{\sum_{j=1}^{N}(\frac{1}{EER_j})} \tag{3.15}$$

3.2.6 Simplified PalmNet Gabor algorithm

The proposed approach uses an innovative procedure based on deep learning and feature selection for palmprint recognition. First, we apply Log-Gabor filters in the pre-

processing step to adjust the pixel luminance of palmprint images. Then, in order to extract discriminative palmprint features, we use the PalmNet Gabor network [68] in feature extraction. Additionally, we employ a Support Vector Machines (SVM) classifier and K-Nearest Neighbour (KNN) classifiers. The key idea of our approach is to use feature selection and dimensionality reduction procedures to improve PalmNet Gabor performance and reduce feature vector size. Therefore, we use the Fisher score and ReliefF feature selection algorithms and dimensionality reduction WPCA algorithm. For the multimodal system, we combined modalities at the matching score level to improve system performance. To validate our method, we applied it to several public palmprint databases.

3.3 Experiments and Results

This section presents the experimental evaluation, by conducting experiments on four popular and publicly available databases which are CASIA multispectral palmprint, PolyU multispectral palmprint, Tongji contactless palmprint, and PolyU 2D/3D contactless palmprint. First, we give a brief description of the adopted palmprint databases (section 3.3.1). Second, we present the setup of our approach in the experimental setup (section 3.3.2). Finally, in the experimental results (section 3.3.3), we discuss and analyse the results.

3.3.1 Databases

The proposed method is tested using four publicly available palmprint databases; the CASIA and PolyU multispectral databases and Tongji and PolyU 2D/3D contactless databases. The aim of employing contact-based and contactless databases is to verify the robustness and high efficiency of our method. A description of these databases is given below.

1. **CASIA Multispectral Palmprint Database V1.0**

   The CASIA Multispectral Palmprint Image Database comprises 7,200 palm images obtained from 100 different individuals using self-designed multiple spectral imaging devices described in [115]. In this database, the images of each hand are collected in two separate sessions. The time interval between two sessions is

more than one month. In each session, there are three samples. Each sample includes six palm images, which are captured at the same time with six different electromagnetic spectrums. Wavelengths of the illuminator corresponding to the six spectrums are 460, 630, 700, 850, 940 nm, and white light, respectively (see Fig 3.4). Between two samples, certain degrees of variations of hand postures are allowed. All palm images are low resolution $< 150dpi$ stored as 8-bit gray-level images per band with dimensions of 128×128.

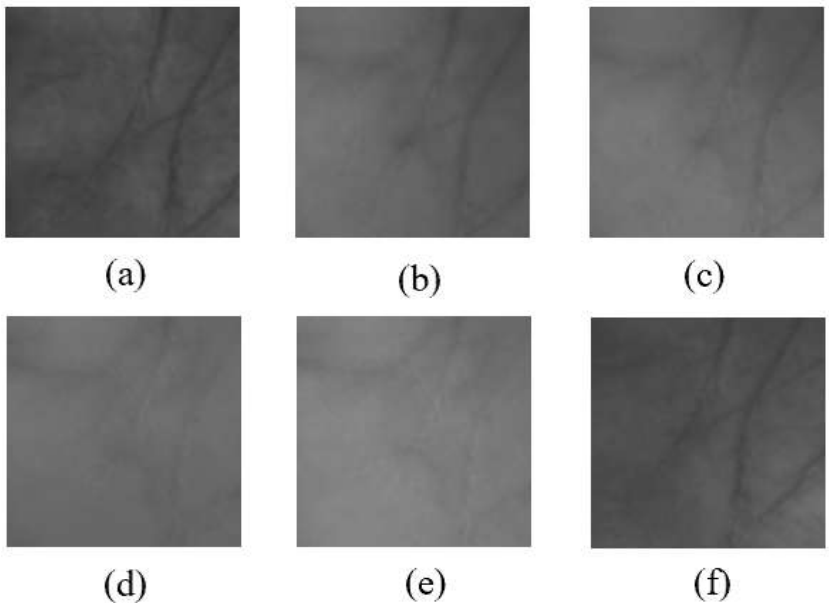

Figure 3.4 – Palmprint ROI samples from the multispectral CASIA database. (a) 460nm, (b) 630nm, (c) 700nm, (d) 850nm, (e) 940nm, and (f) White light.

2. **PolyU Multispectral Palmprint Images Database**

PolyU Multispectral Palmprint Images Database comprises 6000 images obtained from 500 different palms for each band using palmprint images capturing device designed by Hong Kong Polytechnic University researchers described in [30]. The multispectral database contains cropped multispectral palmprint images of four different bands (Red, Green, Blue, and NIR) are shown in Fig 3.5. The images were collected in two separate sessions at a time interval of about two months. In each session, the person provides 6 images per palm, so there are 12 images for each person. Therefore, 48 spectrum images of all illumination from 2 palms were collected from each person. The average time interval between the first and

the second sessions was about nine days. Also, all palm images are low resolution $< 150dpi$ stored as 8-bit gray-level images per band with dimensions of 128×128.

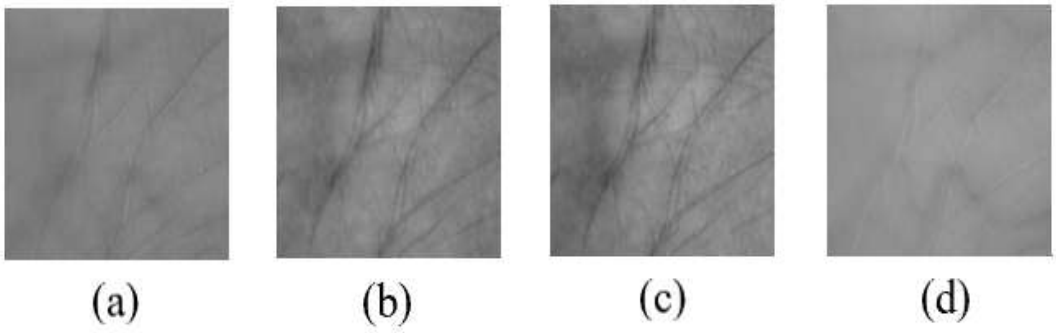

Figure 3.5 – Palmprint ROI samples from the multispectral PolyU database. (a) Red, (b) Green, (c) Blue, and (d) NIR.

3. **Tongji Contactless Palmprint Dataset**

   Tongji Contactless Palmprint Dataset comprises 12,000 images obtained from 600 different palms using the proprietary touchless acquisition device described in [116]. Tongji University collected images from 300 volunteers, including 192 males and 108 females. Among them were 235 people between the ages of 20 and 30 and the others between the ages of 30 and 50. The left and right samples were collected in two separate sessions (see Fig 3.6). In each session, the person provides ten images per palm. Therefore, 40 images from 2 palms were collected from each person. The average period of time between the first and second sessions was approximately 61 days. The minimum and maximum time intervals were 21 days and 106 days, respectively. All palm images are stored as $8-bit$ gray-level images per band with dimensions of 128×128.

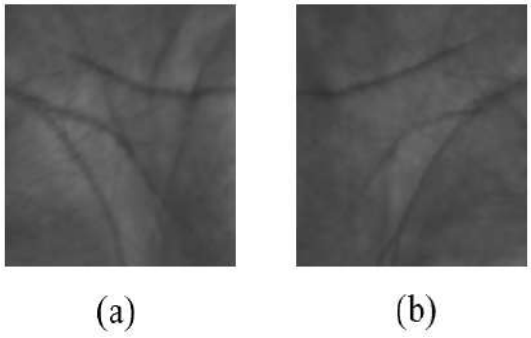

Figure 3.6 – Palmprint ROI samples from the Contactless Tongji database. (a) Left, and (b) Right.

4. **PolyU 2D/3D Contactless Palmprint Dataset**

   The PolyU 2D/3D Contactless Palmprint database contains 8000 images collected from 400 palms of 200 volunteers. The Bio-Research Center (UGC/CRC) of Hong Kong Polytechnic University [117] created the PolyU 2D/3D database. The participants' gender includes 136 males and 64 females with the age range of 18 to 50 years. Each person provided twenty samples for both the left and right palms. The left and right palms from the same person can be considered as belonging to different classes. Thus, there are 400 classes of 2D/3D palmprint image samples. The samples have been collected in two sessions, where ten samples are captured in each session, and the average time between the two sessions is one month. All 2D images in this database are stored as $8-bit$ gray-level images with dimensions of 128×128. In this work, we use only the 2D ROI images. The following figure (Fig 3.7) shows the 2D ROI images from this database.

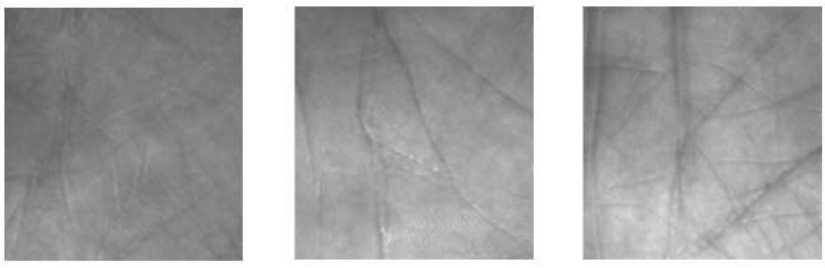

Figure 3.7 – Palmprint 2D ROI samples from the Contactless PolyU 2D/3D database.

3.3.2 Experimental setup

To evaluate the efficiency of our proposed method, the experiments were conducted on two sub-datasets. The first sub-dataset is used for the training phase, while the second is for the testing phase. Each sub-dataset contained 50% of the images in the database.

Moreover, to evaluate the computational time requirements of each algorithm, the performance indicator time refers to the CPU time needed to classify one palmprint image in seconds.

To reach the best possible recognition accuracy on the considered datasets, we experimentally tuned some filter parameters, and we selected the others by considering the optimal values found in the literature [68]. For the Gabor filters, the chosen values of the filter numbers k_1 and k_2 were $k_1 = k_2 = 13$ in two stages. The fixed-scale $2-D$ Gabor filters F is 10 with dimensions $h_1 = h_2 = 31$ and the adaptive multiscale $2-D$ Gabor filters $A^{'}$ is 3.

The feature vector size is computed by using the Eq. 3.7 as follows: $|H| = k_1 n_B 2^{k_2} = 13\ .\ 4\ .\ 2^{13} = 425984$. Where $n_B = 4$ represents the number of non-overlapping blocks with the values of $b_1 = b_2 = 15$ that fit in the input ROI image with size $u = v = 32$. The network parameters are summarized in Table. 3.1.

Table 3.1 – Network Parameters.

Parameter(s)	Description	Value(s)
u, v	Size of the palmprint ROI images	32, 32
k_1	Number of filters in L_1	13
k_2	Number of filters in L_2	13
h_1, h_2	Dimensions of the fixed-scale Gabor filters	31, 31
F	Number of fixed-scale Gabor filters	10
$A^{'}$	Number of adaptive multiscale Gabor filters	3
b_1, b_2	Size of non-overlapping blocks	15, 15

3.3.3 Experimental Results

In our experiments, after extracting the Region of Interest (ROI) from the palmprint images, we resized the images to 32×32 and applied the Log-Gabor filters for adjusting pixel luminance. We used two layers of Gabor filters with an adaptive Gabor-based filter tuning technique for extracting palmprint specific informative features. To increase recognition accuracy and reduce computation time, we used feature selection algorithms Fisher score and ReliefF with the reduction of dimensionality algorithm whitening Principal Component Analysis (WPCA). For classification, we used the Support Vector Machine classifier (SVM) and the Nearest Neighbour classifier (1-NN). Finally, we fuse the spectral bands at the matching score level to improve identification system performance.

All the computation times presented in this chapter are obtained with MATLAB® 2018a in PC with a processor (Intel Core i7-4710MQ) 2.50-GHz and RAM 16 GB.

The experimental results can be divided into three subparts: the first subpart includes the results obtained from the unimodal identification system evaluated on the CASIA and PolyU multispectral databases, and the contactless Tongji and PolyU 2D/3D databases. While in the second subpart, the results of the multimodal identification system are presented. As for the third subpart, we do a comparison study with some works in literature.

1. **Unimodal biometric system performance**

   The unimodal system results were performed on four public multispectral and contactless palmprint databases.

   (a) **CASIA multispectral database results**

   In order to evaluate and test the effectiveness of the proposed method, experiments are done on the CASIA multispectral database with 100 persons and six spectral bands (460, 630, 700, 850, 940 nm, and white light). Since our evaluation adopts random splits for training and testing, we studied the effect of the amount of training on the method's performance. To this end, we run our method using three different random training-testing splits (without Feature selection) (see Table 3.2). From the obtained results, we can observe that the 50% training-testing split gives the best results for all spectral bands. Therefore, the experiments will be conducted using the 50% training-testing splits. Also, to evaluate the performance of the proposed approach, we calculated the performance indicators for several random splits of the training and testing images. Thus, we calculated the standard deviation of the main performance indicators EER and ROR in two cases: without and with FS and dimensionality reduction using the SVM classifier. To this end, we have adopted ten random image splits, each of which contains six images for training and the remaining six images for testing. The number of genuine and impostor comparisons for each spectral band is 600 and 29,700, respectively. Table 3.3 shows the different results of ERR (%) and ROR (%) on the ten random splits for two cases without feature selection (FS) and with FS (Fisher score) and dimensionality reduction (WPCA) of six spectral bands from the CASIA database. This table also shows the mean and standard deviation of ERR (%) and ROR (%). Comparing all the results in the two tables shows that feature selection and dimensionality reduction have improved average performance (i.e., EER and ROR) and reduced standard deviations, implying that performance is relatively stable. Moreover, in the case without feature selection, the best results were obtained with band

630, and in the case with feature selection, with band 460.

Table 3.4 shows the results of the proposed method with two classifiers (1-NN and SVM) and two modes of identification (open-set and closed-set). This table also shows the mean of ERR (%), ROR (%), and time for all spectral bands. By comparing all the obtained findings, it is clear that the spectral band 460 nm gives the best results in terms of EER and ROR values. Firstly, the features' number of the unimodal identification systems is reduced from 12288000 features for the work [68] to 425984 features for our work. In order to reduce features more, applying Fisher score algorithm with ReliefF algorithm or not has allowed reducing the features while maintaining a good identification accuracy. Fig 3.8 and Fig 3.9 show an example of selecting features for a Fisher score algorithm using an SVM classifier based on the performance of EER (%) and GAR (%) against the number of ranked features, respectively. The obtained results show that the insertion of Fisher score with SVM classifier achieves the perfect results with EER equal to 0.000 % in the open set and ROR equal to 100 % in the closed set for spectral band 460 nm with 11500 features. Fig 3.10 illustrates the effectiveness (ROC and CMC curves) of this case for all spectral bands. For the last case, Fisher score algorithm with WPCA algorithm, the system yielded better results compared with previous (without FS), it can achieve an EER of 0.003 % in the open set and a ROR of 99.83 % in the closed set for the 460 nm spectral band while reducing the feature vector size to 410 with CPU time 0.001s instead of 0.478s. Thus, the use of the FS and dimensionality reduction allowed us to reduce the number of features and improve the identification accuracy.

Table 3.2 – Performances comparison of different random training-testing splits.

Spectral bands	**Performance of 25% for training and 75% for testing**		**Performance of 33.33% for training and 66.67% for testing**		**Performance of 50% for training and 50% for testing**	
	ERR (%)	**ROR (%)**	**ERR (%)**	**ROR (%)**	**ERR (%)**	**ROR (%)**
460	6.951	73.55	1.306	92.75	0.333	97.66
630	4.755	85.88	2.000	92.25	0.666	98.00
700	6.057	77.77	2.805	88.62	0.914	95.50
850	8.169	71.44	3.875	86.25	1.650	92.83
940	6.440	78.33	4.345	88.62	1.833	94.66
WHT	9.579	72.33	2.250	86.25	0.500	97.50

Table 3.3 – Mean and standard deviation results using 50% for training and 50% for testing.

Spectral bands	Cases	Random split	1	2	3	4	5	6	7	8	9	10	Mean ± SD
460	Without FS	ERR(%)	0.333	0.833	2.474	2.319	2.440	0.500	0.333	1.883	1.763	0.333	1.321 ± 0.938
		ROR (%)	97.66	96.16	88.66	89.00	91.00	98.16	97.16	90.00	88.83	97.50	93.41 ± 4.208
	FS + dimensionality reduction	ERR(%)	0.003	0.367	1.000	0.833	0.666	0.166	0.166	1.244	0.521	0.166	0.513 ± 0.413
		ROR (%)	99.83	97.83	94.33	96.33	96.66	99.33	98.83	94.83	97.16	99.16	97.42 ± 1.907
630	Without FS	ERR(%)	0.666	0.773	2.666	2.000	1.500	0.500	0.636	1.666	0.996	0.666	1.207 ± 0.722
		ROR (%)	98.00	95.50	88.66	93.00	94.33	98.00	97.00	90.50	94.16	97.83	94.69 ± 3.248
	FS + dimensionality reduction	ERR(%)	0.268	0.333	1.666	0.833	0.693	0.205	0.185	0.744	0.333	0.166	0.542 ± 0.466
		ROR (%)	98.83	99.00	94.33	95.50	96.66	98.50	98.50	95.50	97.33	98.66	97.28 ± 1.688
700	Without FS	ERR(%)	0.914	1.333	4.500	3.056	3.245	0.833	1.133	4.636	2.102	0.850	2.260 ± 1.500
		ROR (%)	95.50	93.33	84.16	87.16	88.00	95.33	95.16	81.66	86.66	95.66	90.26 ± 5.318
	FS + dimensionality reduction	ERR(%)	0.500	1.016	2.666	1.666	1.776	0.500	0.500	2.166	0.666	0.221	1.168 ± 0.841
		ROR (%)	97.66	96.33	90.50	93.50	94.33	98.00	98.50	90.16	95.50	98.33	95.28 ± 3.109
850	Without FS	ERR(%)	1.650	2.833	4.666	4.666	4.333	1.115	1.833	3.833	3.166	1.880	2.997 ± 1.336
		ROR (%)	92.83	90.33	83.66	81.50	83.00	94.16	94.66	85.50	90.16	93.66	88.94 ± 5.067
	FS + dimensionality reduction	ERR(%)	0.934	1.333	3.192	2.333	2.833	0.587	0.666	1.950	1.280	1.000	1.611 ± 0.918
		ROR (%)	96.16	94.33	89.50	92.83	90.83	97.66	97.66	91.50	95.50	96.16	94.21 ± 2.904
940	Without FS	ERR(%)	1.833	2.500	4.500	4.333	3.500	1.166	0.833	3.275	2.333	1.666	2.594 ± 1.273
		ROR (%)	94.66	92.83	85.33	87.16	85.50	96.33	96.83	85.83	90.66	95.16	91.02 ± 4.719
	FS + dimensionality reduction	ERR(%)	0.833	1.368	2.666	2.071	2.166	0.500	0.500	1.967	1.166	1.000	1.424 ± 0.753
		ROR (%)	96.66	94.66	91.83	92.83	90.00	97.83	97.33	92.16	95.16	97.50	94.59 ± 2.764
WHT	Without FS	ERR(%)	0.500	1.677	4.255	3.504	3.500	0.500	0.623	2.746	2.333	0.725	2.036 ± 1.428
		ROR (%)	97.50	94.50	84.16	87.66	86.16	97.66	96.16	81.00	86.50	97.00	90.83 ± 6.349
	FS + dimensionality reduction	ERR(%)	0.271	0.666	2.166	1.204	1.500	0.500	0.166	1.196	1.125	0.040	0.883 ± 0.673
		ROR (%)	98.50	97.33	90.66	94.33	95.33	98.00	99.00	92.83	94.83	99.16	95.99 ± 2.870

Table 3.4 – The unimodal identification system performance for the CASIA database using 50% for training and 50% for testing.

Feature selection schemes	Classifier	Number of features	Spectral bands												Mean ± SD		
			460			630			700			850			940			WHT					
			ERR %	ROR %	Time (s)	EER %	ROR %	Time (s)	EER %	ROR %	Time (s)	EER %	ROR %	Time (s)	EER %	ROR %	Time (s)	EER %	ROR %	Time (s)	EER %	ROR %	Time (s)
Without feat. select.	1-NN	**425984**	0.075	99.50	0.024	0.201	98.66	0.023	0.666	96.83	0.023	0.833	95.66	0.025	1.166	96.00	0.025	0.333	98.66	0.024	0.546 ± 0.416	97.55 ± 1.597	0.024 ± 7.966×10^{-4}
Fisher score		**11500**	0.026	99.50	0.009	0.333	98.50	0.009	0.888	96.33	0.009	1.003	95.00	0.008	1.246	95.33	0.008	0.359	97.83	0.009	0.643 ± 0.471	97.08 ± 1.810	0.009 ± 4.147×10^{-4}
Fisher score+ReliefF		**7000**	0.152	99.83	0.007	0.500	98.00	0.007	0.833	95.83	0.007	1.087	94.33	0.006	1.500	94.83	0.006	0.500	97.66	0.006	0.762 ± 0.482	96.74 ± 2.110	0.007 ± 4.412×10^{-4}
Fisher score+WPCA		**410**	2.333	92.83	7.031×10^{-4}	2.166	93.00	7.032×10^{-4}	3.588	90.16	8.073×10^{-4}	5.500	86.50	7.032×10^{-4}	4.794	88.50	6.770×10^{-4}	2.529	93.00	7.813×10^{-4}	3.485 ± 1.397	90.66 ± 2.752	$7.166 \times 10^{-4} \pm 7.527 \times 10^{-5}$
Without feat. select.	SVM	**425984**	0.333	97.66	0.478	0.666	98.00	0.496	0.914	95.50	0.503	1.650	92.83	0.497	1.833	94.66	0.502	0.500	97.50	0.510	0.982 ± 0.621	96.02 ± 2.054	0.497 ± 0.010
Fisher score		**11500**	**0.00**	**100**	0.014	0.283	98.50	0.014	0.703	97.83	0.013	0.767	96.50	0.013	0.833	96.83	0.015	0.221	98.33	0.014	0.468 ± 0.344	97.99 ± 1.265	0.014 ± 5.696×10^{-4}
Fisher score+ReliefF		**7000**	0.001	99.83	0.009	0.314	98.16	0.008	1.000	97.16	0.008	0.834	96.16	0.009	0.707	96.66	0.008	0.202	98.00	0.009	0.510 ± 0.393	97.66 ± 1.309	0.009 ± 5.564×10^{-4}
Fisher score+WPCA		**410**	0.003	99.83	0.001	0.268	98.83	0.001	0.500	97.66	0.002	0.934	96.16	0.002	0.833	96.66	0.002	0.271	98.50	0.001	0.468 ± 0.359	97.94 ± 1.383	0.001 ± 5.921×10^{-4}

Note: Time= CPU time needed to classify one palmprint image for the CASIA database.

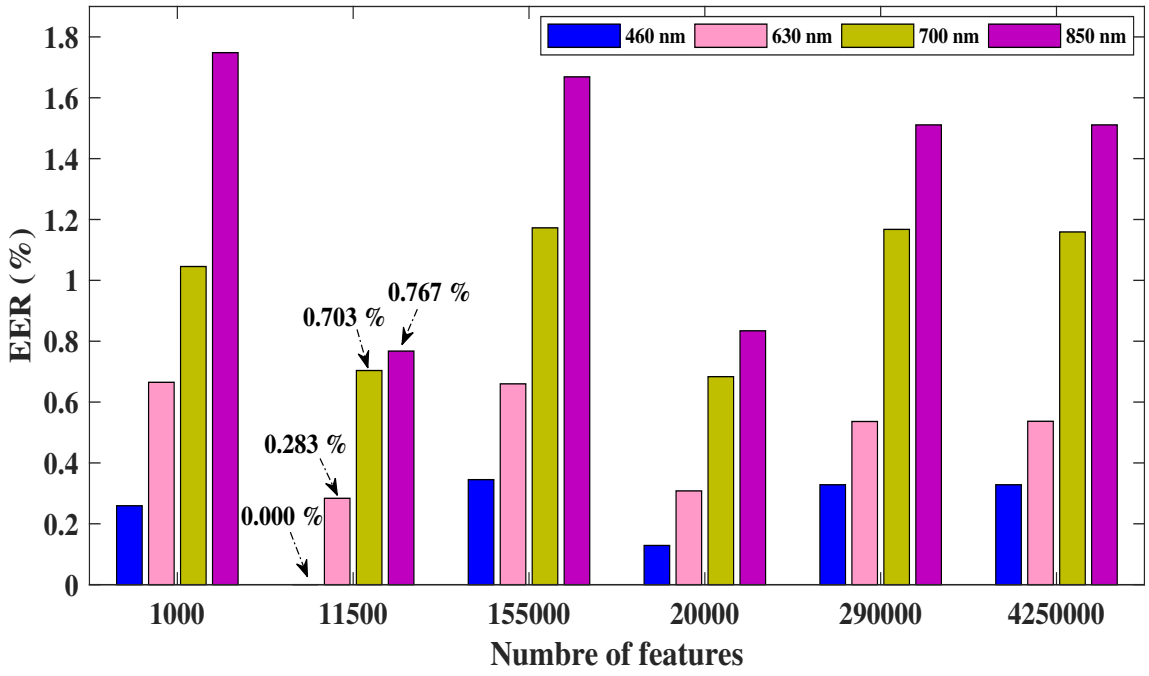

Figure 3.8 – The performance of EER (%) against the Number of ranked features on the CASIA database using 50% for training and 50% for testing.

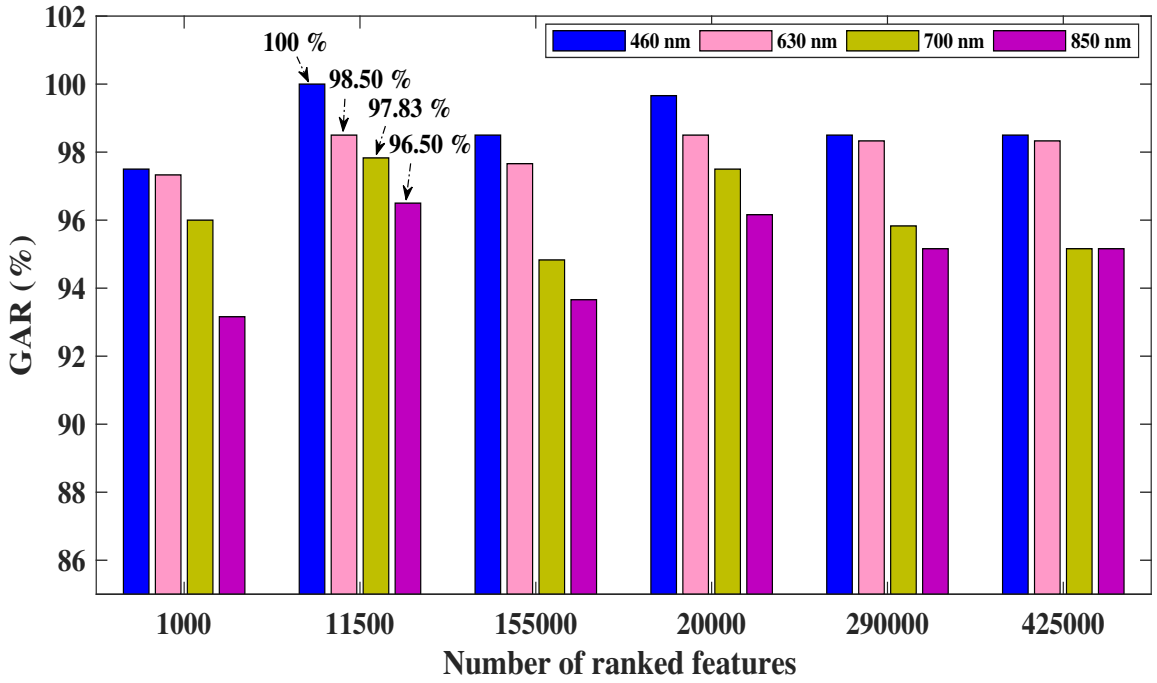

Figure 3.9 – The performance of GAR (%) against the Number of ranked features on the CASIA database using 50% for training and 50% for testing.

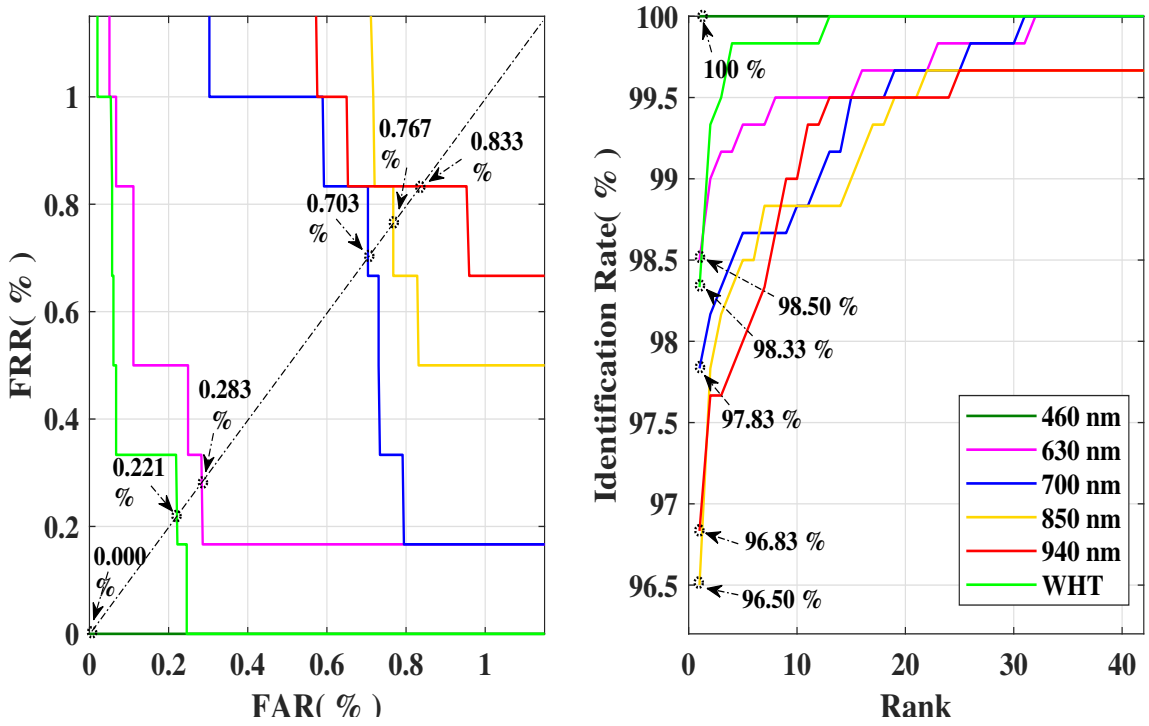

Figure 3.10 – Unimodal system results for the CASIA database using 50% for training and 50% for testing. (a) ROC curves (FRR against FAR) and (b) CMC curves (Identification rate against Rank).

(b) **PolyU multispectral database results**

In the following, we present experimental results of the proposed system evaluated on the PolyU multispectral database, which contains 500 persons and various modalities (Red, Green, Blue, and NIR). In our experiment, six images of each person are selected for training, and the other six for testing. Namely, 3000 images are used for training, and 3000 images are used for testing for each modality. Furthermore, there are 3000 genuine comparisons, and 748,500 impostor comparisons are generated for each band. Thus, in order to see the performance of the biometric system with two modes of identification and CPU time needed to classify one palmprint image, we present the findings in Table 3.5. We can observe from the results obtained by the proposed system that NIR and Blue spectral bands presented the best results in terms of the EER(%) and ROR(%) values. For example, the results of the open-set identification with 1-NN classifier and without FS give EERs equal to 4.008×10^{-4} %

and 8.016×10^{-4} % for NIR and Blue spectral bands, respectively. While, for the closed-set identification, the system achieved a $ROR = 99.96$ % and $CPUtime = 0.121$ s with NIR band, and a ROR of 99.96 % and CPU time equal 0.118 s with Blue. It is also clear that the use of feature selection and dimensionality reduction improves the system's accuracy and reduces computational time. The Fisher score with SVM classifier achieves the perfect results with an $EER = 0.000$ % in the open-set and a $ROR = 100$ % in the closed-set for NIR spectral band. The effectiveness of all spectral bands is shown in Fig 3.11, where the ROC and CMC curves are illustrated. The use of the Fisher score + ReliefF with SVM classifier reduced the feature vector size to 3000 and gave a perfect result with an $EER = 0.000$ % in the open-set and a ROR of 100 % in the closed-set for the blue spectral band. Similarly, the Fisher score + WPCA yielded perfect results with an $EER = 0.000$ % in the open-set and a $ROR = 100$ % in the closed-set and reduced the feature vector size to 410 and CPU time to 0.007 s for NIR spectral band.

Table 3.5 – The unimodal identification system performance for the PolyU database using 50% for training and 50% for testing.

Feature selection schemes	Classifier	Number of features	Spectral bands											
			Red			Green			Blue			NIR		
			EER %	ROR %	Time (s)	EER %	ROR %	Time (s)	EER %	ROR %	Time (s)	EER %	ROR %	Time (s)
Without feat. select.	**NN**	**425984**	0.002	99.90	0.106	0.008	99.93	0.122	8.016×10^{-4}	99.96	0.118	4.010×10^{-4}	99.96	0.121
Fisher score		**15000**	0.002	99.90	0.065	0.008	99.93	0.062	0.002	99.93	0.062	1.336×10^{-4}	99.96	0.061
Fisher score+ReliefF		**3000**	0.009	99.90	0.030	0.024	99.93	0.028	0.008	99.93	0.028	0.010	99.93	0.027
Fisher score+WPCA		**410**	7.984×10^{-4}	99.90	0.003	0.033	99.83	0.003	0.006	99.93	0.003	2.672×10^{-4}	99.96	0.003
Without feat. select.	**SVM**	**425984**	0.033	99.90	12.081	0.034	99.90	9.898	0.013	99.93	16.582	0.003	99.93	15.102
Fisher score		**15000**	0.001	99.93	0.085	0.061	99.90	0.083	0.009	99.93	0.093	0.000	100	0.085
Fisher score+ReliefF		**3000**	0.001	99.93	0.021	0.036	99.93	0.025	0.000	100	0.020	7.001×10^{-4}	99.96	0.023
Fisher score+WPCA		**410**	0.011	99.93	0.009	0.033	99.93	0.008	1.336×10^{-4}	99.96	0.007	0.000	100	0.007

Note: Time= CPU time needed to classify one palmprint image for the PolyU database.

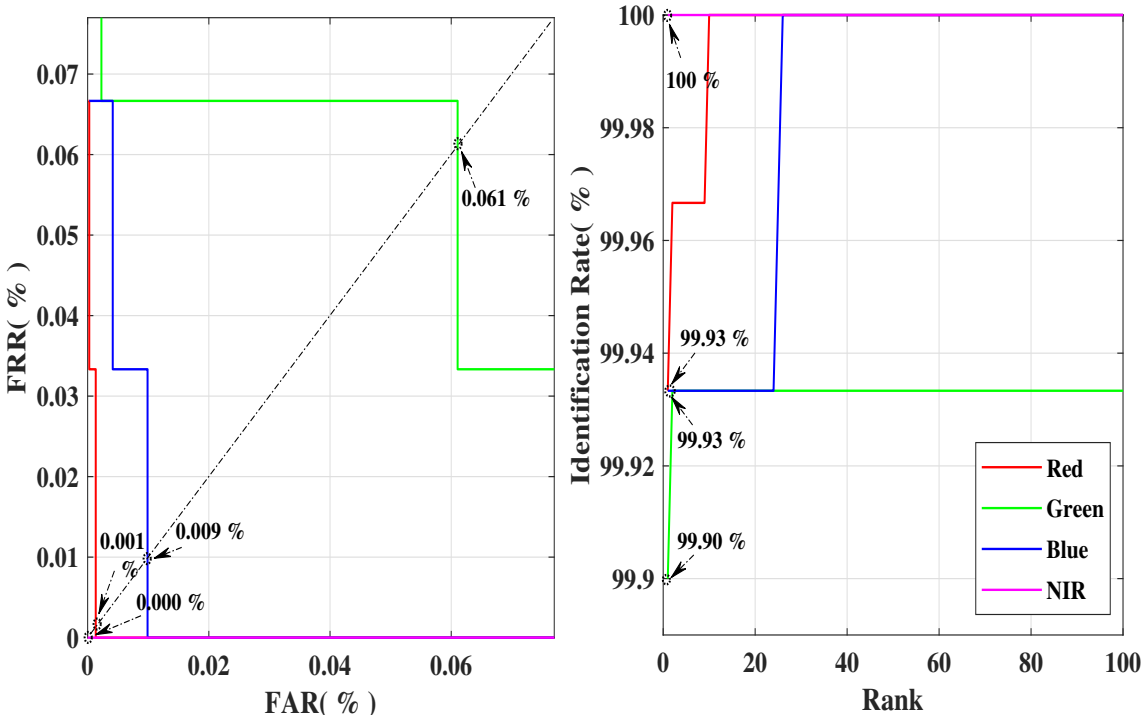

Figure 3.11 – Unimodal system results for the PolyU database using 50% for training and 50% for testing. (a) ROC curves (FRR against FAR) and (b) CMC curves (Identification rate against Rank).

(c) **Tongji contactless database results**

In order to verify the robustness and high efficiency of the proposed method in the contactless database, we used the Tongji database containing 300 persons with two modalities (Left and Right hands). In our experiment, we apply the 10 images of each person for training, and the other ten for testing. Namely, 3000 images are used for training, and 3000 images are used for testing each sample. Thus, 3000 genuine comparisons and 448,500 impostor comparisons are generated. Table 3.6 shows the performance of our unimodal biometric system with two modes of identification system (open-set and closed-set) and the CPU time needed to classify one palmprint image. Compared to all the obtained results, almost all of them give perfect accuracies. The feature selection and dimensionality reduction with two classifiers have not decreased the performance of our identification system. Effectively, with the SVM classifier, the use of the fisher score and the WPCA yielded perfect results with EER of 0.000 % in the

open-set and ROR of 100 % in the closed-set and reduced the feature vector size to 410 and CPU time 0.004 s instead of 6.987 s (without FS) and 0.004 s instead of 7.184 s (without FS) for Left and Right hands, respectively.

Table 3.6 – The performance of unimodal identification systems for the Tongji database using 50% for training and 50% for testing.

Feature selection schemes	Classifier	Number of features	Samples					
			Left			Right		
			EER %	ROR %	Time (s)	EER %	ROR %	Time (s)
Without feat. select.	**NN**	**425984**	0.000	100	0.088	0.000	100	0.083
Fisher score		**10000**	0.000	100	0.070	0.000	100	0.064
Fisher score+ReliefF		**3000**	0.000	100	0.020	0.000	100	0.020
Fisher score+WPCA		**410**	0.000	100	0.005	0.001	99.93	0.005
Without feat. select.	**SVM**	**425984**	0.000	100	6.987	0.000	100	7.184
Fisher score		**10000**	0.000	100	0.036	0.000	100	0.035
Fisher score+ReliefF		**3000**	0.000	100	0.014	0.000	100	0.012
Fisher score+WPCA		**410**	0.000	100	0.004	0.000	100	0.004

Note: Time= CPU time needed to classify one palmprint image for the Tongji database.

In our case, we do not need the fusion for PolyU and Tongji databases because we got perfect results in the unimodal system ($EER = 0.000$ % and $ROR = 100$ %).

(d) PolyU 2D/3D contactless database results

In order to evaluate the efficiency of the proposed method in the contactless database, we utilized the PolyU 2D/3D database, which contains 400 people. In our experiment, we used 2D images from this database splitting each person's 20 images into ten for training and ten for testing. Each sample is tested using 4000 images for training and 4000 images for testing. As a result, there are 4000 genuine comparisons and 798,000 impostor comparisons. Table 3.7 shows the performance of our unimodal biometric system with two modes of identification system (open-set

and closed-set) and the CPU time needed to classify one palmprint image. From the obtained results, we observe that the SVM classifier achieves better performance than the NN classifier, especially in the case of the Fisher score. Furthermore, the use of the fisher score and the WPCA provided perfect results with an EER of 0.000 % in the open-set and ROR of 100 % in the closed-set, reducing the feature vector size to 410 and CPU time 0.007 s instead of 2.394 s (without FS).

Table 3.7 – The performance of unimodal identification systems for the Contactless PolyU 2D/3D database using 50% for training and 50% for testing.

Feature selection schemes	**Classifier**	**Number of features**	**Spectral band**		
			2D		
			EER %	**ROR %**	**Time (s)**
Without feat. select.	**NN**	425984	0.000	100	0.022
Fisher score		10000	0.976	89.85	0.019
Fisher score+ReliefF		3000	0.000	100	0.007
Fisher score+WPCA		410	0.000	100	0.003
Without feat. select.	**SVM**	425984	0.000	100	2.394
Fisher score		10000	0.000	100	0.063
Fisher score+ReliefF		3000	0.000	100	0.022
Fisher score+WPCA		410	0.000	100	0.007

Note: Time= CPU time needed to classify one palmprint image for the Contactless PolyU 2D/3D database.

2. **Multimodal biometric system performance** Unimodal systems suffer from some limitations and cannot provide satisfactory recognition performance in several cases, such as the possibility of noise in the biometric modality and its non-universality [118], which increases system error (EER). Intra-class dissimilarity, as well as inter-class similarity, can also impact the unimodal biometric system and hence the result of identification [119]. An excellent biometric identification system requires a very low EER value, which can be achieved by the multimodal system [120] [121]. Such a system combined several features of each modality at different levels to improve system performance. Matching score level fusion is the

most widely used in the biometric system. In our work, we fuse only the spectral bands of CASIA database palmprint at the matching score level to improve system performance. The other databases have given perfect results with unimodal biometric systems ($EER = 0.000$ % and $ROR = 100$ %). The experiment was conducted with four methods of fusion which are the SUM rule (SUM), the product rule (MUL), and their weighted versions, that is, weighted SUM rule (WHT SUM) and weighted product rule (WHT MUL). The performance of our multimodal identification system is shown in Tables 3.8 and 3.9. The analysis of data showed that the results of the multimodal fusion were much better than those of the unimodal biometric systems. As can be seen from the results, the lowest EER of multimodal identification was obtained by using the combination of all spectral bands that are always better than the lowest results of the unimodal system. In addition, the best results were obtained with an $EER = 0.000$ %. In contrast, the best results of the unimodal biometric system were 0.003 % (case Fisher score+ WPCA with SVM classifier). Figure 3.12 illustrates the CMC and ROC curves for the multimodal identification system.

Table 3.8 – The performance of multimodal identification system fusion between (460, 630, 700) and (850, 940, WHT) using 50% for training and 50% for testing.

Fusion rules	**460- 630- 700**				**850- 940- WHT**			
	Open-Set		**Closed-Set**		**Open-Set**		**Closed-Set**	
	EER (%)	T_0	ROR (%)	RPR	EER (%)	T_0	ROR (%)	RPR
SUM	0.010	0.863	99.00	3	0.046	0.651	100	1
MUL	0.000	0.584	100	1	0.043	0.271	100	1
WHT SUM	0.000	0.985	100	1	0.057	0.647	100	1
WHT MUL	0.000	0.962	100	1	0.006	0.710	100	1

Table 3.9 – The performance of multimodal identification system (fusion between all spectral bands) using 50% for training and 50% for testing.

Fusion rules	**460-630-700-850-940-WHT**			
	Open-Set		**Closed-Set**	
	EER (%)	T_0	ROR (%)	RPR
SUM	0.000	0.940	100	1
MUL	0.000	0.070	100	1
WHT SUM	0.000	0.939	100	1
WHT MUL	0.000	0.940	100	1

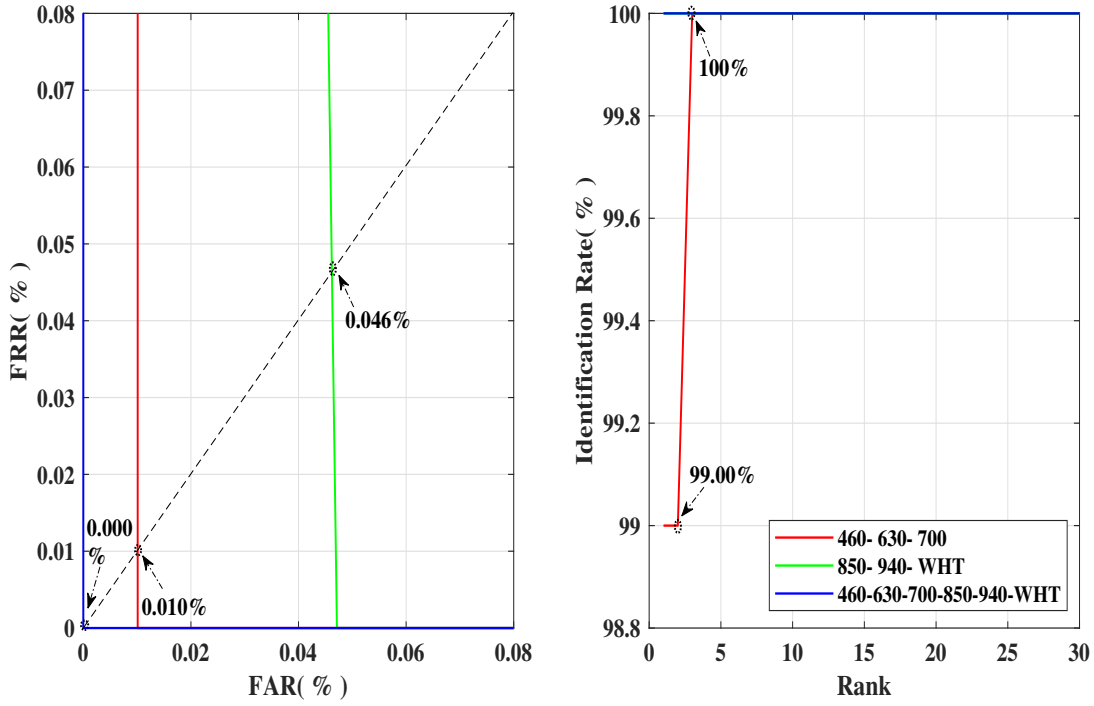

Figure 3.12 – Multimodal system results for the CASIA database (SUM rule) using 50% for training and 50% for testing. (a) ROC curves (FRR against FAR) and (b) CMC curves (Identification rate against Rank).

3. Comparative Study

To prove the effectiveness of the proposed approach against alternative methods, we did a comparative study along with some works found in the literature. Thus, in this chapter, we provided unimodal and multimodal identification systems using multispectral and contactless palmprint images. The results validated the robustness and effectiveness of

the proposed method. The system reached very high identification accuracy ($EER = 0.000$ % and $ROR = 100$ %). Therefore, a comparison of some related and existing techniques must be made on the same databases. Table 3.10 summarizes the works of the unimodal biometric system performed on the multispectral CASIA and PolyU databases, and the contactless Tongji and PolyU 2D/3D databases. To obtain an equitable comparison, we chose works where the percentage of training and testing is 50 %. From this table, we observe that the proposed algorithm (Simplified PalmNet-Gabor) provides high identification performance for multispectral PolyU database and contactless Tongji and PolyU 2D/3D databases, using a substantially lower number of features compared with other methods listed in the same table. On the other hand, for the multispectral CASIA database, a fusion process is used to improve the identification performance. Table 3.10 lists the recognition accuracies of the proposed method and the most recent methods published in the literature with the number of features and computing time of the different classifiers. The computing time represents the CPU time needed to classify one palmprint image. To obtain an equitable comparison, we chose works where the percentage of training and testing is 50 %. From this table, we observe that the proposed algorithm (Simplified PalmNet-Gabor) provides high identification performance for multispectral PolyU database and contactless Tongji and PolyU 2D/3D databases, using a substantially lower number of features compared with other methods listed in the same table. On the other hand, for the multispectral CASIA database, a fusion process is used to improve the identification performance.

Table 3.10 – Performance comparison of the unimodal systems using 50% for training and 50% for testing. For each competing method, the number in parentheses indicates how many times the proposed method is faster.

Method	Databases	Performance		Number of features	Classifier	Computing Time (s)
		ERR (%)	ROR (%)			
Deep scattering convolutional network [62]	$PolyU_M$	-	100	12,512	SVM	0.090 (x 64.3)
PCANet with Two stages [64]	$CASIA_M$	0.006	99.83	46,080	SVM	1.194 (x 852.8)
	$PolyU_M$	0.000	100			
DCTNet with Two stages [67]	$CASIA_M$	0.003	99.83	46,080	SVM	1.552 (x 1109)
	$PolyU_M$	0.000	100			
PalmNet Gabor-PCA [68]	$Tongji_T$	0.720	99.77	12,288,000	KNN	0.151 (x 108.4)
Simplified PalmNet Gabor	$CASIA_M$	**0.003**	**99.83**	**410**	**SVM**	**0.001**
	$PolyU_M$	**0.000**	**100**			
	$Tongji_T$	**0.000**	**100**			
	$PolyU_T$	**0.000**	**100**			

For the multimodal biometric system, a comparative study was performed in Table 3.11 with the works that used fusion at the matching score level and 50% train-test split procedure. It is observed that the proposed algorithm has also given perfect identification performance ($EER = 0.000$ %, $ROR = 100$ %) like the two other works, but it has reduced the features vector to 410 instead of 46,060 for the two other works.

Table 3.11 – Performances comparison of the multimodal systems using 50% for training and 50% for testing.

Method	Performance		Number of features
	EER (%)	ROR (%)	
PCANet with Two stages [64]	0.000	100	46,080
DCTNet with Two stages [67]	0.000	100	46,080
Simplified PalmNet-Gabor	**0.000**	**100**	**410**

3.4 Conclusion

In this work, we proposed efficient unimodal and multimodal identification systems for fast palmprint recognition. The proposed method, namely simplified PalmNet-Gabor, adopts the PalmNet network with enhancements based on feature selection and reduction dimension methods. Therefore, we used feature selection methods to select a subset of relevant features of PalmNet using Fisher score and ReliefF methods and dimensionality reduction by WPCA method to reduce the computational time and improve the accuracy recognition. Furthermore, we applied log-Gabor filters by adjusting the pixel luminance of palmprint images. For the multimodal system, we use the matching score fusion method to improve the performance of the unimodal system. The proposed method effectively improves the accuracy of PalmNet, reduces the number of features, and solves the problem of computational complexity. The proposed approach was evaluated using four popular and publicly available palmprint databases. The extensive experiments presented in this work have validated the robustness and effectiveness of our method by achieving high recognition accuracy with a significantly smaller number of features.

The unimodal identification system performed on multispectral PolyU database and contactless Tongji and PolyU 2D/3D databases obtained a very high identification accuracy ($EER = 0.000$ % and $ROR = 100$ %). It gave a CPU time less than 0.009 s and reduced the feature vector size to 410. Likewise, the multimodal identification system performed on the CASIA database offers perfect results $EER = 0.000$ % for the open-set identification and $ROR = 100$ % for the closed-set identification. In the future, we will test our proposed method with other large databases, such as medical images. We will also employ additional clustering and dimensionality reduction techniques. Furthermore, we will employ the graphics processing unit (GPU) to reduce processing time, which is a highly valuable tool for speeding up the processing speed of computationally intensive algorithms.

Chapter 4

An Improved Multispectral Palmprint System Using Deep CNN-based Palm-Features

4.1 Introduction

NOWADAYS , the adoption of persons and institutions of digitization in their activities has become an urgent necessity. Unfortunately, in this new trend, information is not always safe; this is why information security has become a significant concern for our modern societies [122]. Indeed, one way to achieve this goal is to recognize the identity of the person trying to access the system. In fact, due to the great need for such recognition, researchers have developed several methods related to knowledge-based or token-based [123]. These traditional methods improve security, but they suffer from several limitations that can be overcome effectively by using some characteristics that are inherent to the person or simply biometric technologies [124].

Biometrics refers to the technologies of recognition of individuals based on biometric features that can be extracted from one or more physiological or behavioral traits such as fingerprint, face, iris, speech, hand geometry, etc. Hence, to develop a biometric system, one must first determine the biometric modality we are going to use. In general, this

biometric modality allows us to choose the suitable feature extraction technique that can provide the best success rate [125]. Indeed, two critical parameters are used to select the appropriate biometric modality in a given security application, namely acceptability and precision rates. Human behavior traits have a higher acceptability rate with inferior precision due to their more significant inter-class variability [67]. In contrast to this, the physiological traits offer a good compromise between the acceptability rate and the precision rate. Even in the set of physiological traits, there are biometric traits characterized by low acceptability and others characterized by poor accuracy. For example, face modalities are very acceptable but lead to poor precision. Besides, fingerprints offer high precision but are not acceptable to users in many applications. Currently, many physiological traits have been extracted, and those obtained from the human hand have proven their reliability and acceptability by the user in a wide range of security applications [126]. In particular, from the palm of the human hand, two main biometric modalities, palmprint, and palm-vein can be extracted. Fortunately, with the modern development of multispectral imaging, it is possible to capture these two modalities with a single acquisition device that provides images for the skin and veins of the palm [127]. In other words, the palmprint images, which represent the skin pattern of the inner palm surface, are captured in the visible light spectrum. While the palm-vein images are captured in the near-infrared (NIR) spectrum, they represent the dark lines of the palms and are based on the infrared light absorption (IR) properties of the blood vessel structures.

In the feature extraction task, the acquired biometric image is processed to extract only the discriminant information to form a new representation that must necessarily be unique for each person. In this task, several feature extraction methods, such as Gabor filtering [128], Local Binary Pattern (LBP) [129], and Discrete Cosine Transform (DCT) [55], can be used. However, these methods have big limitations (e.g. large intraclass variability) that affects the accuracy of the system. To overcome these limitations, deep learning techniques [130] have become popular methods that provide a better representation of the image. Compared to conventional methods, one of the main advantages of deep learning methods is flexibility and discriminatively. In these methods, it is possible to use higher-level representation in several levels of representation to extract some discriminant

information from the biometric image. Recently, many feature extraction methods based on deep learning techniques have been proposed in the literature and the Convolutional Neural Network (CNN) technique [131] is almost the first and most effective of these techniques.

This work aims to develop palmprint (palm-vein)-based biometric systems in which biometric images are analyzed using the deep CNN technique. In our experiments, we first evaluate each biometric identification system based on a single spectral band (unimodal system). Also, the results of two or more unimodal systems are fused at the matching score level to create an efficient and robust multimodal identification system.

The rest of the chapter is organized as follows: Section 4.2 describes the proposed multimodal biometric system in which scores are fused at the matching level. Section 4.3 gives an overview of the preprocessing stage. Section 4.4 briefly describes the deep CNN based feature extraction method and classification. The scores normalization and the fusion scheme are illustrated in section 4.5. In section 4.6, the experimental results, obtained using a database of 500 persons, are presented and discussed. Finally, the last section includes the conclusion and the intended perspectives.

4.2 System Framework

In Fig .4.1, we present the technical framework of the proposed multimodal biometric system based on the fusion, at the matching score level, of the palmprint and palm-vein features. In both phases (enrolment and identification), our system includes the image pre-processing and the deep-CNN based feature extraction. For the enrolment phase, the extracted feature vector must be stored in the system database, while for the identification phase, this feature vector is subject to a matching step to decide whether to accept or reject this person at the decision step. It is important to note that before combining the scores obtained from the two unimodal systems, a normalization process is applied. This enhanced scheme takes advantage of each biometric modality and can be used to improve the unimodal biometric system.

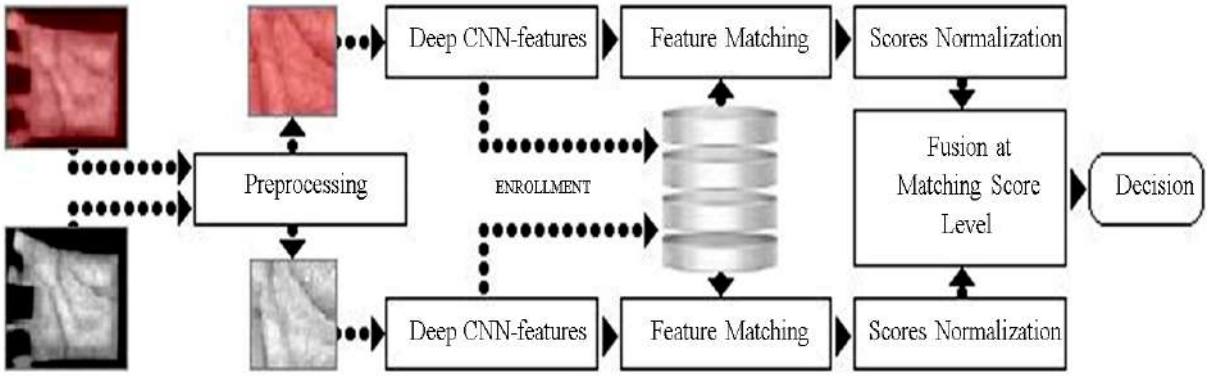

Figure 4.1 – Multimodal biometric identification system based on fusion of Deep features of palmprint & palm-vein

4.3 Prepossessing Stage

Determining the palmprint Region Of Interest (ROI) is an essential step in the biometric based identification system. For this, we used in our work the same algorithm as that used in [30]. It consists of defining a system of coordinates, making it possible to locate the central area of the palm. The gaps between the fingers are used as reference points for determining a coordinate system. As a result, a rectangular ROI sub-image of size $H \times W$ W is located and then extracted.

The main steps of this technique, illustrated in Fig. 4.2, are as follows: (a) the biometric modality (e.g. the palmprint) is filtered with a Gaussian smoothing filter to reduce the noise effect. Then, (b) the resulting image is binarized with the Otsu thresholding algorithm to obtain a binary image containing only one object (the whole hand). (c) A hand contour tracking algorithm is used to extract only the perimeter of the hand. This perimeter is then used to locate the two reference and stable points, located between the ring and the little finger and between the forefinger and the middle finger. (d) The tangent of these two points is calculated to be used to align the palmprint modality. Finally, (e) the central region of the image, i.e. 128×128, is cropped to represent the ROI palmprint. It should be noted that all spectral bands of the image (red, green, blue and near-infrared) are subjected to the same preprocessing steps to extract the ROI sub-image.

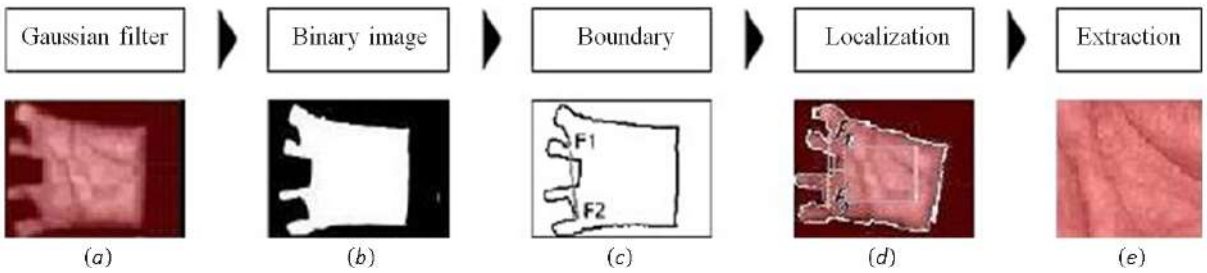

Figure 4.2 – Palmprint region of interest extraction technique. (a) Image filtering, (b) Image binarization, (c) Binary image boundaries with the location points of the ROI sub-image, (d) Location of the central area, and (e) Preprocessing result (ROI sub-image).

4.4 Feature Extraction and Classification

The Convolutional Neural Network (CNN) [132] scans an input image with many banks of convolution filters. It can be run using multiple layers and several filters to extract higher level feature vectors. Indeed, CNN is a kind of deep neural network used in pattern recognition and image processing. The CNN algorithm is a multilayer perceptron explicitly designed for the analysis of two-dimensional signal information like image. Overall, the CNN architecture (see Fig. 4.3) includes three main layers: i) convolutional layers, ii) pooling layers and iii) fully-connected layers. Thus, in the convolutional layer, the input image is convolved with some filters. This task can be applied in several steps. After each convolutional layer and to reduce the size of the obtained feature, which is the role of the pooling layer, the outputs of this layer are reduced by using the max-pooling. Finally, in the output layer, the feature vectors of the input image are obtained and then used as inputs of an ANN for the classification (matching).

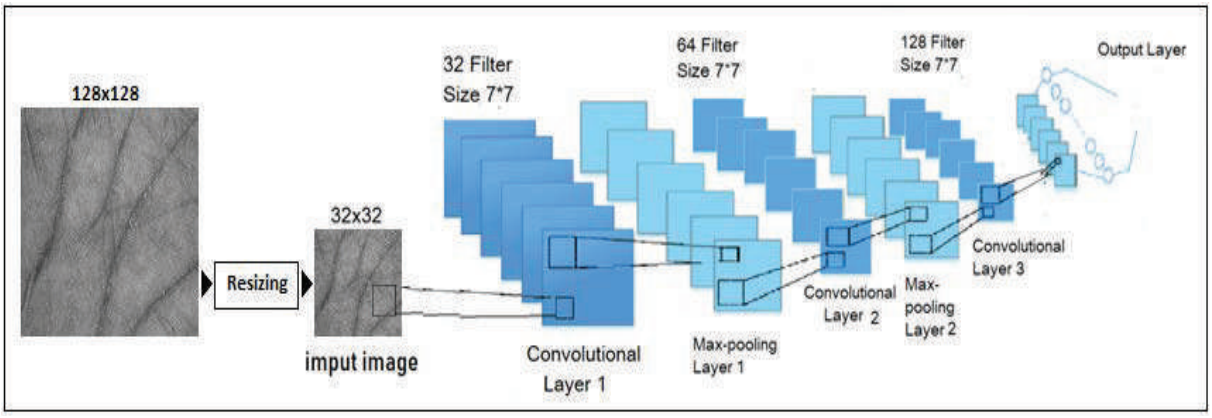

Figure 4.3 – CNN's proposed architecture for biometric feature extraction.

4.5 Scores Normalization and Fusion Schemes

The normalization process that is typically used in multimodal systems (data fusion) allows each measured score to be transformed into a common interval. The most widely used normalization method in biometric identification systems is $Min-Max$. This technique is the more appropriate in the case where the limits (minimum and maximum values) of the scores produced by the systems are known. In this case, we can easily translate the minimum and maximum values of the scores vector into 0 and 1, respectively. The following formula gives the score normalized by the $Min-Max$ method:

$$\hat{V_d} = \frac{V_d - min(V_d)}{max(V_d) - min(V_d)} \tag{4.1}$$

Where the vector V_d comprises all the scores calculated between the test and all the stored feature vectors, while the vector V_d contains the normalized scores.

Generally, the performance of a single-modality based biometric system (or unimodal biometric system) has several limitations. Indeed, to overcome the weaknesses of unimodal biometric systems, the data fusion principle is used. In the biometric system, the fusion process can be applied to one of four levels: sensor level, feature level, matching score level and decision level. Until now, the fusion at matching score level is the most commonly used process due to its simplicity, efficiency and ease of implementation. In this process,

the normalized scores were fused to produce a new score which is used to make a final decision. There are a variety of rules-based fusion techniques. In our work, we used six fusion rules: sum-score rule (SUM), product-score rule (MUL), sum-weighted-score (WHT SUM), product-weighted-score (WHT MUL), min-score (MIN), and max-score (MAX) [124].

The system decision depends on the computed matching score (d_0^i) and the system security threshold (T_0) provided by the system designer (depending on the desired security level). For each user, the system decision is made as follows:

$$Decision = \begin{cases} Accepted & if \quad d_0^i \geq T_0 \\ Rejected & if \quad d_0^i < T_0 \end{cases} \tag{4.2}$$

Where (d_0^i) indicates the calculated score for the i^{th} person and (T_0) the system security threshold.

4.6 Experiments and Results

An excellent biometric system depends on its accuracy. The degree of accuracy is measured with biometric parameters depending on the system used. For this, an evaluation phase is carried out with a dataset of multispectral palmprint images acquired with a capture device developed by the Polytechnic University of Hong Kong (PolyU) [133]. This database contains a large number of images and is widely used in many works, which justifies its use. This dataset is composed of palm images captured under visible light (red, green and blue spectral bands) which represent the modalities of the palmprint and the Near InfraRed (NIR spectral band) representing the palm vein modalities. Thus, 195 males and 55 females contributed to the image collection, which constituted a dataset of 250 persons. These persons represent the students and staff of PolyU University and have a different age, which varies between 20 and 60 years. All of the images in this database were collected in two separate sessions during which each person is asked to provide six images for each palm. These two sessions were separated by an average time interval of 9

days. As a result, for each illumination, 24 images (four spectral bands in every six image) were collected from both palms of each person. The built dataset contains 6000 images of 500 different palms The experiments involved are performed on two sub-datasets. The first sub-dataset is used for training (learning) phase, while the second is for the testing phase. For the CNN algorithm, it is better to adopt a more extensive training set to avoid overfitting. To do this, for each spectral band, six images are selected randomly for the learning phase, containing images of $3000(6 \times 500)$ and six images for the testing phase containing $3000(6 \times 500)$ images.

The set of tests presented in this chapter is divided into three parts. In the first part, an empirical evaluation is used to select the relevant and suitable parameters of the CNN algorithm (which gives the best system accuracy). These parameters are used in the second part to evaluate the performance of the proposed unimodal biometric system using the different spectral bands of the multispectral palmprint database. For this, both identification modes (open-set and closed-set modes) are tested. Finally, in the third and final part, the performance of the multimodal biometric system is evaluated.

Our system is implemented using MATLAB 2018a in an experimental platform as a workstation (HP Z8 G4), with a 64-bit Microsoft Windows 10 operating system, equipped with an Intel Xeon Silver 4108 processor, a 32 GB of RAM and a graphic processing unit (GeForce RTX 2080 Ti).

4.6.1 Experimental Setup

There are many parameters for adjusting a convolutional neural network. To get the best CNN architecture and get a very accurate identification rate, we need to find the relevant parameters that effectively represent our system. In any CNN architecture, there are hyper-parameters and additional parameters. Among the essential hyper-parameters, one can find the number of layers, the activation function, the learning rate, the batch size, the number of epochs and the L_2 regularization. On the other hand, the most important additional parameters are the filters size, the number of filters, the padding, the stride, and the pooling-layer. To have an excellent biometric system with reduced complexity, our study focused on a few parameters that we think are important in our work and on

the fact that other parameters taken by default have given good results. It's good practice to start with a basic model and then try to improve it at every step. Our basic model took the following default settings: stochastic gradient descent with momentum, learning rate = 0.01, L_2 regularization = 0.0001, fixed the maximum number of epochs for training to 30 and used a mini-batch with 128 observations at each iteration. In the rest of this study, we will adopt an empirical evaluation by modifying the number of layers, the size of the filters and the number of filters. It should be noted that each layer of our CNN architecture is composed of a convolution operation, a batch normalization operation to normalize (mean centering and variance scaling) the input given to the layers.

A Relu operation and an optional max-pooling operation which aim to down-sample an input representation (image, hidden layer output matrix, etc.), reducing its dimensionality to retaining the maximum value (activated features) in the sub-regions binned. Table 4.1 illustrates the effect of the above parameters on system performance (Red spectral band). According to this table, the best parameters obtained are the number of layers = 3, the size of the filters = 7×7 and the number of filters is 32, 64, 128 for each layer respectively. We will use these parameters in the next subsections.

4.6.2 Unimodal biometric System Test Results

We continue to evaluate the performance of our biometric system on the other spectral bands (Green, Blue, and NIR) using the parameters obtained in the two identification modes, open-set, and closed-set. Table 4.2 and Fig.4.4 show an objective comparison between the four spectral bands. In this figure, all the spectral bands gave excellent results. The Green and NIR spectral bands and the color palmprint (RGB) slightly outperform the Red and Blue spectral bands. In this case, an Equal Error Rate (EER) of $1,336 \times 10-4$ % is reached. The Red and Blue spectral bands can work with a close EER, with $2,672 \times 10-4$ %. Fig. 4.4.(a) and Fig. 4.4.(b) illustrates the comparison between the four spectral bands and the color component of the palmprint for the open-set identification.

Finally, Fig. 4.4.(c) compare the closed-set identification results. Like the open-set iden-

tification biometric system, the closed-set identification system can achieve high precision with the CNN algorithm. In this case, the system generates a Rank-One Recognition (ROR) equal to 99.93% up to 99.96% with a Rank of Perfect Recognition (RPR) of 2 for all spectral bands and the color component (RGB).

Table 4.1 – Identification System Parameters Selection

NUMBER OF LAYER	[2]	[3]	[4]	[5]
ERR (%)	0.046	0.038	0.626	15.70

NUMBER OF FILTER	[4 4 4]	[4 8 16]	[8 16 32]	[16 32 64]	[32 64 128]	[64 128 256]	[128 128 128]
ERR (%)	0.038	0.006	8.950×10^{-3}	0.010	7.420×10^{-3}	0.015	0.029

FILTER SIZE	[3 3]	[4 4]	[5 5]	[6 6]	[7 7]	[8 8]	[9 9]
ERR (%)	7.420×10^{-3}	0.010	1.730×10^{-3}	7.580×10^{-3}	2.672×10^{-4}	3×10^{-3}	7.980×10^{-4}

Table 4.2 – Unimodal Identification Test Results

SPECTRAL BANDS	OPEN SET		CLOSED SET	
	T_o	ERR (%)	ROR (%)	RPR
RED	0.439	$2,672 \times 10^{-4}$	99.96	02
GREEN	0.982	$1,336 \times 10^{-4}$	99.96	02
BLUE	0.863	$2,672 \times 10^{-4}$	99.93	02
NIR	0.599	$1,336 \times 10^{-4}$	99.96	02
RGB	0.593	$1,336 \times 10^{-4}$	99.96	02

4.6.3 Multimodal Biometric System Test Results

Unimodal systems are subject to a variety of problems, such as the possibility of noise in the biometric modality and its non-universality, which increases the system error (EER) [134]. Intra-class dissimilarity, as well as inter-class similarity, can also affect the unimodal biometric system and hence the result of identification [135]. An excellent biometric identification system requires a very low EER value, which can be achieved by the multimodal system [120]. Such a system combined several features of each modality at different levels to improve system performance. To build a multimodal biometric system, unimodal biometric systems can be combined at four different levels, namely the sensor

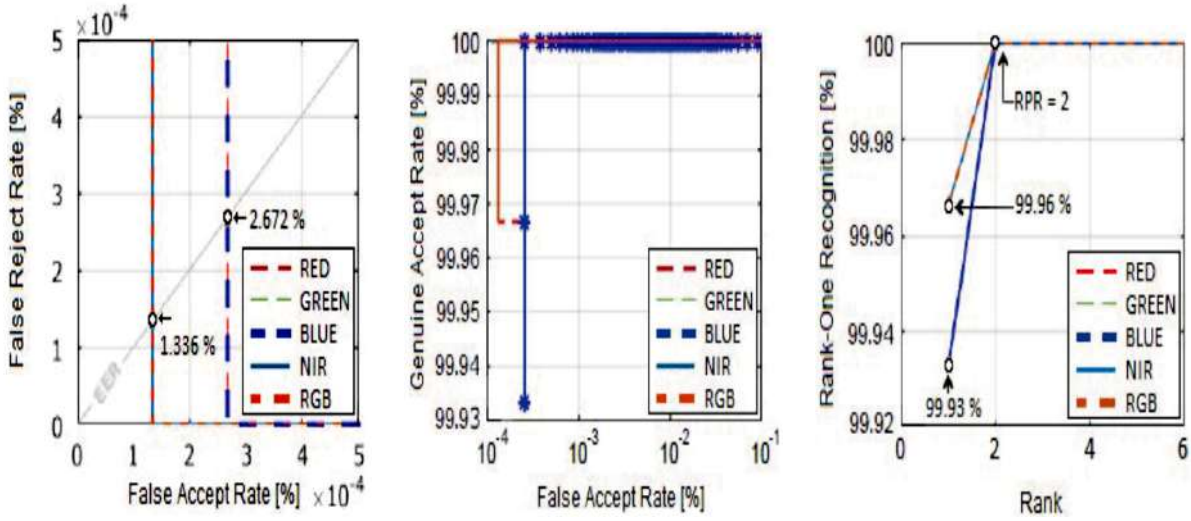

Figure 4.4 – Unimodal biometric identification system test results. (a) ROC curves (FRR against FAR), (b) ROC curves (GAR against FAR) and (c) CMC curves, identification rate against rank.

level [136], the feature level [137], the matching score level [138], and the decision level [139].

Matching score level fusion is the most commonly used biometric information fusion strategy because matching scores are readily available and because they retain enough information to distinguish the genuine matching from impostor matching. In our work, we will combine (fusion) all spectral bands and the RGB palmprint at the matching score level to improve system performance. The experiment was conducted with five methods of fusion which are the sum of the scores (SUM), the sum of the weighted scores (WHT SUM), the product of the scores (MUL), the product of the weighted scores (WHT MUL) and the minimum score (MIN). Several combinations can be made between the four spectral bands and the color images. We limit our tests only to $R+G+B$ and $RGB+NIR$. This choice allows the biometric system to use a device captured under visible light (color image, RGB) or a multispectral image (RGB-NIR).

Table 4.3 and Fig. 4.5 show the results obtained from our multimodal identification system with different fusion rules in open-set mode and closed-set mode. The analysis of the data showed that the results of the multimodal fusion were much better than those of the unimodal biometric systems. As can be seen from the results, the lowest EER of multimodal identification was obtained by using the combination $R+G+B$ with all

fusion rules that are always better than the lowest results of the unimodal system. In addition, the best results were obtained with EER = 0.000%. While the best results of the unimodal biometric system were $1,336 \times 10 - 4$.

The $(RGB + NIR)$ combination did not bring any improvement, except for the closed-set identification biometric system which provides a perfect ROR of 100% (RPR = 1). Same thing for the combination $R + G + B$. In our case, we do not need to fusion the $R + G + B$ combination with the NIR spectral band because we got perfect results with the $R + G + B$ combination.

Table 4.3 – Multimodal Biometric Identification System Test Results

FUSION RULES	RED-GREEN-BLUE				RGB-NIR			
	OPEN SET		CLOSED SET		OPEN SET		CLOSED SET	
	T_o	ERR(%)	ROR(%)	RPR	T_o	ERR(%)	ROR(%)	RPR
SUM	0.913	0.000	100	01	0.596	1.336×10^{-4}	100	01
WHT SUM	0.612	0.000	100	01	0.596	1.336×10^{-4}	100	01
MUL	0.025	0.000	100	01	0.356	1.336×10^{-4}	100	01
WHT MUL	0.138	0.000	100	01	0.596	1.336×10^{-4}	100	01
MIN	0.173	0.000	100	01	0.593	1.336×10^{-4}	100	01

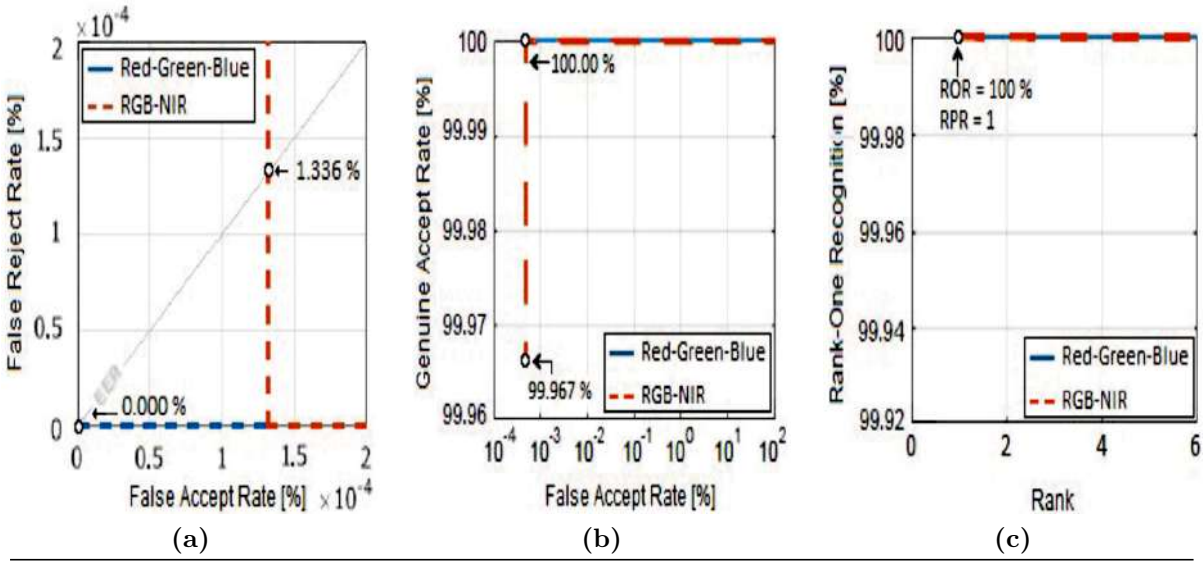

Figure 4.5 – Multimodal biometric identification system test results. (a) ROC curves (FRR against FAR), (b) ROC curves (GAR against FAR) and (c) CMC curves, identification rate against Rank.

4.7 Conclusion and Future Work

In the proposed method for this study, the first multispectral palmprint based unimodal biometric systems were evaluated independently. It was found that the Green spectral band (palmprint modality) and the NIR spectral band (palm-vein modality) gave better results than the other palmprint bands (blue and red spectral bands). Besides, the study evaluated the multimodal system on the fusion of RGB palmprint or all spectral bands at matching scores level. The fusion of the bands was done by five rules fusion. All fusion rules produced the best result with a value of 0% EER in open-set mode and a ROR of 100% in closed-set mode.

In conclusion, the fusion schemes with multimodal systems gave significantly better performances than their unimodal systems. This result suggests that the multimodal identification system is the best choice for our case. The unimodal identification system will be a secondary choice. Due to the effectiveness of the CNN approach in the classification system, our future work focuses on other deep learning techniques (like Deep Belief Network (DBN) and autoencoder neural network) and their use in feature extraction methods.

Chapter 5

Finger Knuckle Print Recognition Using Deep Convolutional Neural Network

5.1 Introduction

SINCE the beginning of the 21^{th} century humans has always been searching for ways to improve their lifestyle in many domains, especially their own security and here we see their huge step in technological evolution towards improving their safety in several sectors taking several ways and methods. Biometrics has emerged to meet this need and even has developed in the science combining biology technology and information technology to utilize physiological or behavioral characteristics in the human body to deal with identifying individuals. It is applied to two main aspects applications, identity verification and identity recognition. A hand has many biometric traits such as fingerprint, palm print, finger/palm vein, finger knuckle, and hand geometry. Among such traits, a finger knuckle is a relatively new biometric trait in contrast with famous biometric traits such as face, fingerprint, and iris.

In this work, one of these systems was chosen for study, which uses the (FKP) trait [88]. This trait has been selected according to many great advantages: accepted by people, easy

to use, simple, permanent, stable throughout life, unique to each and another. Finally, the combination of fingers (ten fingers with both hands) can be used to create a strong and precise recognition system. Our experience is based on convolutional neural network method. CNNs have recently shown remarkable success in image recognition [140][141], computer vision, automated language process, text classification, medicine [142], time series physiological signals [143], electric machine fault diagnosis [144], ultrasonic signal classification [145]. Deep learning techniques have recently been used by many companies, such as Adobe, Apple, Facebook, Baidu, Google, IBM, Microsoft, NEC, Netflix, and NVIDIA [146]. This work aims at achieving the unimodal and multimodal biometric systems based on multi-sample FKP images using the deep CNN technique. Compared with traditional methods, the proposed DCNN could extract more distinctive and deep features and achieve satisfying recognition performance.

In our experiments, we first evaluate each biometric identification system based on a single spectral band (unimodal system). Also, the results of two or more unimodal systems are fused at the matching score level to create an efficient and robust multimodal identification system. The rest of the work is organized as follows: Section 5.2 describes the proposed multimodal biometric system in which scores are fused at the matching level. Section 5.3 briefly describes the deep CNN based feature extraction method and classification. The fusion rules are illustrated in section 5.4. In section 5.5, the experimental results, obtained using a database of 165 persons, are presented and discussed. Finally, the last section includes the conclusion and the intended perspectives.

5.2 System Design

In Fig. 5.1, we present the block diagram of the proposed multimodal identification system based on the fusion (at the matching score level) of finger knuckle print Scores. Each subsystem exploits different biometric techniques, which are Left Index Finger (LIF), Left Middle Finger (LMF), Right Index Finger (RIF) and Right Middle Finger (RMF) modalities. Our system includes the pre-processing image and the deep-CNN based feature extraction with classification. Like all biometric systems, this system work into two phases: the enrollment phase and the identification phase. In the enrollment phase, the

extracted feature vector must be stored in the system database, while for the identification phase, this feature vector is subject to a matching step to decide the decision.
For each user, the system decision is made as follows:

$$Decision = \begin{cases} Accepted, & \text{if} \quad d_0^i \geq \mathcal{T}_{th} \\ Rejected, & \text{if} \quad d_0^i < \mathcal{T}_{th} \end{cases} \tag{5.1}$$

where d_0^i indicates the probability for the i^{th} person and (T_0) the system security threshold provided by the system designer (depending on the desired security level). This enhanced scheme takes advantage of each biometric modality and can be used to improve the unimodal biometric system.

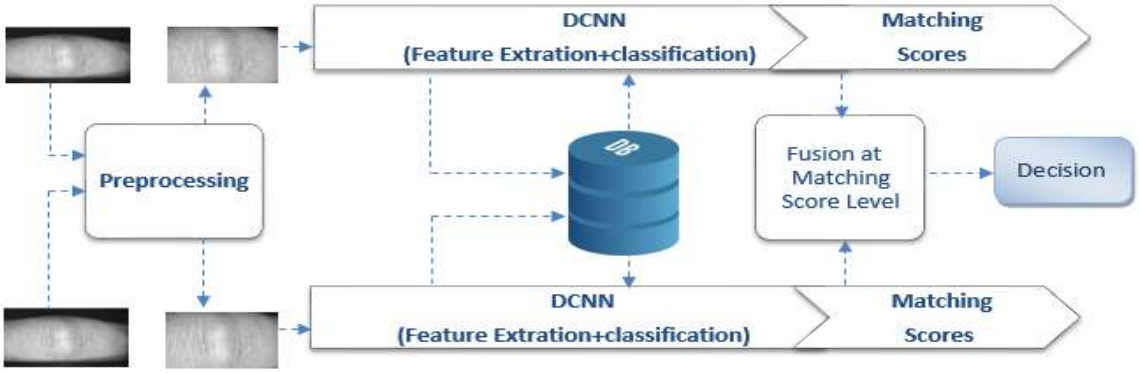

Figure 5.1 – Multimodal Finger Knuckle Print identification system.

5.3 Feature Extraction and Classification

The CNN is a kind of deep neural network where the structure consists of many hidden layers and parameters. (CNN) is a kind of deep neural network inspired by biological processes and designed to recognize patterns directly from pixel images, it has been applied in image processing, natural language processing. CNNs are typically structured in two parts. First part, usually called feature extraction, which uses combinations of convolutional and pooling layers. Second part called classification which uses fully connected layers. Overall, the CNN architecture includes three main layers: i) convolutional layers, ii) pooling layers and iii) fully-connected layers as shown in Fig. 5.2 .

5.3.1 Convolution Layer

is the core building block of the CNN. The prime purpose of convolution is to extract distinct features from the input. These layers are comprised of a series of filters or learnable kernels which aim at extracting local features from the input, and each kernel is used to calculate a feature map or kernel map. The first convolutional layer extracts low-level meaningful features such as edges, corners, textures and lines.

5.3.2 Pooling Layer (Downsampling, or Subsampling Layers)

It reduces the resolution of the previous feature maps through compressing features and computational complexity of the network. It adjusts the features robust to noise and disorder. Another purpose of the pooling layer is to make it robust to small variations for previously learned features, there are mainly two kinds of Pooling: Max and Mean Pooling.

5.3.3 Fully-Connected Layer

The output from the convolutional and pooling layers represent high-level features of the input image. The purpose of the Fully Connected layer is to use these features for classifying the input image into various classes based on the training dataset, this layer is a traditional ANN include a softmax activation function (with Loss function called cross-entropy loss) which outputs a probability (values between zero and one that sum to one) for every classification label.

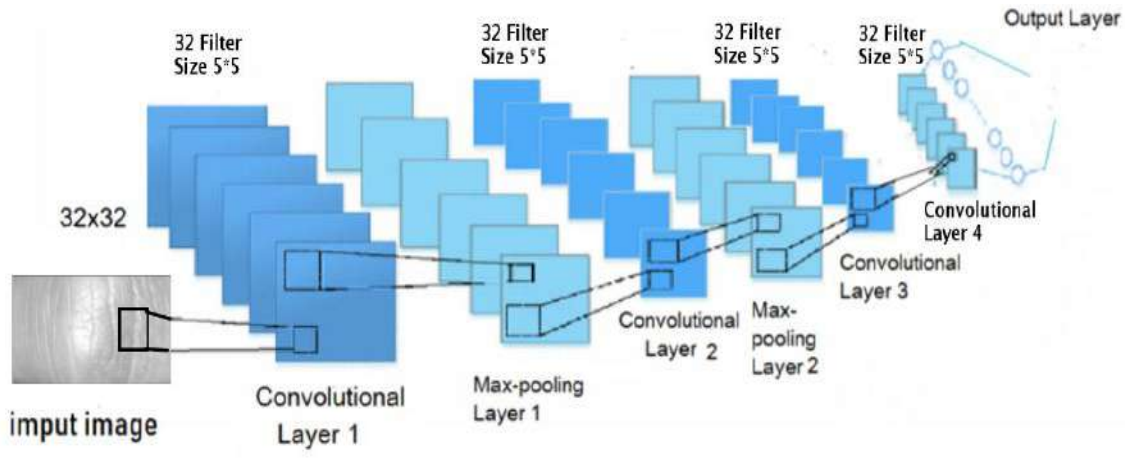

Figure 5.2 – Architecture of the proposed CNN.

5.4 Matching, Fusion Scheme and Decision

Matching score is a measure of similarity between the test (input) and train (template) feature vectors. The high match score can be determined by examining the match scores appertaining to all the comparisons and reporting the identity of the template corresponding to the largest similarity score [67]. Fusion at the matching score level is the most popular and frequently used method because of its good performance and simplicity. The outputs of the two or more matching modules (LIF, LMF, RIF, RMF) are combined using fusion at the matching-score level.

There are several matching-score fusion rules integrate normalized matching scores of a user to produce the final matching score [30].

1. **Simple Sum rule**

   The Simple Sum rule takes the sum of the R matching scores of the $(k)_th$ user as the final matching score S_k of this user. S_k is calculated as follows:

   $$S = 1/N \sum_{i=1}^{N} S_i \tag{5.2}$$

2. **Product rule**

   This rule defines the new scores for each matcher, is calculated as follows:

   $$S = 1/N \prod_{i=1}^{N} S_i \tag{5.3}$$

3. **Minimum rule**

   This rule simply sets a new scores as the minimum score of each matcher's scores, is calculated as follows:

   $$S = min(S_i) \tag{5.4}$$

4. **Maximum rule**

   This rule simply sets a new scores as the maximum score of each matcher's scores, is calculated as follows:

   $$S = max(S_i) \tag{5.5}$$

   The final result of the fusion is a new matching score, which is the basis for the classification decision of the entire system.

5. **Weighted Sum rule**

   The weighted sum of the R matching scores, which is shown in (6), is considered as the final matching score of the k_{th} user.

$$S = \sum_{i=1}^{N} w_i S_i \tag{5.6}$$

   whereW_i represents the weight of the matching score of the i_{th} biometric trait of the k_{th} user. And

$$w_i = \frac{1/\sum_{i=1}^{N} 1/EER_j}{EER_i} \tag{5.7}$$

6. **Weighted Product rule**

   Let W_i stand for the weight of the matching score of the i_{th} biometric trait of the k_{th} user. A Weighted Product rule can determine the final matching score of the k_{th} user using

$$S = \prod_{i=1}^{N} w_i S_i \tag{5.8}$$

   The final result of the fusion is a new matching score, which is the basis for the classification decision of the entire system.

5.5 Experimental Results and Discussion

To evaluate the performance of the proposed biometric system and choose their appropriate parameters, a database of FKP images is required. Thus, our experiment tests were performed using the FKP Database from the Poly University (The Hong Kong Polytechnic University 2018) [147]. The database has a total of 7920 images from 660 different fingers obtained by 165 persons. This dataset including 125 males and 40 females. Among them, 143 subjects were 20-30 years old and the others are 30-50 years old. These images are collected in two separate sessions. The average time interval between the first and the second sessions were about 25 days. The maximum and minimum intervals were 96 and 14 days, respectively. In each session, the subject (person) was asked to provide 12 image samples for each of Left Index Fingers *LIF*, Left Middle Fingers *LMF*, Right Index

Fingers *RIF* and Right Middle Fingers *RMF*. Therefore, 48 image samples from 4 finger types were collected from each subject. To develop a finger knuckle print recognition system, it is necessary to have two databases: a database to perform training (learning) and another techniques to test and determine their performance. For the CNN algorithm, it is better to adopt a more extensive training set to avoid overfitting. In our series of tests, we divided the database as follows: The odd images of each person are used for the learning phase, the remaining 6 (even) images of each individual were used for the various tests. In order to properly analyze our identification system, and in order to achieve satisfactory results, we divided our work into three parts: In the first part, an empirical evaluation is used to select the relevant and suitable parameters of the CNN algorithm (which gives the best system accuracy). These parameters are used in the second part to evaluate the performance of the proposed unimodal biometric system using the different FKP finger knuckle print samples. For this, both identification modes (open-set and closed-set modes) are tested. Finally, in the third and final part, the performance of the multimodal biometric system is evaluated. Our system is implemented using MATLAB 2019a in an experimental platform as a workstation (HP Z8 G4), with a 64-bit Microsoft Windows 10 operating system, equipped with an Intel Xeon Silver 4108 processor, a 32 GB of RAM and a graphic processing unit (GeForce RTX 2080 Ti).

5.5.1 Experimental Setup

To get the best CNN architecture and get a very accurate identification rate, there are many parameters for adjusting a convolutional neural network. In any CNN architecture, there are hyper-parameters and additional parameters. In the essential hyper-parameters, we can find the number of layers, the activation function, the learning rate, the batch size, the number of epochs and the L_2 regularization. On the other hand, the most important additional parameters are the filters size, the number of filters, the padding, the stride, and the pooling-layer. To have an excellent biometric system with reduced complexity, our study focused on a few parameters that we think are important in our work and on the fact that other parameters taken by default have given good results. It's good

practice to start with a fundamental model and afterward attempt to improve it at every step. Our basic model took the following default settings: stochastic gradient descent with momentum, L_2 regularization $= 0,0001$, learning rate $= 0,01$, fixed the maximum number of epochs for training to 30 and used a mini-batch with 128 observations at each iteration. In the rest of this study, we will adopt an empirical evaluation by modifying the number of layers, the size of the filters and the number of filters. It should be noted that each layer of our CNN architecture is composed of a convolution operation, a Relu operation and an optional max-pooling operation which aims to down-sample an input representation (image, hidden layer output matrix, etc.), reducing its dimensionality to retaining the maximum value (activated features) in the sub-regions binned. Table 5.1 illustrates the effect of the above parameters on system performance (LIF). According to this table, the best parameters obtained are the number of layers $= 4$, the size of the filters $= [5,5]$ and the number of filters is $[32;32;32,32]$ for each layer respectively. We will use these parameters in the next subsections.

5.5.2 Performance of the unimodal biometric system

The goal of this experiment is to evaluate the system performance when we using information from each modality (each finger). For this, in Open Set identification we found the performance under different modalities (LIF, LMF, RIF, RMF). Table 5.2 and Fig. 5.3 compares the performance of the unimodal system using CNN feature extraction for various fingers. The experimental results indicate that the LIF, LMF perform better than the RIF and RMF in terms of EER. They give $EER = 1.590 \times 10^{-1}, 2.020 \times 10^{-1}\%$ respectively. Fig. 5.3 (c) compare the closed-set identification results. Like the open-set identification biometric system, the closed-set identification system can achieve high precision with the CNN algorithm. In this case, the system generates a Rank-One Recognition (ROR) equal to 99.93% up to 99.96% with a Rank of Perfect Recognition (RPR) equal to 21 up to 71 for all spectral bands.

Table 5.1 – Identification Rate Under The Design Parameters.

Number Of Layer	**[2]**	**[3]**	**[4]**	**[5]**		
ERR (%)	5.520×10^{-1}	2.120×10^{-1}	1.590×10^{-1}	8.900×10^{-1}		
Number Of Filter	**[8 16 32 64]**	**[16 16 32 64]**	**[32 32 32 32]**	**[32 48 64 128]**	**[64 64 64 64]**	**[32 64 64 32]**
ERR (%)	6.060×10^{-1}	5.480×10^{-1}	1.590×10^{-1}	4.040×10^{-1}	4.040×10^{-1}	2.020×10^{-1}
Filter Size	**[3 3]**	**[4 4]**	**[5 5]**	**[6 6]**	**[7 7]**	**[8 8]**
ERR (%)	4.650×10^{-1}	3.520×10^{-1}	1.590×10^{-1}	4.040×10^{-1}	3.810×10^{-1}	3.706

Table 5.2 – Unimodal Identification Test Results

Fingres	**Open Set**		**Closed Set**	
	T_o	**ERR (%)**	**ROR (%)**	**RPR**
LIF	0.168	1.590×10^{-1}	99.96	21
LMF	0.137	2.020×10^{-1}	98.44	28
RIF	0.082	4.040×10^{-1}	97.77	32
RMF	0.056	5.050×10^{-1}	97.27	71

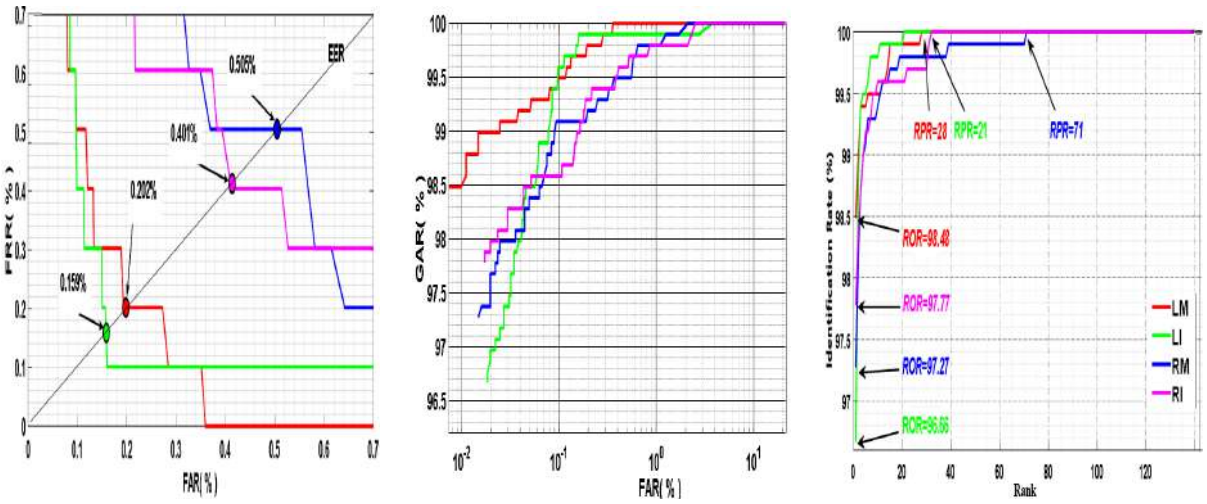

(a) **(b)** **(c)**

Figure 5.3 – Unimodal biometric identification system test results. (a) ROC curves (FRR against FAR), (b) ROC curves (GAR against FAR) and (c) CMC curves, identification rate against rank.

5.5.3 Performance of the multimodal biometric system

Unimodal systems are Faced several problems, such as the possibility of noise in the biometric modality and its non-universality, which increases the system error (EER) [134].

Intra-class dissimilarity, as well as inter-class similarity, can also affect the unimodal biometric system and hence the result of identification [135]. An excellent biometric identification system requires a very low EER value, which can be achieved by the multimodal system [120]. Such a system combined several features of each modality at different levels to improve system performance. To build a multimodal biometric system, unimodal biometric systems can be combined at four different levels, namely the sensor level [136], the feature level [137], the matching score level [138], and the decision level [139].

The goal of the fusion process is to improve the performance by fusing the information from different modalities. To improve more our results, we will try to merge the different scores for different finger to obtain a multimodal system. In this case, we merge the different samples of some fingers (LIF and LMF, RIF and RMF) and at the end we realize a system based on the fusion between the two fingers (LF*RF). Table 5.3 and Fig 5.4 show the performance of the multimodal identification system using different fusion rules, from the results, we note that the PROD rule gives the best result with the LIF+LMF and RIF +RMF in combinations, they gives $EER = 2.210 \times 10 - 2\%$, 0.000% respectively.

In closed set, the system generates a Rank-One Recognition (ROR) equal to 100%. The analysis of the data showed that the results of the multimodal fusion were much better than those of the unimodal biometric systems. The multimodal system have a ($EER = 0.000\%$) and an ($ROR = 100\%$) and an ($RPR = 01$), there by obtaining a perfect result. This ideal precision can be reduced to a large database. The PROD rule is the best compared to another rules because it gives a perfect result and it is simple to use.

Table 5.3 – Multimodal Biometric Identification System Test Results

FUSION RULES	LIF-LMF				RIF-RMF			
	Open Set		Closed Set		Open Set		Closed Set	
	T_o	ERR (%)	ROR (%)	RPR	T_o	ERR(%)	ROR(%)	RPR
SUM	0.559	2.210×10^{-2}	100	01	0.288	1.010×10^{-1}	100	01
WHT SUM	0.559	2.210×10^{-1}	98.78	02	0.279	1.010×10^{-1}	100	01
PROD	0.366	3.690×10^{-3}	100	01	0.034	2.210×10^{-2}	100	01
WHT PROD	0.569	7.390×10^{-3}	100	01	0.221	2.210×10^{-2}	100	01
MIN	0.366	7.380×10^{-3}	100	01	0.067	1.010×10^{-1}	100	01
MAX	0.388	1.010×10^{-1}	97.57	02	0.988	5.660×10^{-2}	99.39	02

LF-RF-ALL Fingers				
Fusion rules	Open Set		Closed Set	
	T_o	ERR(%)	ROR(%)	RPR
SUM	0.854	1.230×10^{-3}	100	01
WHT SUM	0.717	4.920×10^{-3}	100	01
PROD	0.089	0.000	100	01
WHT PROD	0.441	0.000	100	01
MIN	0.137	3.690×10^{-3}	100	01
MAX	0.988	5.660×10^{-2}	96.96	02

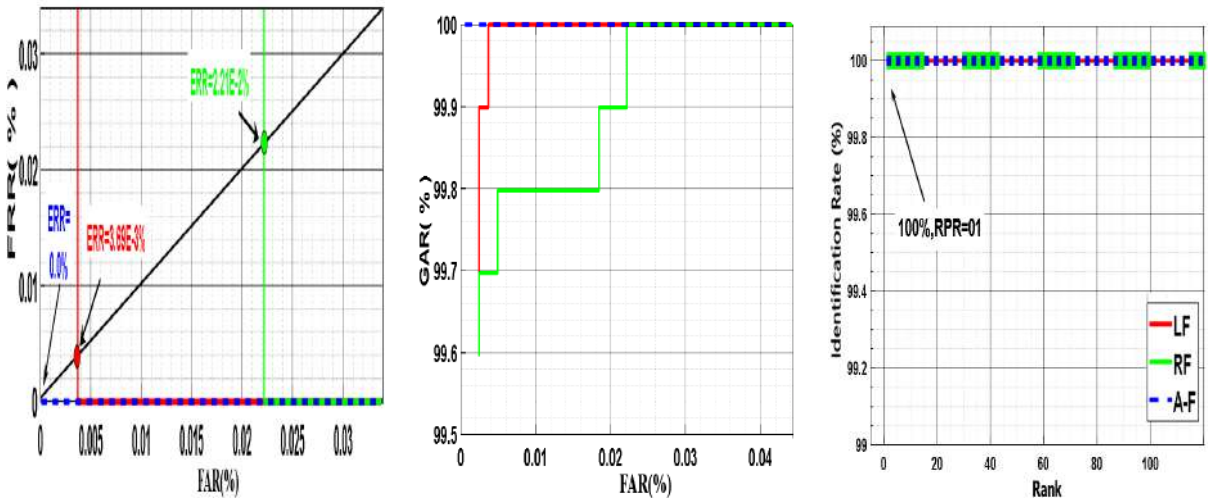

(a) (b) (c)

Figure 5.4 – Multimodal biometric identification system test results. (a) ROC curves (FRR against FAR), (b) ROC curves (GAR against FAR) and (c) CMC curves, identification rate against rank.

5.6 Conclusion and Further Work

This work provides a multimodal biometric system based on fusion of the sub-systems outputs at matching score level by using the FKP database (which consists LIF, LMF, RIF and RMF fingers). In this context, we have implemented the CNN deep learning

technique. The experimental results show that the combination of fingers modalities images performs better against the one finger modality and results up to EER of 0.000% for open-set identification and a ROR of 100% for closed-set identification.

In conclusion, the fusion schemes with multimodal systems gave significantly better performances than their unimodal systems. Our future work will project to use other finger knuckle print databases (CASIA) with other deep learning techniques (like Deep Belief Network (DBN) and autoencoder neural network) and their use in feature extraction methods.

Chapter 6

General conclusion and Perspectives

6.1 General Conclusion

The study discussed in this thesis concerns the automatic identification of individuals based on their biometric characteristics. We have proposed unimodal and multimodal biometric systems based on the two most important biometric modalities: the palmprint and the finger knuckle print. This thesis aims to improve the performance of identification systems using palmprints and finger knuckle prints by employing various approaches and sets of operations.

We used deep learning methods for feature extraction in the first proposed system based on palmprint recognition. For this reason, we have developed the simplified PalmNet–Gabor using Log-Gabor filters to increase the pixel for preprocessing. In order to decrease the feature vector size and increase recognition accuracy, we have selected relevant features using Fisher score, ReliefF, and dimensionality reduction (WPCA) methods. Besides, we fused modalities at the matching score level for the multimodal system to improve system performance. The experimental results performed on the multispectral PolyU database and contactless Tongji and PolyU 2D/3D databases using a single modality (unimodal) obtained a very high identification accuracy (EER = 0:000% and ROR =

100%). It gave a CPU time of less than 0.009 s and reduced the feature vector size to 410. Likewise, the multimodal identification system performed on the CASIA database offers perfect results with EER = 0:000% for the open-set identification and ROR = 100% for the closed-set identification.

We designed unimodal and multimodal based on palmprint recognition for the second proposed system. Our method uses a Convolutional Neural Network (CNN) deep learning technique for feature extraction and classification. The experiment evaluated the multimodal system on the fusion of palmprint and palm-vein modalities at the matching scores level using five methods of fusion, which are the sum of the scores (SUM), the sum of the weighted scores (WHT SUM), the product of the scores (MUL), the product of the weighted scores (WHT MUL) and the minimum score (MIN). All fusion rules produced the best result with a value of 0% EER in open-set mode and a ROR of 100% in closed-set mode.

The last proposed systems were unimodal and multimodal based on finger knuckle print recognition. We used the Convolutional Neural Network (CNN) deep learning technique to extract deep palmprint features. In our experiments, we first evaluate each biometric identification system based on a single spectral band (unimodal system). Then, the results of two or more unimodal systems are fused at the matching score level to create an efficient and robust multimodal identification system. Therefore, the experimental results were obtained using a large and available FKP database (which consists of LIF, LMF, RIF, and RMF fingers) and show that the combination of finger modalities images performs better against the one finger modality and results up to EER of 0.000% for open-set identification and a ROR of 100% for closed-set identification. Moreover, the results indicate that the proposed method is more efficient than other approaches in the literature. In conclusion, the fusion schemes with multimodal systems gave significantly better performances than their unimodal systems.

6.2 Perspectives

Although the proposed approaches have demonstrated high performance for hand modalities recognition, they could be developed and improved in future works.

1. We will test our first proposed method with other large databases, such as the Hyperspectral PolyU or 3D databases. We will also employ additional clustering and dimensionality reduction techniques. Furthermore, we will employ the graphics processing unit (GPU) to reduce processing time, which is a valuable tool for speeding up the processing speed of computationally intensive algorithms. Moreover, we will test our proposed method on another trait, such as the face or Iris.

2. We will test our second proposed method on other deep learning techniques (like Deep Belief Network (DBN) and autoencoder neural network) and their use in feature extraction methods. We will also change other classifiers and other distance measures.

3. We will try to use large finger knuckle print databases like the CASIA database with other deep learning techniques and an autoencoder neural network for the last proposed method. We will test our proposed method on another trait, such as the face or iris.

Personal Contributions

Publications

— **Trabelsi, Selma** & Samai, Djamel & Dornaika, Fadi & Benlamoudi, Azeddine & Bensid, Khaled & Taleb-Ahmed, Abdelmalik. (2022). **Efficient palmprint biometric identification systems using deep learning and feature selection methods.** Neural Computing and Applications. https://doi.org/10.1007/s00521-022-07098-4.

International Communications

— **S. Trabelsi**, D. Samai, A. Meraoumia, K. Bensid and A. Taleb-Ahmed, **"An Improved Multispectral Palmprint System Using Deep CNN-based Palm-Features,"** 2019 International Conference on Advanced Electrical Engineering (ICAEE), Algiers, Algeria, 2019, pp. 1-6, https://doi.org/10.1109/ICAEE47123.2019.9015074.

— **S. Trabelsi**, D. Samai, A. Meraoumia, K. Bensid, A. Benlamoudi, F. Dornaika and A. Taleb-Ahmed, **"Finger-Knuckle-Print Recognition Using Deep Convolutional Neural Network,"** 020 1st International Conference on Communications, Control Systems and Signal Processing (CCSSP), EL OUED, Algeria, 2020, pp. 163-168, https://doi.org/10.1109/CCSSP49278.2020.9151531.

Bibliography

[1] A. K. Jain, P. Flynn, and A. A. Ross, *Handbook of biometrics*. Springer Science & Business Media, 2007.

[2] D. D. Zhang *et al.*, *Palmprint authentication*. Springer Science & Business Media, 2004.

[3] R. Ren, K. Han, P. Zhao, J. Shi, L. Zhao, D. Gao, Z. Zhang, and Z. Yang, "Identification of asphalt fingerprints based on atr-ftir spectroscopy and principal component-linear discriminant analysis," *Construction and Building Materials*, vol. 198, pp. 662–668, 2019. [Online]. Available: https://doi.org/10.1016/j.conbuildmat.2018.12.009

[4] Y. Yang, C. Hou, Y. Lang, D. Guan, D. Huang, and J. Xu, "Open-set human activity recognition based on micro-doppler signatures," *Pattern Recognition*, vol. 85, pp. 60–69, 2019.

[5] L. Fei, B. Zhang, W. Zhang, and S. Teng, "Local apparent and latent direction extraction for palmprint recognition," *Information Sciences*, vol. 473, pp. 59–72, 2019. [Online]. Available: https://doi.org/10.1016/j.ins.2018.09.032

[6] C. Wang, J. Muhammad, Y. Wang, Z. He, and Z. Sun, "Towards complete and accurate iris segmentation using deep multi-task attention network for non-cooperative iris recognition," *IEEE Transactions on information forensics and security*, vol. 15, pp. 2944–2959, 2020. [Online]. Available: https://doi.org/10.1109/TIFS.2020.2980791

[7] T. Tuncer and S. Dogan, "Novel dynamic center based binary and ternary pattern network using m4 pooling for real world voice recognition," *Applied Acoustics*, vol.

156, pp. 176–185, 2019.

[8] I. Adjabi, A. Ouahabi, A. Benzaoui, and A. Taleb-Ahmed, "Past, present, and future of face recognition: A review," *Electronics*, vol. 9, no. 8, p. 1188, 2020. [Online]. Available: https://doi.org/10.3390/electronics9081188

[9] S. Trabelsi, D. Samai, A. Meraoumia, K. Bensid, and A. Taleb-Ahmed, "An improved multispectral palmprint system using deep cnn-based palm-features," in *International Conference on Advanced Electrical Engineering (ICAEE)*. IEEE, 2019, pp. 1–6.

[10] N. Charfi, H. Trichili, A. M. Alimi, and B. Solaiman, "Personal verification system using hand modalities." *Journal of Information Assurance & Security*, vol. 11, no. 3, 2016.

[11] A. Kong, D. Zhang, and M. Kamel, "A survey of palmprint recognition," *pattern recognition*, vol. 42, no. 7, pp. 1408–1418, 2009. [Online]. Available: https://doi.org/10.1016/j.patcog.2009.01.018

[12] N. Charfi, "Biometric recognition based on hand schape and palmprint modalities," Ph.D. dissertation, Ecole nationale supérieure Mines-Télécom Atlantique, 2017.

[13] F. Belhadj, "Biometric system for identification and authentication," Ph.D. dissertation, Ecole nationale Supérieure en Informatique Alger, 2017.

[14] A. Kong, D. Zhang, and M. Kamel, "Palmprint identification using feature-level fusion," *Pattern Recognition*, vol. 39, no. 3, pp. 478–487, 2006. [Online]. Available: https://doi.org/10.1016/j.patcog.2005.08.014

[15] X. Wu, D. Zhang, and K. Wang, "Palm line extraction and matching for personal authentication," *IEEE Transactions on Systems, Man, and Cybernetics-Part A: Systems and Humans*, vol. 36, no. 5, pp. 978–987, 2006.

[16] W. Li, L. Zhang, and D. Zhang, "Three dimensional palmprint recognition," in *IEEE International Conference on Systems, Man and Cybernetics*. IEEE, 2009, pp. 4847–4852. [Online]. Available: https://doi.org/10.1109/ICSMC.2009.5346053

[17] A. Morales, M. A. Ferrer, and A. Kumar, "Towards contactless palmprint authentication," *IET computer vision*, vol. 5, no. 6, pp. 407–416, 2011.

[18] L. Fei, G. Lu, W. Jia, S. Teng, and D. Zhang, "Feature extraction methods for palmprint recognition: A survey and evaluation," *IEEE Transactions on Systems, Man, and Cybernetics: Systems*, vol. 49, no. 2, pp. 346–363, 2018.

[19] D. Zhang, W.-K. Kong, J. You, and M. Wong, "Online palmprint identification," *IEEE Transactions on pattern analysis and machine intelligence*, vol. 25, no. 9, pp. 1041–1050, 2003. [Online]. Available: https://doi.org/10.1109/TPAMI.2003.1227981

[20] A. Kumar and D. Zhang, "Integrating shape and texture for hand verification," *International Journal of Image and Graphics*, vol. 6, no. 01, pp. 101–113, 2006.

[21] L. Zhang and D. Zhang, "Characterization of palmprints by wavelet signatures via directional context modeling," *IEEE Transactions on Systems, Man, and Cybernetics, Part B (Cybernetics)*, vol. 34, no. 3, pp. 1335–1347, 2004.

[22] D. Zhang and W. Shu, "Two novel characteristics in palmprint verification: datum point invariance and line feature matching," *Pattern recognition*, vol. 32, no. 4, pp. 691–702, 1999.

[23] A. Kumar, D. Wong, H. C. Shen, and A. K. Jain, "Personal verification using palmprint and hand geometry biometric," in *International conference on audio-and video-based biometric person authentication*. Springer, 2003, pp. 668–678.

[24] X. Wu, D. Zhang, and K. Wang, "Fisherpalms based palmprint recognition," *Pattern recognition letters*, vol. 24, no. 15, pp. 2829–2838, 2003.

[25] G. Lu, D. Zhang, and K. Wang, "Palmprint recognition using eigenpalms features," *Pattern Recognition Letters*, vol. 24, no. 9-10, pp. 1463–1467, 2003. [Online]. Available: https://doi.org/10.1016/S0167-8655(02)00386-0

[26] W. Zuo, D. Zhang, and K. Wang, "An assembled matrix distance metric for 2dpca-based image recognition," *Pattern Recognition Letters*, vol. 27, no. 3, pp. 210–216, 2006.

[27] D. Han, Z. Guo, and D. Zhang, "Multispectral palmprint recognition using wavelet-based image fusion," in *2008 9th International Conference on Signal Processing*. IEEE, 2008, pp. 2074–2077.

[28] Z. Guo, D. Zhang, and L. Zhang, "Is white light the best illumination for palmprint recognition?" in *International conference on computer analysis of images and patterns*. Springer, 2009, pp. 50–57.

[29] Y. Hao, Z. Sun, T. Tan, and C. Ren, "Multispectral palm image fusion for accurate contact-free palmprint recognition," in *15th IEEE International Conference on Image Processing*. IEEE, 2008, pp. 281–284.

[30] D. Zhang, Z. Guo, G. Lu, L. Zhang, and W. Zuo, "An online system of multispectral palmprint verification," *IEEE transactions on instrumentation and measurement*, vol. 59, no. 2, pp. 480–490, 2009. [Online]. Available: https://doi.org/10.1109/TIM.2009.2028772

[31] Z. Khan, A. Mian, and Y. Hu, "Contour code: Robust and efficient multispectral palmprint encoding for human recognition," in *2011 International Conference on Computer Vision*. IEEE, 2011, pp. 1935–1942.

[32] J.-R. Cui, "Multispectral palmprint recognition using image-based linear discriminant analysis," *International Journal of Biometrics*, vol. 4, no. 2, pp. 106–115, 2012.

[33] X. Xu, Z. Guo, C. Song, and Y. Li, "Multispectral palmprint recognition using a quaternion matrix," *Sensors*, vol. 12, no. 4, pp. 4633–4647, 2012.

[34] Z. Guo, L. Zhang, and D. Zhang, "Feature band selection for multispectral palmprint recognition," in *2010 20th International Conference on Pattern Recognition*. IEEE, 2010, pp. 1136–1139.

[35] D. Zhang, G. Lu, W. Li, L. Zhang, and N. Luo, "Palmprint recognition using 3-d information," *IEEE Transactions on Systems, Man, and Cybernetics, Part C (Applications and Reviews)*, vol. 39, no. 5, pp. 505–519, 2009.

[36] D. Zhang, V. Kanhangad, N. Luo, and A. Kumar, "Robust palmprint verification using 2d and 3d features," *Pattern Recognition*, vol. 43, no. 1, pp. 358–368, 2010.

[37] J. Cui, "2d and 3d palmprint fusion and recognition using pca plus tptsr method," *Neural Computing and Applications*, vol. 24, no. 3, pp. 497–502, 2014. [Online]. Available: https://doi.org/10.1007/s00521-012-1265-y

[38] A. d. Santos Sierra, C. Sánchez Ávila, J. Guerra Casanova, and G. B. d. Pozo, "Invariant hand biometrics feature extraction," in *Chinese Conference on Biometric Recognition*. Springer, 2011, pp. 108–115.

[39] A. Genovese, V. Piuri, and F. Scotti, *Touchless palmprint recognition systems*. Springer, 2014, vol. 60.

[40] L. Liu, D. Zhang, and J. You, "Detecting wide lines using isotropic nonlinear filtering," *IEEE Transactions on image processing*, vol. 16, no. 6, pp. 1584–1595, 2007.

[41] Y. Wang and Q. Ruan, "Palm-line extraction using steerable filters," in *2006 8th international Conference on Signal Processing*, vol. 3. IEEE, 2006.

[42] X. Wu, K. Wang, and D. Zhang, "Hmms based palmprint identification," in *International Conference on Biometric Authentication*. Springer, 2004, pp. 775–781.

[43] W. W. Boles and S. Chu, "Personal identification using images of the human palm," in *TENCON'97 Brisbane-Australia. Proceedings of IEEE TENCON'97. IEEE Region 10 Annual Conference. Speech and Image Technologies for Computing and Telecommunications (Cat. No. 97CH36162)*, vol. 1. IEEE, 1997, pp. 295–298.

[44] S.-Y. Kung, S.-H. Lin, and M. Fang, "A neural network approach to face/palm recognition," in *Proceedings of 1995 IEEE Workshop on Neural Networks for Signal Processing*. IEEE, 1995, pp. 323–332.

[45] D.-S. Huang, W. Jia, and D. Zhang, "Palmprint verification based on principal lines," *Pattern Recognition*, vol. 41, no. 4, pp. 1316–1328, 2008. [Online]. Available: https://doi.org/10.1016/j.patcog.2007.08.016

[46] M. K. Leung, A. C. M. Fong, and S. C. Hui, "Palmprint verification for controlling access to shared computing resources," *IEEE Pervasive Computing*, vol. 6, no. 4, pp. 40–47, 2007.

[47] M. R. Diaz, C. M. Travieso, J. B. Alonso, and M. A. Ferrer, "Biometric system based in the feature of hand palm," in *38th Annual 2004 International Carnahan Conference on Security Technology*. IEEE, 2004, pp. 136–139.

[48] A.-K. Kong and D. Zhang, "Competitive coding scheme for palmprint verification," in *Proceedings of the 17th International Conference on Pattern Recognition, ICPR*, vol. 1. IEEE, 2004, pp. 520–523.

[49] A. Kong, K.-H. Cheung, D. Zhang, M. Kamel, and J. You, "An analysis of biohashing and its variants," *Pattern recognition*, vol. 39, no. 7, pp. 1359–1368, 2006. [Online]. Available: https://doi.org/10.1016/j.patcog.2005.10.025

[50] W. Jia, D.-S. Huang, and D. Zhang, "Palmprint verification based on robust line orientation code," *Pattern Recognition*, vol. 41, no. 5, pp. 1504–1513, 2008.

[51] W. Zuo, Z. Lin, Z. Guo, and D. Zhang, "The multiscale competitive code via sparse representation for palmprint verification," in *IEEE Computer Society Conference on Computer Vision and Pattern Recognition*. IEEE, 2010, pp. 2265–2272.

[52] L. Fei, Y. Xu, W. Tang, and D. Zhang, "Double-orientation code and nonlinear matching scheme for palmprint recognition," *Pattern Recognition*, vol. 49, pp. 89–101, 2016.

[53] L. Fei, B. Zhang, Y. Xu, and L. Yan, "Palmprint recognition using neighboring direction indicator," *IEEE transactions on human-machine systems*, vol. 46, no. 6, pp. 787–798, 2016.

[54] Y. Xu, L. Fei, J. Wen, and D. Zhang, "Discriminative and robust competitive code for palmprint recognition," *IEEE transactions on systems, man, and cybernetics: systems*, vol. 48, no. 2, pp. 232–241, 2016.

[55] X.-Y. Jing and D. Zhang, "A face and palmprint recognition approach based on discriminant dct feature extraction," *IEEE Transactions on Systems, Man, and Cybernetics, Part B (Cybernetics)*, vol. 34, no. 6, pp. 2405–2415, 2004. [Online]. Available: https://doi.org/10.1109/TSMCB.2004.837586

[56] Y.-T. Luo, L.-Y. Zhao, B. Zhang, W. Jia, F. Xue, J.-T. Lu, Y.-H. Zhu, and B.-Q. Xu, "Local line directional pattern for palmprint recognition," *Pattern Recognition*, vol. 50, pp. 26–44, 2016.

[57] W. Kang, Y. Liu, Q. Wu, and X. Yue, "Contact-free palm-vein recognition based on local invariant features," *PloS one*, vol. 9, no. 5, p. e97548, 2014.

[58] A. A. Altun, "A combination of genetic algorithm, particle swarm optimization and neural network for palmprint recognition," *Neural Computing and Applications*, vol. 22, no. 1, pp. 27–33, 2013.

[59] S. Minaee and Y. Wang, "Palmprint recognition using deep scattering network," in *IEEE international symposium on circuits and systems (ISCAS)*. IEEE, 2017, pp. 1–4.

[60] D. Zhong, X. Du, and K. Zhong, "Decade progress of palmprint recognition: A brief survey," *Neurocomputing*, vol. 328, pp. 16–28, 2019. [Online]. Available: https://doi.org/10.1016/j.neucom.2018.03.081

[61] X. Wang, L. Lei, and M. Wang, "Palmprint verification based on 2d–gabor wavelet and pulse-coupled neural network," *Knowledge-Based Systems*, vol. 27, pp. 451–455, 2012.

[62] S. Minaee and Y. Wang, "Palmprint recognition using deep scattering convolutional network," *arXiv preprint arXiv:1603.09027*, 2016.

[63] J. Svoboda, J. Masci, and M. M. Bronstein, "Palmprint recognition via discriminative index learning," in *23rd International Conference on Pattern Recognition (ICPR)*. IEEE, 2016, pp. 4232–4237.

[64] A. Meraoumia, F. Kadri, H. Bendjenna, S. Chitroub, and A. Bouridane, "Improving biometric identification performance using pcanet deep learning and multispectral palmprint," in *Biometric security and privacy*. Springer, 2017, pp. 51–69.

[65] J. Cheng, Q. Sun, J. Zhang, and Q. Zhang, "Supervised hashing with deep convolutional features for palmprint recognition," in *Chinese Conference on Biometric Recognition*. Springer, 2017, pp. 259–268.

[66] J. Zhou, Y. Wang, Z. Sun, Z. Jia, J. Feng, S. Shan, K. Ubul, and Z. Guo, *Biometric Recognition: 13th Chinese Conference, CCBR 2018, Urumqi, China, August 11-12, 2018, Proceedings*. Springer, 2018, vol. 10996.

[67] K. Bensid, D. Samai, F. Z. Laallam, and A. Meraoumia, "Deep learning feature extraction for multispectral palmprint identification," *Journal of Electronic Imaging*, vol. 27, no. 3, p. 033018, 2018.

[68] A. Genovese, V. Piuri, K. N. Plataniotis, and F. Scotti, "Palmnet: Gabor-pca convolutional networks for touchless palmprint recognition," *IEEE Transactions on Information Forensics and Security*, vol. 14, no. 12, pp. 3160–3174, 2019. [Online]. Available: https://doi.org/10.1109/TIFS.2019.2911165

[69] S. Zhao and B. Zhang, "Joint constrained least-square regression with deep convolutional feature for palmprint recognition," *IEEE Transactions on Systems, Man, and Cybernetics: Systems*, vol. 52, no. 1, pp. 511–522, 2020.

[70] L. Fei, Y. Xu, B. Zhang, X. Fang, and J. Wen, "Low-rank representation integrated with principal line distance for contactless palmprint recognition," *Neurocomputing*, vol. 218, pp. 264–275, 2016.

[71] G. Arora, S. Kalra, A. Bhatia, and K. Tiwari, "Palmhashnet: Palmprint hashing network for indexing large databases to boost identification," *IEEE Access*, vol. 9, pp. 145 912–145 928, 2021.

[72] W. Kim, J. M. Song, and K. R. Park, "Multimodal biometric recognition based on convolutional neural network by the fusion of finger-vein and finger shape using near-infrared (nir) camera sensor," *Sensors*, vol. 18, no. 7, p. 2296, 2018. [Online]. Available: https://doi.org/10.3390/s18072296

[73] A. M. Kumar, A. Chandralekha, Y. Himaja, and S. M. Sai, "Local binary pattern based multimodal biometric recognition using ear and fkp with feature level fusion," in *IEEE International Conference on Intelligent Techniques in Control, Optimization and Signal Processing (INCOS)*. IEEE, 2019, pp. 1–5.

[74] R. Hammouche, A. Attia, and S. Akrouf, "A novel system based on phase congruency and gabor-filter bank for finger knuckle pattern authentication," *ICTACT J Image Video Process*, vol. 10, no. 3, pp. 2125–2131, 2020.

[75] L. Zhang, L. Zhang, D. Zhang, and H. Zhu, "Ensemble of local and global information for finger–knuckle-print recognition," *Pattern recognition*, vol. 44, no. 9, pp. 1990–1998, 2011. [Online]. Available: https://doi.org/10.1016/j.patcog.2010.06.007

[76] ——, "Online finger-knuckle-print verification for personal authentication," *Pattern recognition*, vol. 43, no. 7, pp. 2560–2571, 2010.

[77] C. Hegde, P. D. Shenoy, K. Venugopal, and L. Patnaik, "Fkp biometrics for human authentication using gabor wavelets," in *IEEE Region 10 Conference*. IEEE, 2011, pp. 1149–1153.

[78] G. Badrinath, A. Nigam, and P. Gupta, "An efficient finger-knuckle-print based recognition system fusing sift and surf matching scores," in *International Conference on Information and Communications Security*. Springer, 2011, pp. 374–387.

[79] S. Aoyama, K. Ito, and T. Aoki, "A finger-knuckle-print recognition algorithm using phase-based local block matching," *Information Sciences*, vol. 268, pp. 53–64, 2014. [Online]. Available: https://doi.org/10.1016/j.ins.2013.08.025

[80] G. Jaswal, R. Nath, and A. Kaul, "Fkp based personal authentication using sift features extracted from pip joint," in *2015 third international conference on image information processing (ICIIP)*. IEEE, 2015, pp. 214–219.

[81] A. Nigam, K. Tiwari, and P. Gupta, "Multiple texture information fusion for finger-knuckle-print authentication system," *Neurocomputing*, vol. 188, pp. 190–205, 2016.

[82] A. B. Waghode and C. Manjare, "Biometric authentication of person using finger knuckle," in *2017 International Conference on Computing, Communication, Control and Automation (ICCUBEA)*. IEEE, 2017, pp. 1–6.

[83] Y. Zhai, H. Cao, L. Cao, H. Ma, J. Gan, J. Zeng, V. Piuri, F. Scotti, W. Deng, Y. Zhi *et al.*, "A novel finger-knuckle-print recognition based on batch-normalized cnn," in *Chinese conference on biometric recognition*. Springer, 2018, pp. 11–21.

[84] M. Chaa, N.-E. Boukezzoula, and A. Meraoumia, "Features-level fusion of reflectance and illumination images in finger-knuckle-print identification system," *International Journal on Artificial Intelligence Tools*, vol. 27, no. 03, p. 1850007, 2018. [Online]. Available: https://doi.org/10.1142/S0218213018500070

[85] A. Attia, A. Moussaoui, M. Chaa, and Y. Chahir, "Finger-knuckle-print recognition system based on features-level fusion of real and imaginary images," *Journal on Image and Video Processing*, 2018.

[86] J. Kim, K. Oh, B.-S. Oh, Z. Lin, and K.-A. Toh, "A line feature extraction method for finger-knuckle-print verification," *Cognitive Computation*, vol. 11, no. 1, pp. 50–70, 2019. [Online]. Available: https://doi.org/10.1007/s12559-018-9593-6

[87] A. Muthukumar and A. Kavipriya, "A biometric system based on gabor feature extraction with svm classifier for finger-knuckle-print," *Pattern Recognition Letters*, vol. 125, pp. 150–156, 2019. [Online]. Available: https://doi.org/10.1016/j.patrec.2019.04.007

[88] R. Chlaoua, A. Meraoumia, K. E. Aiadi, and M. Korichi, "Deep learning for finger-knuckle-print identification system based on pcanet and svm classifier," *Evolving Systems*, vol. 10, no. 2, pp. 261–272, 2019. [Online]. Available: https://doi.org/10.1007/s12530-018-9227-y

[89] A. Attia, M. Chaa, Z. Akhtar, and Y. Chahir, "Finger kunckcle patterns based person recognition via bank of multi-scale binarized statistical texture features," *Evolving Systems*, vol. 11, no. 4, pp. 625–635, 2020.

[90] T. Joshi, S. Dey, and D. Samanta, "Multimodal biometrics: state of the art in fusion techniques," *International Journal of Biometrics*, vol. 1, no. 4, pp. 393–417, 2009.

[91] D. Zhang, Z. Guo, and Y. Gong, "Multispectral biometrics systems," in *Multispectral biometrics*. Springer, 2016, pp. 23–35. [Online]. Available: https://doi.org/10.1007/978-3-319-22485-5_2

[92] J. Deng, J. Guo, N. Xue, and S. Zafeiriou, "Arcface: Additive angular margin loss for deep face recognition," in *Proceedings of the IEEE/CVF conference on computer vision and pattern recognition*, 2019, pp. 4690–4699.

[93] K. W. Bowyer and M. J. Burge, "Introduction to the handbook of iris recognition," in *Handbook of Iris Recognition*. Springer, 2016, pp. 1–22.

[94] C. Wan, L. Wang, and V. V. Phoha, "A survey on gait recognition," *ACM Computing Surveys (CSUR)*, vol. 51, no. 5, pp. 1–35, 2018.

[95] L. Eljawad, R. Aljamaeen, M. Alsmadi, I. Almarashdeh, H. Abouelmagd, S. Alsmadi, F. Haddad, R. Alkhasawneh, M. Alazzam *et al.*, "Arabic voice recognition

using fuzzy logic and neural network," *International Journal of Applied Engineering Research*, pp. 651–662, 2019.

[96] E. A. Kochegurova, E. Gorokhova, and A. Mozgaleva, "Development of the keystroke dynamics recognition system," in *Journal of Physics: Conference Series*, vol. 803, no. 1. IOP Publishing, 2017, p. 012073.

[97] M. Elhoseny, A. Nabil, A. E. Hassanien, and D. Oliva, "Hybrid rough neural network model for signature recognition," in *Advances in Soft Computing and Machine Learning in Image Processing*. Springer, 2018, pp. 295–318.

[98] W. El-Tarhouni, L. Boubchir, M. Elbendak, and A. Bouridane, "Multispectral palmprint recognition using pascal coefficients-based lbp and phog descriptors with random sampling," *Neural Computing and Applications*, vol. 31, no. 2, pp. 593–603, 2019. [Online]. Available: https://doi.org/10.1007/s00521-017-3092-7

[99] A. Serrano, I. M. de Diego, C. Conde, and E. Cabello, "Recent advances in face biometrics with gabor wavelets: A review," *Pattern Recognition Letters*, vol. 31, no. 5, pp. 372–381, 2010.

[100] N. Xu, Q. Zhu, X. Xu, and D. Zhang, "An effective recognition approach for contactless palmprint," *The Visual Computer*, vol. 37, no. 4, pp. 695–705, 2021.

[101] A. Tahmasebi and H. Pourghassem, "Robust intra-class distance-based approach for multimodal biometric game theory-based rank-level fusion of ear, palmprint and signature," *Iranian Journal of Science and Technology, Transactions of Electrical Engineering*, vol. 41, no. 1, pp. 51–64, 2017. [Online]. Available: https://doi.org/10.1007/s40998-017-0017-5

[102] X. Bai, Z. Meng, N. Gao, Z. Zhang, and D. Zhang, "3d palmprint identification using blocked histogram and improved sparse representation-based classifier," *Neural Computing and Applications*, vol. 32, no. 16, pp. 12 547–12 560, 2020.

[103] M. Farmanbar and Ö. Toygar, "Feature selection for the fusion of face and palmprint biometrics," *Signal, Image and Video Processing*, vol. 10, no. 5, pp. 951–958, 2016.

[104] I. Guyon, S. Gunn, M. Nikravesh, and L. A. Zadeh, *Feature extraction: foundations and applications*. Springer, 2008, vol. 207. [Online]. Available: https://doi.org/10.1007/978-3-540-35488-8

[105] G. Roffo, "Feature selection library (matlab toolbox)," *arXiv preprint arXiv:1607.01327*, 2016.

[106] J. E. Tapia and C. A. Perez, "Clusters of features using complementary information applied to gender classification from face images," *IEEE Access*, vol. 7, pp. 79 374–79 387, 2019.

[107] S. Chormunge and S. Jena, "Correlation based feature selection with clustering for high dimensional data," *Journal of Electrical Systems and Information Technology*, vol. 5, no. 3, pp. 542–549, 2018. [Online]. Available: https://doi.org/10.1016/j.jesit.2017.06.004

[108] S. Hijazi, "Semi-supervised margin-based feature selection for classification," Ph.D. dissertation, Université du Littoral Côte d'Opale; École Doctorale des Sciences et de Technologie (Beyrouth)), 2019.

[109] S. Alelyani, J. Tang, and H. Liu, "Feature selection for clustering: A review," *Data Clustering*, pp. 29–60, 2018.

[110] E. Hancer, B. Xue, and M. Zhang, "A survey on feature selection approaches for clustering," *Artificial Intelligence Review*, vol. 53, no. 6, pp. 4519–4545, 2020.

[111] K. Kira and L. A. Rendell, "A practical approach to feature selection," in *Machine learning proceedings 1992*. Elsevier, 1992, pp. 249–256.

[112] I. Kononenko, E. Šimec, and M. Robnik-Šikonja, "Overcoming the myopia of inductive learning algorithms with relieff," *Applied Intelligence*, vol. 7, no. 1, pp. 39–55, 1997. [Online]. Available: https://doi.org/10.1023/A:1008280620621

[113] J. Cervantes, F. Garcia-Lamont, L. Rodríguez-Mazahua, and A. Lopez, "A comprehensive survey on support vector machine classification: Applications, challenges and trends," *Neurocomputing*, vol. 408, pp. 189–215, 2020.

[114] D. Zhang, F. Song, Y. Xu, and Z. Liang, *Advanced pattern recognition technologies with applications to biometrics*. IGI Global, 2009.

[115] C. A. of Sciences, "Casia multispectral palmprint database," *I.o.A.*, 2008.

[116] L. Zhang, L. Li, A. Yang, Y. Shen, and M. Yang, "Towards contactless palmprint recognition: A novel device, a new benchmark, and a collaborative representation based identification approach," *Pattern Recognition*, vol. 69, pp. 199–212, 2017. [Online]. Available: https://doi.org/10.1016/j.patcog.2017.04.016

[117] H. K. P. U. Hong Kong Polytechnic University, *PolyU 2D/3D Contact-free palmprint database*, 2011.

[118] F. Wang and J. Han, "Robust multimodal biometric authentication integrating iris, face and palmprint," *Information technology and control*, vol. 37, no. 4, 2008.

[119] M. O. Oloyede and G. P. Hancke, "Unimodal and multimodal biometric sensing systems: a review," *IEEE access*, vol. 4, pp. 7532–7555, 2016.

[120] W. Yang, J. Hu, S. Wang, and C. Chen, "Mutual dependency of features in multimodal biometric systems," *Electronics Letters*, vol. 51, no. 3, pp. 234–235, 2015.

[121] C. Kant and S. Chaudhary, "A multimodal biometric system based on finger knuckle print, fingerprint, and palmprint traits," in *Innovations in Computational Intelligence and Computer Vision*. Springer, 2021, pp. 182–192.

[122] L. Wang, "Some issues of biometrics: technology intelligence, progress and challenges," *International Journal of Information Technology and Management*, vol. 11, no. 1-2, pp. 72–82, 2012.

[123] S. Majumder, K. J. Devi, and S. K. Sarkar, "Singular value decomposition and wavelet-based iris biometric watermarking," *IET biometrics*, vol. 2, no. 1, pp. 21–27, 2013. [Online]. Available: https://doi.org/10.1049/iet-bmt.2012.0052

[124] H. Supreetha Gowda, G. Hemantha Kumar, and M. Imran, "Multi-modal biometric system on various levels of fusion using lpq features," *Journal of Information and Optimization Sciences*, vol. 39, no. 1, pp. 169–181, 2018. [Online]. Available: https://doi.org/10.1080/02522667.2017.1372918

[125] A. Meraoumia, H. Bendjenna, and S. Chitroub, "Towards a robust palmprint representation for person identification," *International Journal of Information and Communication Technology*, vol. 14, no. 1, pp. 89–109, 2019.

[126] M. Drahanský and M. Dvořák, *Hand shape recognition and palm-print recognition using 2D and 3D features*, ser. IET Book Series on Advances in Biometrics. The Institution of Engineering and Technology, 2018, pp. 283–307. [Online]. Available: https://www.fit.vut.cz/research/publication/11713

[127] A. Genovese, V. Piuri, and F. Scotti, *Palmprint Biometrics*. Cham: Springer International Publishing, 2014, pp. 49–109. [Online]. Available: https://doi.org/10.1007/978-3-319-10365-5_4

[128] B. Ammour, T. Bouden, and L. Boubchir, "Face–iris multi-modal biometric system using multi-resolution log-gabor filter with spectral regression kernel discriminant analysis," *IET Biometrics*, vol. 7, no. 5, pp. 482–489, 2018. [Online]. Available: https://doi.org/10.1049/iet-bmt.2017.0251

[129] L. Liu, S. Lao, P. W. Fieguth, Y. Guo, X. Wang, and M. Pietikäinen, "Median robust extended local binary pattern for texture classification," *IEEE Transactions on Image Processing*, vol. 25, no. 3, pp. 1368–1381, 2016.

[130] K. He, X. Zhang, S. Ren, and J. Sun, "Deep residual learning for image recognition," in *Proceedings of the IEEE conference on computer vision and pattern recognition*, 2016, pp. 770–778.

[131] A. Rattani, N. Reddy, and R. Derakhshani, "Convolutional neural network for age classification from smart-phone based ocular images," in *IEEE international joint conference on biometrics (IJCB)*. IEEE, 2017, pp. 756–761.

[132] C. Lin and A. Kumar, "A cnn-based framework for comparison of contactless to contact-based fingerprints," *IEEE Transactions on Information Forensics and Security*, vol. 14, no. 3, pp. 662–676, 2018. [Online]. Available: https://doi.org/10.1109/TIFS.2018.2854765

[133] H. K. P. U. Hong Kong Polytechnic University, *PolyU Multispectral palmprint database*, 2009.

[134] S. D. Jamdar and Y. Golhar, "Implementation of unimodal to multimodal biometrie feature level fusion of combining face iris and ear in multi-modal biometric system,"

in *2017 International Conference on Trends in Electronics and Informatics (ICEI)*. IEEE, 2017, pp. 625–629.

[135] K. Fakhar, M. El Aroussi, M. N. Saidi, and D. Aboutajdine, "Fuzzy pattern recognition-based approach to biometric score fusion problem," *Fuzzy Sets and Systems*, vol. 305, pp. 149–159, 2016. [Online]. Available: https://doi.org/10.1016/j.fss.2016.05.005

[136] S. Soviany and M. Jurian, "Multimodal biometric securing methods for informatic systems," in *Proceedings of the 2011 34th International Spring Seminar on Electronics Technology (ISSE)*, 2011, pp. 447–450.

[137] Y. Xin, L. Kong, Z. Liu, C. Wang, H. Zhu, M. Gao, C. Zhao, and X. Xu, "Multimodal feature-level fusion for biometrics identification system on iomt platform," *IEEE Access*, vol. 6, pp. 21 418–21 426, 2018.

[138] M. He, S.-J. Horng, P. Fan, R.-S. Run, R.-J. Chen, J.-L. Lai, M. K. Khan, and K. O. Sentosa, "Performance evaluation of score level fusion in multimodal biometric systems," *Pattern Recognition*, vol. 43, no. 5, pp. 1789–1800, 2010.

[139] Q. Tao and R. Veldhuis, "Threshold-optimized decision-level fusion and its application to biometrics," *Pattern Recognition*, vol. 42, no. 5, pp. 823–836, 2009. [Online]. Available: https://doi.org/10.1016/j.patcog.2008.09.036

[140] A. Krizhevsky, I. Sutskever, and G. E. Hinton, "Imagenet classification with deep convolutional neural networks," *Advances in neural information processing systems*, vol. 25, 2012.

[141] K. Simonyan and A. Zisserman, "Very deep convolutional networks for large-scale image recognition," *arXiv preprint arXiv:1409.1556*, 2014.

[142] U. R. Acharya, H. Fujita, S. L. Oh, Y. Hagiwara, J. H. Tan, and M. Adam, "Application of deep convolutional neural network for automated detection of myocardial infarction using ecg signals," *Information Sciences*, vol. 415, pp. 190–198, 2017. [Online]. Available: https://doi.org/10.1016/j.ins.2017.06.027

[143] K. Wang, Y. Zhao, Q. Xiong, M. Fan, G. Sun, L. Ma, and T. Liu, "Research on healthy anomaly detection model based on deep learning from multiple time-series physiological signals," *Scientific Programming*, vol. 2016, 2016.

[144] R. Liu, G. Meng, B. Yang, C. Sun, and X. Chen, "Dislocated time series convolutional neural architecture: An intelligent fault diagnosis approach for electric machine," *IEEE Transactions on Industrial Informatics*, vol. 13, no. 3, pp. 1310–1320, 2016.

[145] M. Meng, Y. J. Chua, E. Wouterson, and C. P. K. Ong, "Ultrasonic signal classification and imaging system for composite materials via deep convolutional neural networks," *Neurocomputing*, vol. 257, pp. 128–135, 2017.

[146] Y. Jia, E. Shelhamer, J. Donahue, S. Karayev, J. Long, R. Girshick, S. Guadarrama, and T. Darrell, "Caffe: Convolutional architecture for fast feature embedding." Association for Computing Machinery, 2014.

[147] T. H. K. P. U. Hong Kong Polytechnic University, "Polyu finger knuckleprint database," 2018. [Online]. Available: http://www.comp.polyu.edu.hk/biometrics/FKP.htm